RECIPROCATING WEAR RESPONSE OF Ti(C,N)-Ni_3Al CERMETS

by

Stephen T.J. Buchholz

Submitted in partial fulfilment of the requirements
for the degree of Master of Applied Science

at

Dalhousie University
Halifax, Nova Scotia
December 2011

DALHOUSIE UNIVERSITY

DEPARTMENT OF PROCESS ENGINEERING AND APPLIED SCIENCE

The undersigned hereby certify that they have read and recommend to the Faculty of Graduate Studies for acceptance a thesis entitled "RECIPROCATING WEAR RESPONSE OF Ti(C,N)-Ni_3Al CERMETS" by Stephen T.J. Buchholz in partial fulfilment of the requirements for the degree of Master of Applied Science.

Dated: December 5, 2011

Co-Supervisors: _____

_____

Readers: _____

_____

DALHOUSIE UNIVERSITY

DATE: December 5, 2011

AUTHOR: Stephen T.J. Buchholz

TITLE: RECIPROCATING WEAR RESPONSE OF Ti(C,N)-Ni_3Al CERMETS

DEPARTMENT OR SCHOOL: Department of Process Engineering and Applied Science

DEGREE: MASc CONVOCATION: May YEAR: 2012

_____

Signature of Author

DEDICATION PAGE

I would like to dedicate this work to all those who have helped me get to where I am today, and to overcome the innumerable problems that have plagued the last few years. This is especially true for Dr. Kevin Plucknett, my mother and brother, all my friends, and especially Rachel, for keeping me sane.

Table of Contents

List of Tables

List of Figures

Abstract

Titanium carbonitride (Ti(C,N)) cermets have become more popular in recent research due to their mix of high hardness, high hot hardness, good ductility, chemical stability, and low densities. These mechanical properties make Ti(C,N)-cermets especially desirable as a replacement for current 'hardmetals', such as tungsten carbide cobalt (WC-Co), as it is known that WC-Co exhibits poor mechanical behaviour at elevated temperatures. Additional interest and research has been conducted in reference to binders which enhance the cermet's capability to retain strength at high temperatures while remaining ductile. One such binder, Ni_3Al actually increases in yield strength up to a temperature of ~900°C. In this thesis, the production method utilizing melt infiltration for TiC, $Ti(C_{0.7},N_{0.3})$, $Ti(C_{0.5},N_{0.5})$, and $Ti(C_{0.3},N_{0.7})$-based cermets with Ni_3Al binder contents of 20, 30 and 40 vol. % have successfully been developed and utilized. This process produced high density samples at each nitrogen content for all binder contents, excluding $Ti(C_{0.3},N_{0.7})$. $Ti(C_{0.3},N_{0.7})$-Ni_3Al samples at 20 and 30 vol. % suffered from poor infiltration and could not be tested. The reciprocating wear mechanisms were examined, using a ball-on-flat test, utilizing WC-Co spheres with a diameter of 6.35 mm as a counter-face, and test parameters of 20 Hz, 2 hrs., and applied loads of 20, 40, 60 and 80 N. The wear tracks were examined using optical profilometry, SEM, and EDS to determine the volumetric wear rate, and the dominant wear mechanisms. The wear volume, and wear mechanisms were compared with the effect of binder content, nitrogen content, and applied load.

List of Abbreviations and Symbols Used

CIP	Cold Isostatic Press
EDS	Energy-dispersive x-ray spectroscopy
HV	Vickers Hardness
LPS	Liquid Phase Sintering
SEM	Scanning Electron Microscope
UMT	Universal Micro-Tribometer
XRD	X-ray Diffraction

Acknowledgements

I would like to acknowledge the constant support of my supervisor, Dr. Kevin Plucknett, who has aided with his support, guidance and feedback throughout all endeavours in this project. Without this aid, the body of this work would not have been possible. I would like to thank Dr. Zoheir Farhat, my co-supervisor, for his aid and advice, especially with the wear testing and related portions of this project.

I would like to thank the people who helped me throughout this thesis, with assistance with experiments, analysis, suggestions, and in keeping the equipment I required running or fixing it quickly on the many occasions it was not. I would like to make special mention of Brad Collier, Winston Mosher, Hung-Wei Liu, Mathew Harding and Md. Aminul Islam. Their help was essential in set-up and utilization of equipment throughout this project. I also thank Dean Grijm, for his aid in all of the many mechanical issues throughout this work.

I would also like to thank Petroleum Research Atlantic Canada (PRAC) and the Natural Sciences and Engineering Research Council of Canada (NSERC), the Canada Foundation for Innovation, the Atlantic Innovation Fund, and and the others who helped fund the Facilities for Materials Characterisation.

Chapter 1: Introduction

Titanium carbonitride (Ti(C,N)), the solid solution of titanium carbide (TiC) and titanium nitride (TiN)), is a ceramic material which is gaining in popularity in research and industrial applications. Ti(C,N) has excellent properties, having high hardness, high thermal conductivity, high thermal shock resistance, high hot strengths, good chemical resistance, low friction, and relatively good (for a ceramic) toughness. This, when compared to tungsten carbide cobalt (WC-Co) and other cemented carbides (including TiC) make Ti(C,N) an appealing substitute in many applications, such as high speed cutting tools. Combining Ti(C,N) with an appropriate binder, such as nickel aluminide (Ni_3Al) will greatly improve its ability to withstand impacts and shock, allowing the cermet which is formed to be successfully applied in situations for which neither material alone would be applicable. This is especially true in a direct comparison with WC-Co, as these materials are known to decompose at elevated temperatures, while Ti(C,N)-Ni_3Al is known to actually increase in yield strength up to ~900°C. The ability to withstand harsh environments while retaining its mechanical properties makes Ti(C,N)-Ni_3Al and appealing material for further research and the topic of this thesis project.

This project focus was split into two stages, the development of a production method for TiC and Ti(C,N)-Ni_3Al cermets through melt infiltration and the development/ implementation of a reciprocal wear testing method. Melt infiltration, a method by which the metallic phase of a cermet is introduced to the ceramic phase through capillary action, requires the use of compacted preforms. These compacts were produced though a combination of uniaxial and isostatic pressing, requiring a wax binder for the Ti(C,N)-Ni_3Al cermets. These cermets were created for compositions of TiC, Ti($C_{0.7}$,$N_{0.3}$), Ti($C_{0.5}$,$N_{0.5}$), and Ti($C_{0.3}$,$N_{0.7}$) and Ni_3Al at binder volumes of 20, 30 and 40 vol. %. Once the fabrication method was optimized, including post sintering machining and polishing, attention was shifted to material evaluation using reciprocating wear testing. Though it was initially attempted to optimize the reciprocating wear for mass loss measurements, the limited accuracy of testing required the subsequent use of optical profilometry to determine the wear rates of the materials. This method allowed for the accurate

measurement of volume loss while allowing for the pseudo three-dimensional examination of the wear track. Further examinations were conducted using scanning electron microscopy (SEM) and Energy-dispersive x-ray spectroscopy (EDS). Together, with the coefficient of friction gathered from the reciprocating wear testing, the wear mechanisms of the cermets could be investigated.

This thesis is divided into seven chapters, which follow the progression of the work throughout the project. Chapter 2 details the theory and literature review necessary for the reader to attain the background required to understand the theory and principals covered throughout this research. Chapter 3 and 4 detail the materials, methods, and the results produced throughout this study, focussing on the matters not detailed throughout Chapters 5 or 6. Chapters 5 and 6 are the manuscripts in submission for publication, which have been altered only to include the numbering of titles, figures and tables to correspond to the current work's numbering scheme. Chapter 7 details the overall conclusions gathered throughout this project and recommendations given for future work.

Chapter 2: Literature Review

2.1 Cermets

Ceramic-metal composites, or cermets, are structural materials composed of ceramic phase(s) that act as the hard phase (reinforcing phase), where the hard phase is made up of approximately equiaxed fine grains, and a metal matrix or binding phase that is comprised of one or more metal(s) or alloy(s).(1-3) The reasons for the creation of cermets are the same as those for standard metal matrix composites; to suppress the undesirable properties of metals and ceramics while incorporating their desirable qualities.(2, 3) However, instead of striving simply to add the favourable properties of ceramics to metals, such as abrasion resistance, and specific strength, cermets have been created to provide the benefits of metals to ceramics, including ductility and creep resistance. Cermets tend to be light in weight when compared to "hard metals", such as tungsten carbide with a cobalt binder (WC-Co), and have high mechanical strength, toughness, corrosion resistance, and thermal conductivity.(3) By having a high thermal conductivity, lower temperature gradients are created during use, which in turn produces lower thermal stresses and less cracks. Because of the combination of these properties, cermets are preferred for use as high speed cutting tools, since durability, high mechanical strengths, ability to handle wear, and the ability to endure thermal shock are all necessary traits for cutting tools. It has been found that cermet cutting tools perform better than their hard metal counterparts in general, allowing for a greater control of geometry accuracy in work pieces, greater chip and tolerance control, improved surface finishes, and increased feed rates, while they also provide consistent maintenance of critical dimensions, and longer tool life. (2, 3)

In order to control the desired properties of cermets, the metal additions that make up the binder phase may be customised. These binders are chosen from a wide variety of alloys, commonly including Fe, Al, Ni, and Co as primary additions. Each alloying element will bring specific qualities to the cermets, such as ductility, oxidation resistance, hardness, thermal conductivity, and/or thermal shock resistance. By adding various amounts or compositions of the binder alloys, cermets are able to be tailored to specific

purposes. It is important to note that the mechanical properties of the metals are not solely responsible for determining their effect on the cermet, and that their sintering behaviour will greatly impact the final product. If the metallic binders fail to wet the ceramic particles during sintering, the mechanical properties will be adversely affected, possibly causing the material to no longer be suitable for the desired application.

Recently, research has been focussed upon attempts to replace WC-Co, leading to a greater focus on TiC and Ti(C,N) cermets. These cermets are of particular interest as they may overcome the deficiencies of WC-Co, namely degradation at elevated temperatures, limited ductility, and heavy weights. The following section is focussed on Ti(C,N) cermets and the research previously done to attain their properties, and their wear characteristics.

2.1.1 Titanium Carbonitride

Titanium carbonitride (Ti(C,N)), as a cermet, that has been studied for close to 80 years (3), and in that time has been studied using many additives and various binders. Table 1 gives a brief outline of the progression of research concerning the various cermet combinations that have been researched (2).

Table 1. Progression of Ti(C,N) research from 1931-1991. (2)

Year of Establishment	Hard Phase	Binder Phase
1931	Ti(C,N)	Ni(Co, Fe)
1970	Ti(C,N)	Ni-Mo
1974	(Ti,Mo)(C,N)	Ni-Mo
1980-1983	(Ti,Mo,W)(C,N)	Ni-Mo-Al
1988	(Ti,Ta,Nd,V,Mo,W)(C,N)	(Ni, Co)-Ti_2AlN
1988	(Ti,Ta,Nd,V,W)(C,N)	Ni-Co
1991	(Ti,Ta,Nd,V,Mo,W, etc.)(C,N)	Ni-Cr

These cermets have been created to fill the niche that the WC-Co hard metals currently fill. It is desirable to replace hard metals because they are significantly denser, on average, than standard cermets, and because cermets may be tailored to fulfill specific demands, such as improved wear resistance and high mechanical strength.(2, 3) Ti(C,N) has been created in an effort to blend the attributes of titanium carbide (TiC) and titanium nitride (TiN), in order to take advantage of the favourable properties of both substances. Table 2 provides a comparison of various ceramics and ceramic based materials.(3, 4) Table 3 displays the mechanical properties of the constituents of Ti(C,N) (TiC and TiN),whereas Figure 4 compares TiC to Ti(C,N) based cermets.

Table 2. Comparison of various ceramics and ceramic based materials. (3, 6)

Material	Hardness, in kg/mm²	Hardness, in lbs/in²
Single-crystal diamond	7000–9500	10.0–13.5 million
Polycrystalline diamond	7000–8600	10.0–12.2 million
Cubic boron nitride (CBN)	3500–4750	5.0–6.7 million
Boron carbide (B_4C)	3200	4.5 million
Titanium carbide (TiC)	2800	4.0 million
Silicon carbide (SiC)	2300–2900	3.3–4.1 million
Aluminum oxide (sapphire or polycrystalline)	2000	2.8 million
Tungsten carbide – cobalt "cermet" (94% WC-6% Co)	1500	2.1 million
Zirconium oxide (ZrO_2)	1100–1300	1.6–1.8 million
Silicon dioxide (SiO_2)	550–750	0.8–1.1 million
Borosilicate glass (such as ovenware)	530	0.75 million

Table 3. Comparison of TiC and TiN. (2, 3)

	Melting Temperature °C	Micro Hardness kgf/mm^2	Density g/cm^2	Electrical Resistance μΩ cm	Thermal Conductivity Watt/m/deg	Lattice Parameter Å	Young's Modulus GPa
TiC	3140	3200	4.92	68	10	4.322	491
TiN	2930	2000	5.22	25	23	4.242	600

Table 4. Comparison of TiC cermets to Ti (C, N) cermets. (2, 3)

Cermet	Microhardness at 1000°C kg/mm^2	Strength (TRS) at 900°C MPa	Oxidation Rate at 1000°C mg/cm^2*h	Thermal Conductivity at 1000°C watt*deg/m
TiC-Cermet	500	1050	11.8	24.7
Ti(C,N)-Cermet	600	1360	1.6	42.3

These various tables have been included to provide a direct comparison of the respective properties of the materials that Ti(C,N) cermets are competing against, and to summarise the properties of the individual constituents of Ti(C,N). As may be seen in Table 2, WC and TiC both have high hardnesses which allow for their preferred application as high speed cutting tools and wear resistant coatings, since these uses may expect high temperatures, high wear due to friction, and oxidation to be incurred. However, WC based cermets are limited in their use since they may not be applied in high cutting rate applications due to softening from heating and chemical degradation. (2, 3) This is a common difficulty faced by all cutting tools and as such, new, more resilient materials have been sought. TiC cermets have been researched and applied as a replacement for WC cermets, due to their improved hardnesses and lower densities. This tends to allow parts to be created or coated in TiC that will have longer tool lives, and the ability to machine materials at higher speeds. Unfortunately, TiC is still susceptible to cracking from thermal shock and from corrosion, which limit the application of such tools. To prevent this, coatings or tools of TiN have been used in many situations to mitigate cracking and wear, because it has superior tribological and corrosion properties, as well as higher thermal conductivity. These factors allow tools to have longer lives under harsher conditions. Unfortunately, TiN is not as hard as TiC, so although it may handle the heat generated from faster production rates more easily, it will not be able to cut materials that require a greater hardness.

As a result, Ti(C,N), is a solid solution of TiC and TiN, where it is anticipated to benefit from the favourable properties of both end-member components. Because

Ti(C,N) is its own distinct material, and different from the basic materials that it is comprised of, the mechanical properties are also different and change with its varying compositions. The purpose of such a combination is to produce a material that may be put to use under conditions that neither TiC or TiN alone can function under, or to out perform those materials in their current applications. Due to the varying compositions of Ti(C,N), often represented as $Ti(C_{1-x},N_x)$ where x is the atomic fraction of nitrogen, the material properties vary widely and are difficult to ascertain ahead of time. However, the general trends for the various properties are known. As the nitrogen content increases in $Ti(C_{1-x},N_x)$, the attributes of the material change from resembling those of TiC to favouring those of TiN. This means that as the nitrogen content is increased, the hardness at room temperature, the coefficient of friction, and the lattice parameters all decrease. Conversely, the hot hardness, the thermal conductivity, the corrosion resistance, the chemical inertness, the wear rate, the stability (at increased temperatures), and the density all increase.(2, 3, 5) These attributes allow $Ti(C_{1-x},N_x)$ to cut at faster speeds and be used for machining more difficult materials (such as super alloys), while still producing better surface finishes.

One of the attributes that make Ti(C,N) such a versatile material is that TiC and TiN are isomorphous, with a face-centered-cubic (FCC) crystal structure, with lattice parameters of 0.4320mm and 0.4240mm, respectively. For Ti(C,N) the carbon and nitrogen atoms are in the ½, ½, ½ sites within the Ti super lattice, and are substituted at random. (2, 3) This allows for the stoichometry of $Ti(C_{1-x},N_x)$ to be maintained at all times, regardless of the varying amounts of carbon and nitrogen, since there is no requirement for an ordered lattice. The non-ordered arrangement of carbon and nitrogen also allows for the substitution of atoms to be carried out without a large distortion (or other defects) in the crystal lattice, as the material progresses from one composition to another. Figure 1 illustrates the isomorphous nature of the FCC crystal structure of Ti(C,N). First displaying the original theory that all elements (Ti, C, and N) were interchangeable within the FCC structure), and the current theory (depicting only C and N to be interchangeable). Figure 2 is an image captured during a selected area diffraction pattern using transmission electron microscopy. Figure 3 is an image captured using a

scanning electron microscope (SEM). All tests were conducted using Ti ($C_{0.50}$, $N_{0.50}$) powder and are shown to demonstrate the FCC crystal lattice of Ti(C,N). (6)

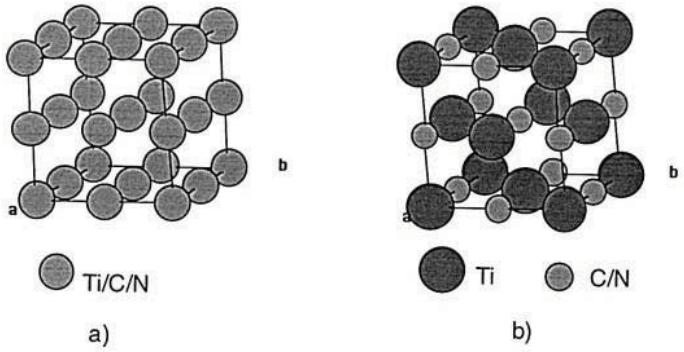

Figure 1. Diagrams of Ti (C, N) crystal structures where a) depicts the original theory and b) depicts the current theory. (8)

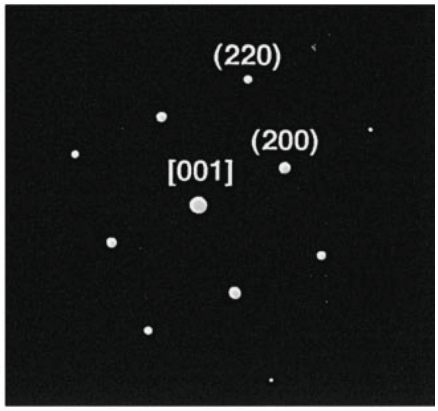

Figure 2. TEM diffraction image of Ti ($C_{0.50}$, $N_{0.50}$) displaying its FCC crystal structure.(8)

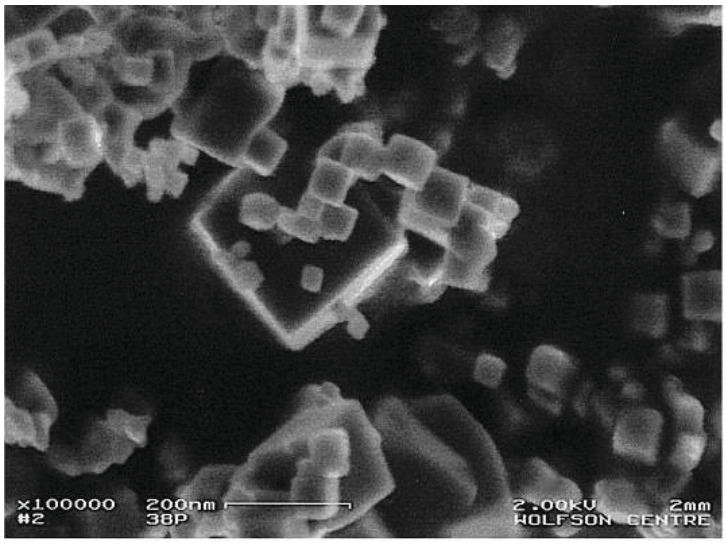

Figure 3. SEM image of Ti ($C_{0.50}$, $N_{0.50}$) displaying its FCC crystal lattice.(8)

Unfortunately, Ti(C,N) has two severe difficulties in its production; decarburization and denitridation during sintering, solutionising, or from reactions taking place with the binding agent. As may be seen in the ternary and binary combination phase diagrams presented in Figure 4, and the more detailed binary phase diagram in Figure 5(2, 5), there is an area that indicates, even at 1150°C, that graphite will be produced in the presence of high dissolved amounts of carbon.(2, 6)

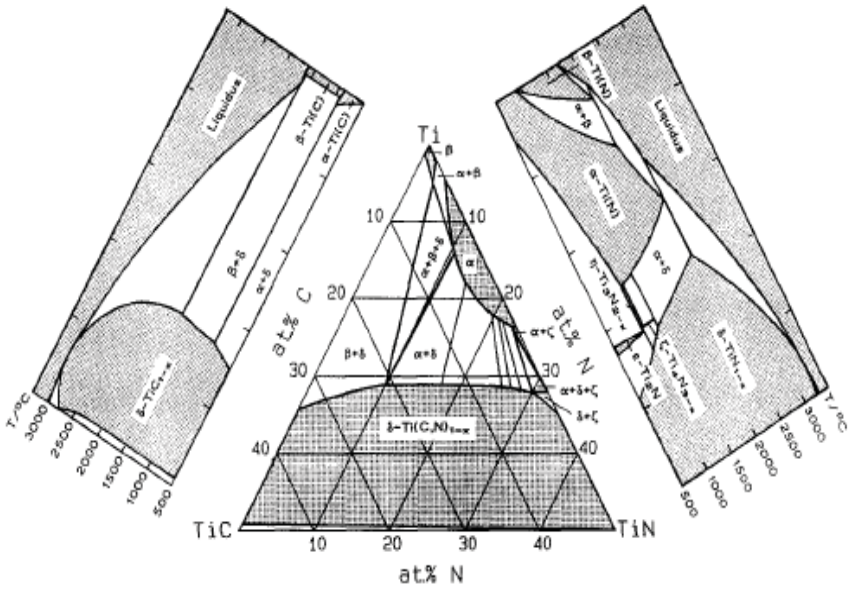

Figure 4. Ternary phase diagram of the Ti-C-N system at 1150°C with TiC and TiN binary phase diagrams included. (7)

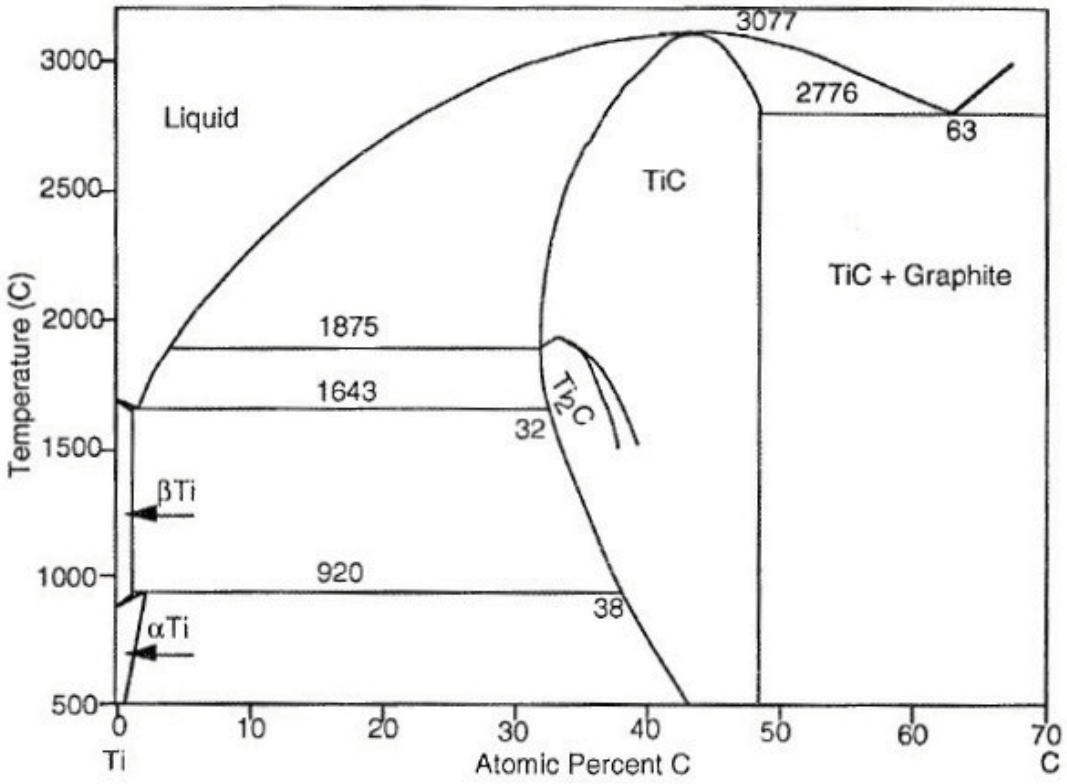

Figure 5. The binary phase diagram Ti-C, displaying the range of stable TiC and TiC+graphite over a range of carbon amounts. (2)

As the partial pressure of nitrogen increases a greater amount of free carbon will be produced, while less carbon will be produced as the temperature increases. The denitridation occurs during the formation of $Ti(C_{1-x},N_x)$ or during sintering, when the TiN particles are denitrided and carburized. This changes the nitrogen content of the ceramic from the predetermined amount, thus altering both the chemical composition and the desired properties. In addition to this, when nitrogen is lost, bubbles are formed within the particles and nitrogen gas is trapped between the particles, creating porosity within the material that acts as sites for crack propagation. Further denitridation takes place through chemical reactions during the addition of the binding phase, as the metal binder reacts to the Ti (C_{1-x}, N_x) hard phase.

Table 5(2) shows data obtained for various sintering temperatures and compositions of $Ti(C_{1-x},N_x)$, along with the stable phases, so as to illustrate the changing stability of $Ti(C_{1-x},N_x)$ at increasing temperatures.

Table 5. Stability of $Ti(C_{1-x},N_x)$ where x is the amount of nitrogen, at various temperatures. (2)

Temperature °C	Stable Phase		
	TiN + C	$Ti(C_{1-x},N_x)$ + C	$Ti(C_{1-x},N_x)$
1400	no data	no data	$x>0.06$
1527	$x\leq 0.2$	$0.2\leq x\leq 0.625$	$x > 0.65$
1800	no data	no data	$x > 0.35$
2027	does not exist	$x\leq 0.16$	$x > 0.16$

As both the temperature and the nitrogen partial pressure may be carefully controlled, the decarburization may also be controlled, or alternatively determined through testing in order to mitigate its effects on the material. Denitridation has traditionally been solved with the addition of molybdenum, which bonds with the $Ti(C_{1-x},N_x)$ particles in a core rim structure, shown in Figure 6.(7) A more recent solution involves using a pre-solid solution sintering treatment, which does not require the addition of Mo. Both processes have positive and negative aspects, and may be chosen on the basis of the mechanical properties that are desired, together with cost.(2, 7) Figure 6 displays the hard phase of Ti(C,N) as the dark grey core in the particles, while Mo_2C with minor amounts of dissolved Ti is in the intermediate, light grey rim phase; Co binder is present as the white areas between particles.

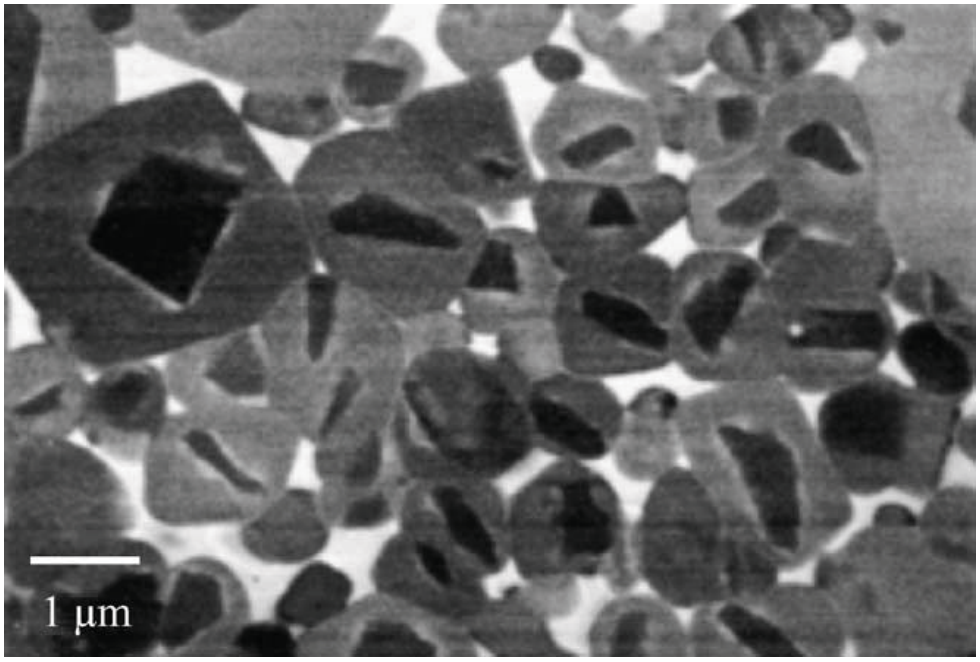

Figure 6. SEM image of the core rim structure of Ti(C,N). (7)

When molybdenum is added to $Ti(C_{1-x},N_x)$ or any of the other carbonitrides from groups IV_b, V_b, and VI_b of the periodic table of the elements, it is added in the form of Mo_2C. By adding the Mo_2C, the sinterability of the carbonitride is greatly improved, denitridation is reduced or eliminated, graphite formation is suppressed, and grain growth is retarded. These gains however come at the cost of machinability of the material.(2, 3) The sinterability of the material is increased because Mo_2C has a greater wettability for the currently used binders than TiC.(2) Wetting is improved when there is preferential absorption of atoms at an interface, which lowers the interfacial energy, or by establishing a diffusion gradient across a solid-liquid interface, which reduces the contact angle. This is manifested in the carbides of groups IV_b, V_b, and $VI_{b\ elements}$ by their stability, which is greater at lower heats of formation. Since Mo_2C is the least stable, as displayed by Table 6 (2), its reactivity is the highest, and therefore its wetting angle is the smallest, leading to the greatest wettability (2).

Table 6. A comparison of heats of formation for carbides of elements in groups IV_b, V_b, and VI_b of the periodic table of the elements. (2)

IV_b	kJ/mol	V_b	kJ/mol	VI_b	kJ/mol
TiC	-183.7	VC	-126.4	Cr_3C_2	-89.7
ZrC	-199.2	NbC	-142.3	Mo_2C	-17.6
HfC	-209.2	TaC	-161.1	WC	-35.1

Mo_2C reduces the denitridation by separating the $Ti(C_{1-x},N_x)$ particle core from the liquid phase with an intermediate phase during sintering. This separation ensures that the contact required to chemically react with the liquid phase, and to allow increased mass transport during LPS, is eliminated for $Ti(C_{1-x},N_x)$. This ensures that nitrogen cannot freely leave the $Ti(C_{1-x},N_x)$ particles and, as such, greatly reduces the denitridation. The grain growth of $Ti(C_{1-x},N_x)$ is also retarded, since the intermediate phase does not allow the required mass transport to take place during LPS. Since the nitrogen content will effectively not be changing, graphite formation will also be hindered, as the composition of the hard phase will not change to a composition where graphite is the stable phase. In addition to this, the Mo_2C addition creates a strong bond with $Ti(C_{1-x},N_x)$ while also bonding with the metallic binding phase. This increases the hardness of the material, which in many cases may be desired. Unfortunately, this increase of hardness also comes with a decrease in the toughness of the cermet. This affects the cermet negatively as both, the increased hardness and more brittle behavior decrease the machinability of the material. This makes production more difficult, costly, and time consuming. (6)

The treatment of forming a pre-sintering solid solution (PSSS) is a method of production where the desired solid solution is formed before the sintering process. In using this method to create cermets, the solid solution hard phase is typically formed at a temperature greater than the sintering temperature, milled to create a fine powder, and then processed as per the original powder, including the sintering steps. This approach overcomes the same problems that have been solved by the addition of Mo_2C, such as the solubility of the carbide in the binder during LPS and the reactions allowing for denitridation to occur, but solves these difficulties in a different manner. By first forming the solid solution, the difficulties of denitridation are immediately mitigated. Since the

loss of nitrogen may be predetermined, it may be dealt with by providing additional nitrogen in the starting material. In this manner, the final nitrogen content that is desired will remain after the solid solution is formed, and only the excess nitrogen is lost. In addition to this, the problems of gaseous bubbling are also mitigated, by re-pulverizing the material after forming the solid solution; this eliminates any stress concentrating bubbles that formed during denitridation. Decarburization may be controlled as previously stated, through prior knowledge of nitrogen partial pressure and the temperature at which the process is carried out, and may be applied in the same manner for both PSSS and for the addition of Mo.

The final benefit that PSSS provides to the production of $Ti(C_{1-x},N_x)$ is that of increased stability. One of the factors that greatly harm the creation of carbonitride cermets is that of mass transport during the LPS, and the solubility of the carbides in the most common metal matrices, such as cobalt and nickel. Carbides tend to have an increased solubility in both Ni and Co (carbon having a solubility of approximately 10 at%(2, 3)in Ni and Co), and they will dissolve during LPS and precipitate during cooling, causing grain growth. Nitrogen is much less soluble than carbon in both binders, and this is true with nitrides as well. This means that nitrides will not dissolve appreciably in these binders and therefore will not contribute to grain growth during LPS. Thus, when combined to form carbonitrides, the nitrogen will suppress the dissolution of the compound as a whole, greatly decreasing grain growth while still allowing the partial solubility that is required for LPS. This allows for high nitrogen content carbonitrides to be manufactured, resulting in increased ductility, improved tribological properties, high strength, and high toughness, while still retaining good machinability.

Due to the various advantages gained from PSSS, the Mo_2C that was previously believed to be an indispensable ingredient in the formation of carbonitrides may be greatly reduced or eliminated completely. This allows for the desired attributes of the carbonitrides to be attained, without the negative qualities of Mo_2C addition to be imparted into the material.

Table 7 displays a comparison of several properties for Ti(C,N) cermets, with and without PSSS treatment, with hard phase amounts of 80-85%.

Table 7. A comparison of materials with and without PSSS treatment, and the addition of Mo_2C. (2, 3)

Cermet	Hard Phase %	PSSS Treatment	Contains 5% Mo_2C	Hardness Hv kg/mm^2	Fracture Toughness MPa* $m^{1/2}$	Strength TRS kg/mm^2	Crater depth mm	Flank Wear mm
A	85	yes	no	1600	8.5	200	0.05	0.08
C	85	no	no	1300	9	180	too worn	too worn
B	80	yes	yes	1630	5.5	180	0.23	0.08
D	80	no	yes	1500	5.5	180	0.25	0.12

As is shown, all of the attributes listed increase for the PSSS treated substances and (excluding hardness) are better than those obtained when Mo_2C is added. This is chiefly due to the avoidance of increased hardness and decreased ductility that are induced with Mo_2C addition, which has significant impacts on tribological attributes. However, despite the promising affects of PSSS treatment, it is limited in effectiveness to nitrogen contents of approximately 60% (i.e. $Ti(C_{0.4},N_{0.6})$.(2, 3) Past this amount of nitrogen, denitridation is once again encountered during sintering. PSSS treatment still provides positive results past this ratio, but Mo_2C needs to be added to the material in order to prevent denitridation, albeit in lower amount than if the PSSS treatment had not taken place.

The final consideration to be taken into account when forming a $Ti(C_{1-x},N_x)$ cermet is the metal binder that is used to form the composite. When choosing a binding phase, it is important to select one that wets the ceramic phase well, has a slight solubility for the hard phase, and has the physical attributes that are desired. The first two requirements for the metal are obvious as they are determining factors for both LPS and for the ability of the metal to infiltrate the green body. However, matching the first two criteria with the final desired properties has proven difficult.

As shown in Table 1, nickel, and nickel mixed with iron or cobalt were the original choices for the binder phases during the initial research. As time progressed, the binder alloys became more complicated but remained relatively limited. This limitation stems from the fact that Ti (C_{1-x}, N_x) is best wet by the transition metals. Because of this, although the properties of non-transitional metals may be desired or preferred, because they do not wet the ceramic phase very well, if at all, the overall benefits of adding the non-transitional metal binders may be destroyed by the negative effects of poor wetting. In addition to this, the wetting increases as the atomic weight decreases. This means that transition metals occupying period 4 of the periodic table of the elements will generally wet better than elements in the same group in period 5. Attempts to combine more ductile or chemically resistant materials, such as aluminum and various compounds, have also been made hoping for gains that are greater than the losses suffered by decreased wetting.(2, 3, 8)

In addition to the properties of the powders and binders, the method of production will affect the properties of the final product. Beneficial and adverse attributes will be associated with each individual method of production. A common method used for powdered materials is a simple press and sinter technique. The following section details both uniaxial and isostatic pressing, as both methods are used in this study.

2.2 Pressing

A common production method for simple parts, whether for powder metallurgy or for ceramics, is the compaction of dry powders (<2 wt. % water) and semi-dry powders (~5 to 20 wt. % water) using a press.(9) Commonly used methods to achieve this compaction are uniaxial pressing and isostatic pressing (both cold and hot). Both of these methods have the benefits of rapidly producing green bodies with simple shapes and accurate dimensions. However, each of these compaction methods has positive and negative aspects that are specific to their particular process, which will be discussed in brief in the following sections.

Uniaxial pressing, as the name implies, involves a press that compresses powders in a single direction, normally vertically. Consisting of an upper punch or punches, a

lower punch or punches, and a die; the classification of the press is determined by the actions each of the pieces involved and are displayed in Figure 7.

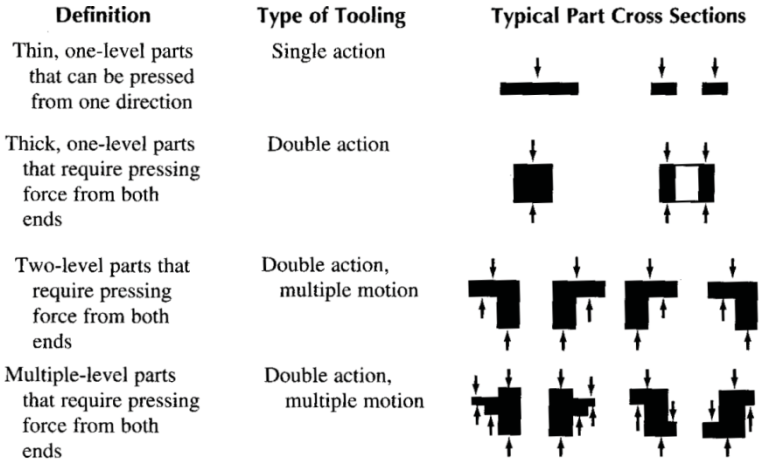

Figure 7. Uniaxial press types. (4)

All of the processes listed in Figure 7 may be carried out either mechanically, or hydraulically, and can be created on a single punch press, rotary press (many single punch dies that are used one after another), or a toggle press (the punch volume remains constant while the powders used are the only factor that change the properties of the green body). The mechanical presses have a high production rate and are easily automated, allowing for a larger number of simple parts to be produced in a given amount of time. Hydraulic presses are slower and not as easily automated, but are able to be larger; leading to their use for pieces that require more customization and pressure. (4) However, regardless of how it is accomplished, uniaxial pressing is still one of the most widely used operations in the ceramics industry.(9) This is due to the good overall production rate, the ease of operation, the high tolerances of the produced pieces (± 1% tolerances for dry powder pressing and ± 2% tolerances for wet powder pressing), and the general easy of automation.

Unfortunately, there are many difficulties that affect the end product formed through uniaxial pressing that limit its effectiveness as a production method. Four of the chief problems that are encountered during production are improper powder density or size, die wear, cracking, and density variation.(4) These difficulties negatively affect

different aspects of the green body, such as the overall density, the density uniformity, the fracture toughness, and the ability to produce products within a designated tolerance.

Improper density or size means that there is a variation in the powders that are being used as compared to their normal traits. The powder may for some reason be made up of particles of approximately the same size, there may be particles present that are extremely oversized, and/or the particles may be heterogeneously distributed instead of homogeneously. This causes poor packing to occur, and allows the green body to have a poor local or overall density. This type of defect may be determined through constant quality control, and can be handled without much difficulty.

Die wear is the degradation of the die itself over time, through the continual contact and abrasion from powders. As the die wears, the pieces being produced will undergo a progressive change in dimensions, eventually leading to pieces outside of tolerance. This problem may be detected through continual quality control of the components being produced. To mitigate this problem, the die should be replaced or repaired as specified by the manufacturer, or be given a coating that is more wear resistant than the die itself. It should be noted that the extent of die wear will increase with increasing compaction pressure.

Cracking, though obvious to see in many cases, is more difficult to determine the cause of than either of the previous issues. It may be caused by many reasons, including: rebound during ejection from the mold, die wall friction, improper design of the mold, and die wear.(4) This is not a complete list of reasons for why cracks form, but a list of those that are more common. Rebound during ejection, or removal of the top punch, causes cracking by allowing non-uniform changes in geometry to occur. When the top punch is removed, the piece may rebound upwards, but may be restricted at the edges due to die wall friction, causing large stresses to build up in localized areas and initiate cracking. During ejection, the piece rebounds to a larger cross section as it is raised out of the die. When this occurs, large stresses are built up in the region still in the mold, and may initiate cracks. Die wall friction, other than the already mentioned method of restricting rebound, may cause cracks by applying greater forces on the edge of the piece during ejection than are applied throughout the bulk, allowing the piece to crack if the stresses are high enough. If the mold is improperly designed, or has suffered from die

wear, pieces may crack due to flaws caused by uneven pressure gradients, which lead to variation in green density, allowing the pieces to crack upon ejection and rebound. There are many ways to reduce the likelihood for cracks to form, ranging from replacing or augmenting the die being used to utilising more lubricant during the pressing, and each process will have to be customized using one or more of the methods to prevent cracking, depending on the mechanisms present. (4)

Density variation is the largest problem that faces uniaxial pressing, and cannot be completely overcome. Since densification occurs due to a uniaxial application of pressure, and since the die wall and particle-particle friction dissipate this pressure as particles slide along the wall and against each other, non-uniform pressure gradients are formed. In addition to this, the pressure decreases as the length to diameter ratio increase due to particle-particle friction, causing a pressure gradient that is depicted in Figure 8 (4). This pressure differential is especially pronounced in single action presses, where the only source of pressure acts upon the top of the piece, but is still present in double action presses. This difference in densities is depicted in Figure 9 (4), where it can be seen that though double action presses still have the density gradient, it is symmetrical as compared to that of the single action press.

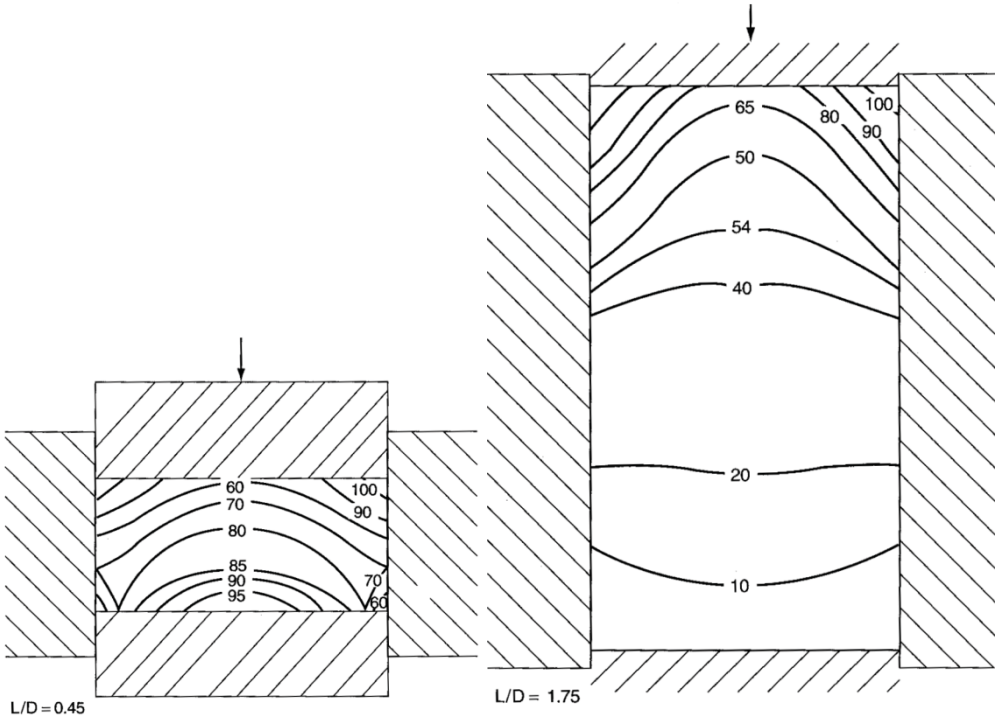

Figure 8. Uniaxial compaction giving densities in percentages.(4)

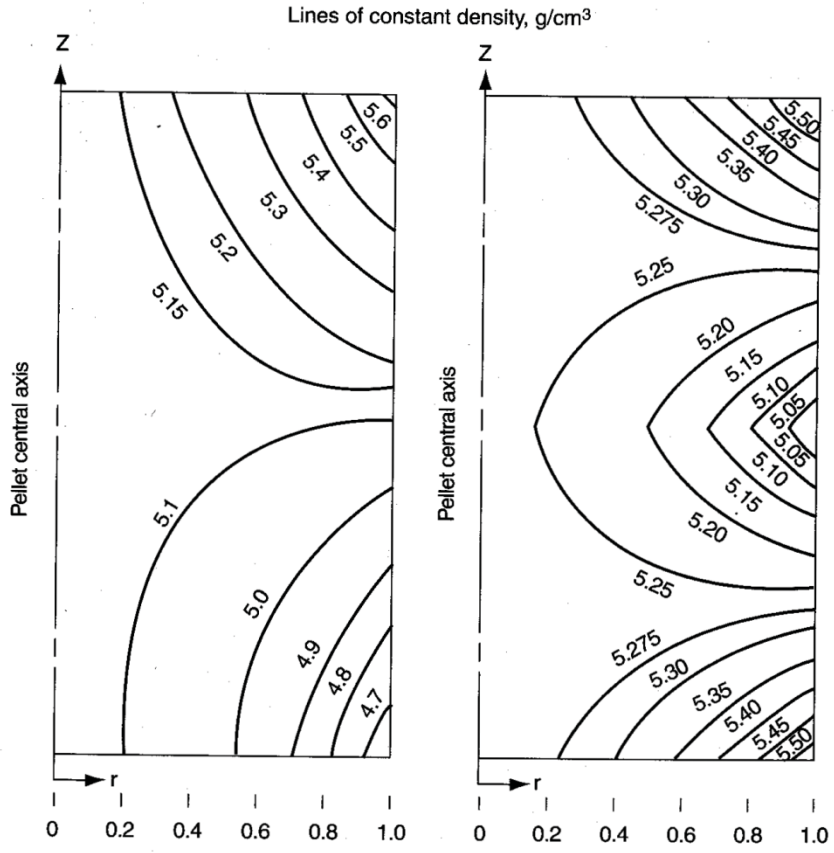

Figure 9. Uniaxial pressing with single action on left, double action compaction on right. (4)

The general method to alleviate the problems of density variation is to reduce the die wall friction and particle-particle friction through the use of suitable lubricants and binders. Lubricants are used to decrease the particle-particle and particle-die wall friction, allowing the particles to rearrange more easily during compaction, and therefore resulting in a greater and more uniform density. Binders are used to form granules out of the smaller particles or to hold the compact together in general, allowing for a greater packing to occur. However, they also have the ability to act as a minor lubricant during compression, helping in the same manner as other lubricants, although not to the same degree.

It is apparent that there are many flaws in uniaxial pressing that restrict its usefulness as a production method despite its many positive attributes. The foremost of these flaws, the inherent particle-die wall friction, may only be mitigated through the use

of lubricants, and occurs due to the problem that pressure may only be applied in one direction. This problem, as well as others, may be eliminated by applying pressure in all directions at once during compaction. Various designs have been created to accomplish this application of pressure, and are all grouped under the greater heading of isostatic pressing.

Isostatic pressing is performed by placing the powder or green body to be compressed into a flexible mold which is then compressed by pressurizing an incompressible liquid inside of a pressure chamber. There are two basic fields of isostatic pressing, wet-bag and dry-bag, and are named according how the pressure is applied to the mould during compaction. In wet-bag isostatic pressing, the powder or green body is placed and sealed into either a flexible rubber mould or a flexible fine mesh (fine enough to not allow the powder to seep though) and suspended in a incompressible liquid, to which the compacting force is applied. Using this method (as long as the mold being used can fit into the pressure chamber, and the pressure is adequate to provide the desired green density) a large variety of shaped molds may be used. This technique allows for pieces with large length-width aspect ratios and/or complex shapes to be fabricated without the need to purchase additional equipment (except for molds). Unfortunately, due to the loading methods for the different pieces, this method is relatively slow, difficult to automate, and takes a large amount of manual labor to operate. However, these drawbacks are offset by the uniformity of the density of the product, the versatility of the process, and the low cost of tooling.

Dry-bag isostatic pressing varies from wet-bad pressing in how the liquid is used to compress the mold, and in the variety of parts that may be produced with each setup. In a dry-bag press, the mold is a part of the pressure chamber itself, and is not removed between batches. Instead, there are channels between the outside of the mold and the inside of the pressure chamber that allow the incompressible liquid to enter and surround the mold, applying pressure through the mold and onto the piece, and then allowing the liquid to be drained off. A schematic of a dry bag press is shown in Figure 10.(4)

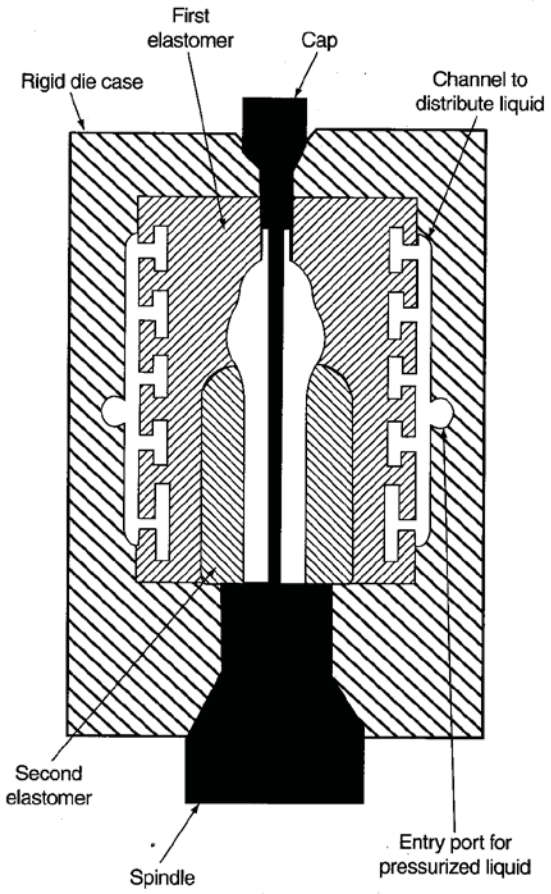

Figure 10. Dry bag isostatic compression schematic. (4)

The benefits of dry bag pressing are that it may be automated and has an increased production rate as compared to the wet bag isostatic press. This allows for its use if there is a demand for the production of the same part repeatedly, such as for spark plug insulators (4). However, since the mold is effectively a piece of the pressure chamber, it is more difficult to change, and therefore it does not have the versatility of the wet bag process.

Following compaction, cermets must undergo further densification. A common method used to accomplish this is sintering. Sintering may be done in either a solid state method, or using liquid phase sintering. Due to its common use and application in this study, the following section describes sintering, with a focus on liquid phase sintering.

2.3 Sintering

Sintering, for the powder processing of ceramics, is a technique where powder compacts are consolidated via thermal energy. This consolidation causes the powder preforms to shrink, to reduce in porosity, and increase in mechanical integrity. This is brought about by the coalescence of the powder particles into a more dense mass, due to diffusion occurring at the grain boundaries. Figure 11 is a diagram that shows what occurs between particles during sintering in stages:

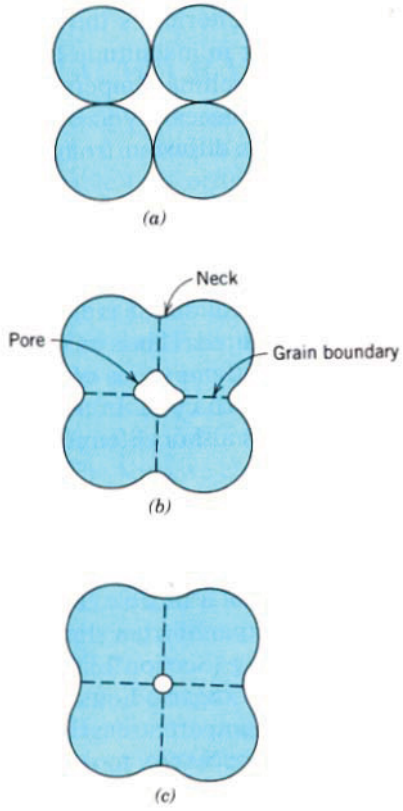

Figure 11. Images (a)-(c) illustrate the different stages encountered during sintering. (10)

Initially, the particles are in contact with each other, as can be seen in Figure 11 (a). This contact has been created during initial compaction of the formed piece, and normally includes only point contacts (when using ceramic powders, with the assumed shape of a sphere), since they will not plastically deform during processing. During the initial stages of the sintering process, diffusion begins, and mass starts to flow away from the exposed edges and to the contact sites, causing necks to form along the point of contact. The grains at the point of contact begin to merge, and new grain boundaries form

at the edges of the necks. This eventually causes the space between each particle to become part of an interconnected network of porosity, as shown in Figure 11 (b). As sintering continues, the pores become smaller and more spherical, and eventually can become isolated, closed pores; as shown in Figure 11 (c). The driving force behind this mass transfer is the reduction of interfacial energy, and occurs below the melting temperature of the particles, normally forcing the diffusion (mass transfer) to occur at the contact points since no liquid is present.(10)

In the case where liquid is present during sintering, the process is named liquid phase sintering (LPS). This process has two major advantages over solid state sintering; it has enhanced sintering kinetics, and that it has tailorable properties.(2) The enhanced kinetics result due to the greater mass transport through the liquid phase. The reason for the increase in mass transport is that the diffusion coefficient for the solute atoms in the liquid and the contact area of the liquid are both greater than those of the grain boundary (the grain boundary mechanics normally dominate at sintering temperatures). Additionally, the pressure gradient of the liquid/solid interface (low pressure), and the liquid/vapor interface (high pressure) provides an additional driving force to increase the mass transport. Both of these features increase the density of the part, allowing for improved physical properties. The final mechanism, Ostwald ripening, allows for particles that are below a critical value to dissolve and the larger grains to grow, leaving pores that may be filled in by liquid where the small particles used to be.(9)

The properties attainable in LPS can be tailored due to the choices that may be made for the material making up the liquid phase, and the amount that will be used. When choosing an additive to use in a LPS, the material needs to wet the ceramic particles well, have an appreciable solubility for the solid, and have a low viscosity. (2, 9) With a low viscosity, the liquid is able to flow into the pores due to capillarity action, while minimizing the drag on the particles it is passing, allowing the homogeneity of the preform to remain intact. If the solid is appreciably soluble in the liquid, the mass transportation will be increased during sintering, and the bonding between the particles and the binder will become stronger, since there will be a chemical bond as well as a physical bond.(2, 3) If the liquid wets the solid well it will cover the particles completely, allowing for better bonding and mass transportation and generally increasing the strength

of the material. Wetting means that the contact angle between the liquid and the particle will be between 90° and 0°; as non-wetting occurs at contact angles above 90°, and complete wetting (or spreading) occurs at a contact angle 0°.

In standard LPS, the particles that form the liquid as well as those that remain solid have normally been previously compacted. This method has the benefit of decreasing the distance required for the liquid to travel to fill voids. However, the particles that form the liquid may cause residual porosity as material flows away to fill current voids. To prevent this, melt infiltration may be conducted, where the liquid phase is initially separate from the ceramic phase.

2.3.1 Melt Infiltration

Melt infiltration is not a production method that is performed to attain the hard phase in a cermet, but is a method of applying the binder phase once a green body has been formed from the hard phase. In this approach, liquid phase sintering must be the method used to sinter the piece, as the liquid binding phase must be free to move in order to infiltrate the green body.

When conducting melt infiltration, the metal phase (normally a powder) is placed into contact with the ceramic green body, by either placing the green body on top of a powder bed, placing the powder onto of the green body, or by surrounding the green body with the powdered metal. The most common of these methods when creating a cermet is the second option, as it allows the green body more support during infiltration, and helps prevent warping. If the liquid wets the hard phase, then the liquid will flow freely into the pores through capillary action, driven by the reduction of free energy; in this instance the process is called pressureless. If the hard phase is significantly soluble in the liquid, then the areas where particles meet at grain boundaries will diffuse preferentially as the liquid wicks through the pores, and may cause the green body to destabilize. If there is no wetting or there is poor wetting, the liquid may be forced into the green body by an increased external pressure. This is called pressure assisted melt infiltration, and typically creates a poor bond between the particles and the binder. In general, since it is less

expensive and sintering is more effective if the wetting is good, pressureless infiltration is preferred.

2.4 Tribology

Due to their high hardnesses and wear resistance, cermets are often used as tools or coatings in applications where materials are expected to be in contact and in motion. To assess the ability of any specific cermet to withstand the continued contact between surfaces, the tribological characteristics must be investigated. Tribology is the science of friction, wear, and lubrication of interacting surfaces in relative motion (11). This field of research covers a wide range of applications, including testing, manufacturing, transportation, chemical processing, medicine, etc. and governs the use of many materials in day-to-day life. The reason that tribology is such a far reaching field is that wear and friction are found in every application where solids interact with other materials. Wear is especially important as it is accountable for the loss of mechanical properties and a majority of material wastage. Thus, improvements in wear resistance will increase the operating lifespan and therefore generate savings for most tools throughout the world. This may be seen in the need to replace the brakes of a car, the loss of efficiency of a bearing, the use in erasers, or even the collapse of some structures (11-13).

Tribology is used to understand friction, wear, and lubrication so that the desired mechanical properties may be employed for a designated application. This means that it is not always the case that both friction and wear need be reduced, as one or both of those properties may be required for proper function. Lubrication may also be chosen according to specific needs, as it may not always be possible to operate without it. Figure 12 illustrates the fact that in many cases friction and/or wear may be necessary to allow for the desired function of a material (11-13).

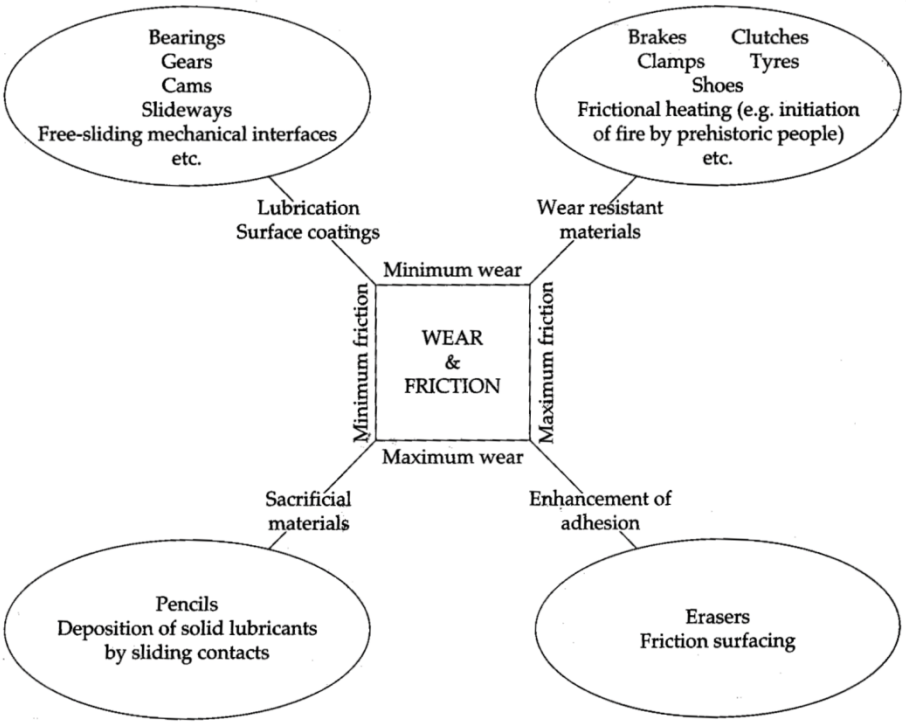

Figure 12. Examples of both, low and high requirements for wear and friction (11).

It is interesting to note that no one material is used to prevent or increase friction and wear, and that the specific application will determine what material is used. An extreme example of this would be in increasing the friction between a car and the road using a rubber tire and increasing friction on a conveyor in a continuous sintering kiln operated at 1000°C. In these two examples, the operating conditions (the temperature) prevent rubber's use in one application but not the other.

Friction, which is the force that opposes the motion for objects in contact, and acts in a direction normal to the surfaces in contact, may be broken up into two components, static and kinetic friction. Static friction is the force that must be overcome in order to initiate motion from rest. It is larger than that of kinetic friction and is best visualized by a block on a wedge, as shown in Figure 13. When describing friction, it is useful to visualize the surfaces in contact as shown in Figure 14. The friction that is caused between the two bodies as they slide over one another may be attributed, in general, to the energy required to overcome the bonding that occurs between the surfaces, or the energy required to force an asperity to pass through/over another (11-14).

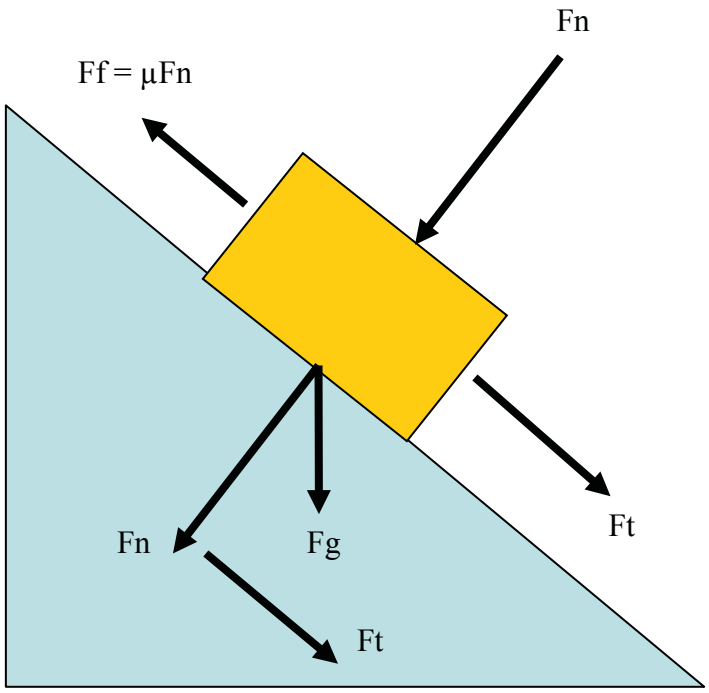

Figure 13. Demonstration of friction.

Where: F_n = normal force, F_f = frictional force, F_g= force of gravity, F_t = force acting tangentially

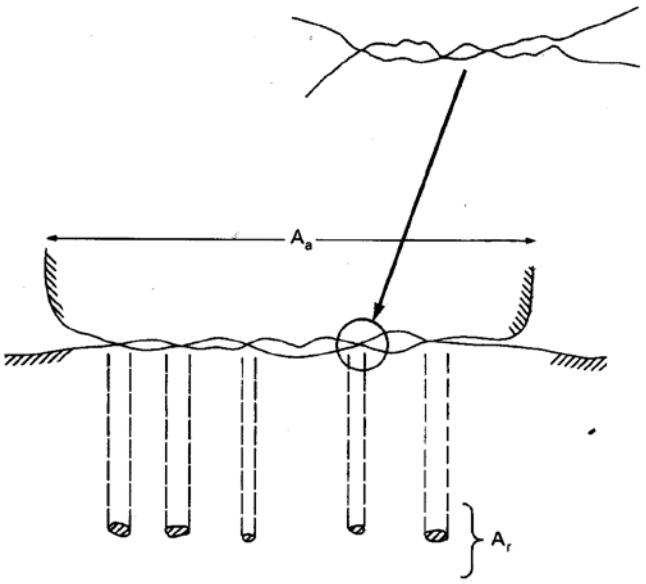

Figure 14. Contact interface, showing asperity contact, submicron contact (upper right) and areas of frictional energy concentration (12).

Referring back to Figure 13, if the force on the block is too low to overcome the static friction then the block will remain in place. If the force is increased and becomes greater than the static friction, the block will begin to move and will slide down the wedge. Once the block has initiated motion, the force required to maintain that motion is smaller than that of the static friction, and is named kinetic friction. Friction is normally represented by the friction coefficient μ, and will vary in magnitude depending on the extent of the attraction between the materials. In these terms, static friction is the force required to break the bonds that hold two materials together in place, while kinetic friction is the force required to prevent bonding to reoccur, and to break any minor bonding that takes place during motion. Even though both components of friction must be considered for the application of a material, one may be dominant in a situation. Static friction would be the dominant concern in cases where there are fast repetitions of stopping and starting, whereas kinetic friction will dominate in a continuous process that stops rarely. This is an over simplification, but it provides the required knowledge required to understand the basic approaches to counteract friction, namely lubrication and alteration of the surface layer(s) (11-14).

Lubrication is one of the most prevalent methods by which to decrease friction. When lubricating a contact, any material that decreases the friction between surfaces may be used, as long as it remains stable while providing the benefit. These materials are in many cases liquids, such as oils, but may also be gases or solids. Both gases and liquids perform in a similar manner, by providing full fluid films or mixed films, and may thus be classified together under the heading of hydrodynamic lubrication. Solid materials used for lubrication are classified under the term solid lubrication. In all cases, the lubricant acts to separate the surfaces and prevent their contact, while providing low shear strength at the contact points. The subject of lubrication is very extensive, and of great practical use, but will not be covered in depth within this thesis, as the experimental studies performed were all conducting under dry sliding conditions (11-14).

The alteration of the surface layers to reduce friction is of great importance as a friction/wear decreasing treatment. This may be done in various ways, such as providing an alloyed coating, chemically altering the surface layer (oxidizing, carburizing, etc.), or choosing materials of different wear properties. By changing the surface layer, it is

possible to provide a wear resistant contact between materials while making use of the bulk material's mechanical properties (11). In general, soft materials wear more quickly when in contact with a surface of greater hardness (11-14).

Wear is the loss of material from an object(s) and occurs as contact surfaces move in relative motion to each other, while transmitting force from one contact to the other. The term transmitting is used because the surfaces are not required to be in direct contact to cause wear, such as in the case of lubricated parts. There are four different regimes for lubrication: rigid full fluid film, elastic full fluid film, mixed, and boundary. A "general" full fluid film, a mixed, and a boundary region are shown schematically in Figure 15 (11-14).

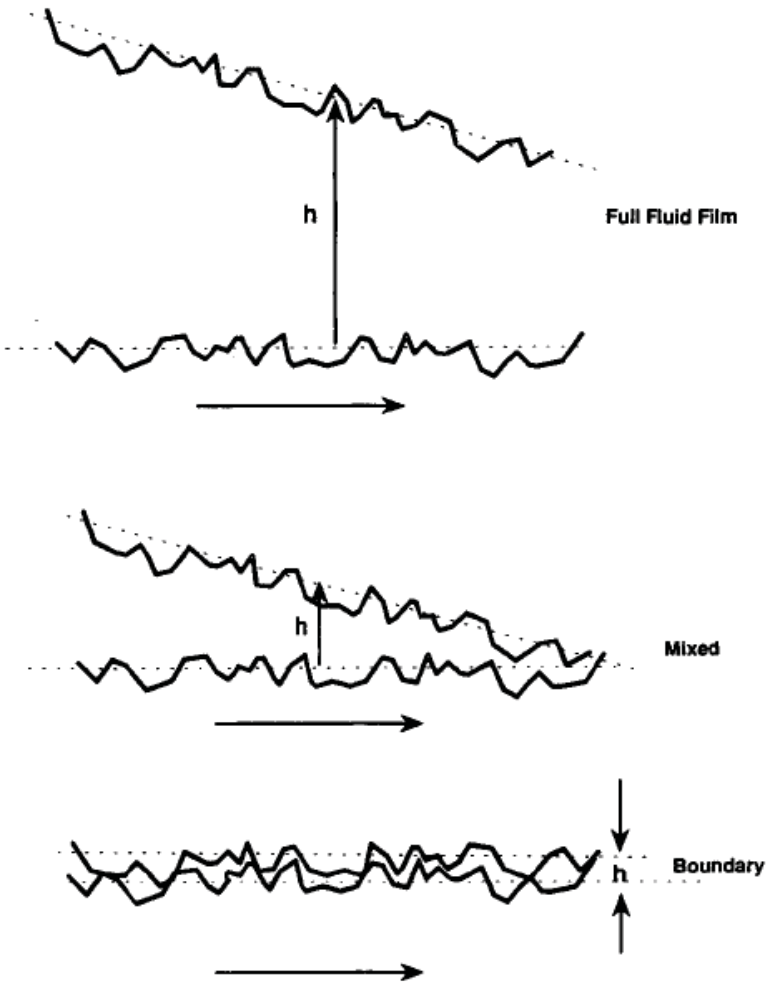

Figure 15. Lubrication regimes (14).

Each regime represents contacts ranging between lubricated surfaces, and unlubricated surfaces. However, as this thesis is solely assessing solid on solid interface contacts, only those contacts of unlubricated/boundary will be considered.

When two materials are in contact, regardless of how smooth the surface may appear, there is always some surface irregularity. This irregularity will affect the tribology of the materials in contact in various ways, including determining the frictional forces and wear rates. In terms of tribology, both friction and wear have various components and it must be specified which is dominant in each physical situation.

Wear is a complicated subject and may be broken into many different forms, based on the mechanisms that cause material loss. These include, but are not limited to, adhesive, abrasive, and fatigue wear. Unfortunately, these mechanisms are not mutually exclusive and usually many forms of wear are incorporated at the same time. This tendency to have many forms of wear acting at the same time makes it difficult to determine the exact cause of material loss in every application. However, there is usually a dominant form of wear that may be assessed, predicted, or determined, based on the different types of contact, or the characteristics of the wear damage (11-14).

The following sections describe three common forms of wear: abrasion, adhesion, and fatigue. Each of these forms of wear is distinct, yet will likely occur simultaneously and is presented in order of relative wear rates (abrasion producing the fastest wear rate, and fatigue producing the least). Although some mechanisms will cause wear at slower rates, each is important and must be addressed.

2.4.1 Abrasive Wear

Abrasive wear is any form of wear that is initiated by damaging the asperities and/or surface of a material by the contact and loading from particles or asperities of another material. It is caused by either repeated deformation of the material of interest, microcutting, microfracture, or the pull-out of individual grains, and will arise from contact with particles of ≥ 0.8 equal hardness to the material (11). Abrasion is a very common cause of wear, and is responsible in many cases for accelerated wear of industrial equipment. This has led to a large amount of research to determine the mechanisms of wear and to predict their effects in a particular application, in order to

prevent or mitigate those effects. Unfortunately, it is very difficult to predict wear in advance, as it not normally caused by single method, but by many acting in conjunction. However, it has been determined that there are two modes by which abrasion takes place, namely two-body and three-body wear (10-17).

The differing modes of wear are determined by the way that the surfaces pass over each other. In two-body wear (2-body wear), the hard particles that cause the abrasion are held rigidly in a second material as it contacts the primary material's surface. It is unable to move as it contacts or passes through the material, and may be likened to the example of sandpaper on wood or quartz particles held firmly in soil against a shovel. It is likely that 2-body wear will produce long gouges in the material via microcutting or ploughing. Three-body wear (3-body wear) is conducted when the hard particles are trapped between two materials and yet may freely roll or slip as they pass over the material of interest. In this mode, the particles will contact the surface of interest successively and will gradually remove material by repeated contact instead of a series of scratches, as in 2-body wear. Both wear modes are shown schematically in Figure 16 (10-13, 16-18).

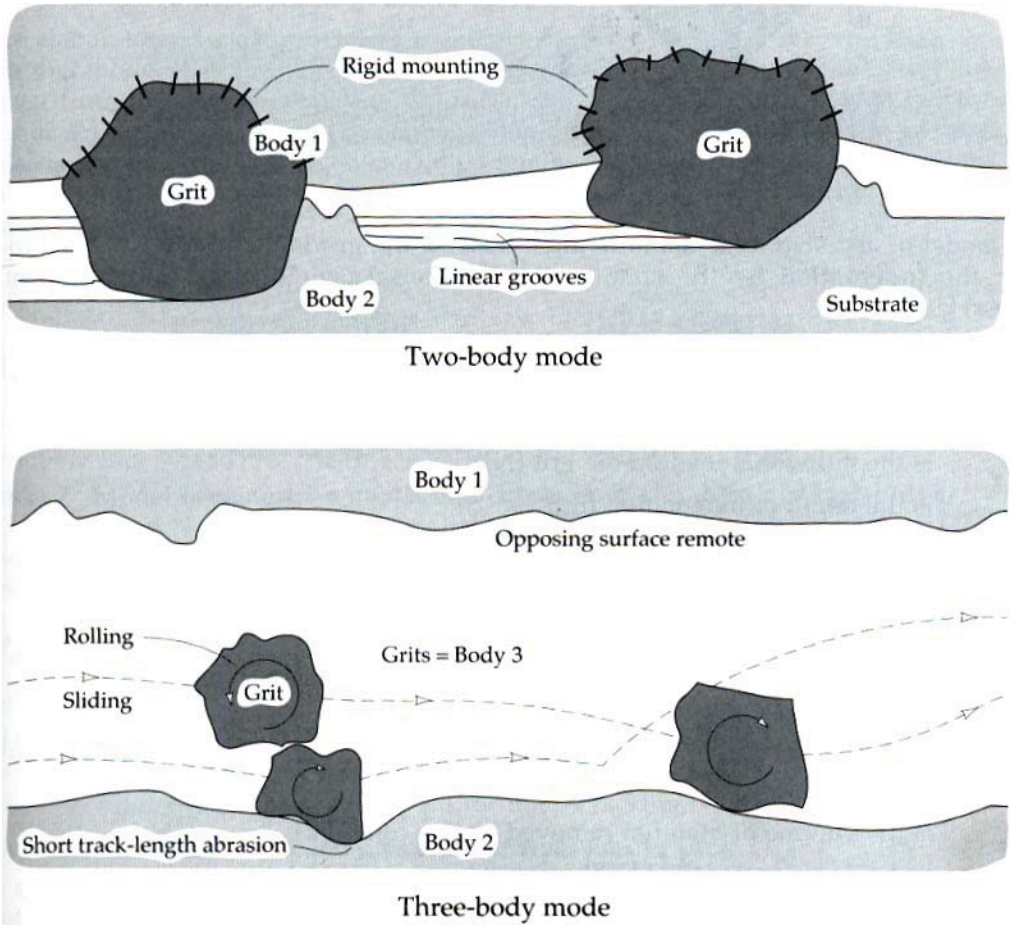

Figure 16. Two-body and three-body wear (11).

Two-body wear is a much more severe mechanism than that of three-body wear, and will result in material loss that is approximately 10 times faster (11). This is believed to be due to the ability of 2-body wear to preform microcutting and ploughing with each particle, rather than requiring repeated impacts and stressing to damage the material. 2-body wear is of special interest as well for many practical applications, such as for cutting tools. In this case, the two materials will be in intimate contact, usually at high velocities, and with high forces, both of which increase the wear rates. Additionally, the cutting tool will be at elevated temperatures due to friction, and as such will usually wear faster since the normal trend is for mechanical properties to decrease as temperatures increase (10-13,16-18).

Both 2-body and 3-body wear appear capable of generating damage that is caused by repeated deformation of the material of interest, microcutting, microfracture, and/or

the pull-out of individual grains. Repeated deformation is the mechanism by where the material is plastically deformed repeatedly by the particles, either by striking the material and work hardening it, or by ploughing/gouging tracks into the surface that displace the material in the trough of the track to the outer edges. In both cases, the material is stressed repeatedly, causing voids to form and cracks to initiate and propagate. The crack then either produces a particle by completely separating a portion of the material from the bulk, or by decreasing the mechanical properties until the next impact will remove the particle. This mechanism is also often termed fatigue wear. Figure 17 demonstrates the trough and lip formed in a Ti(C,N) coating (19). Figure 18 (a), (b), and (c) depict the theoretical representations of the wear tracks caused by ploughing/gouging, respectively (10-13, 16-18).

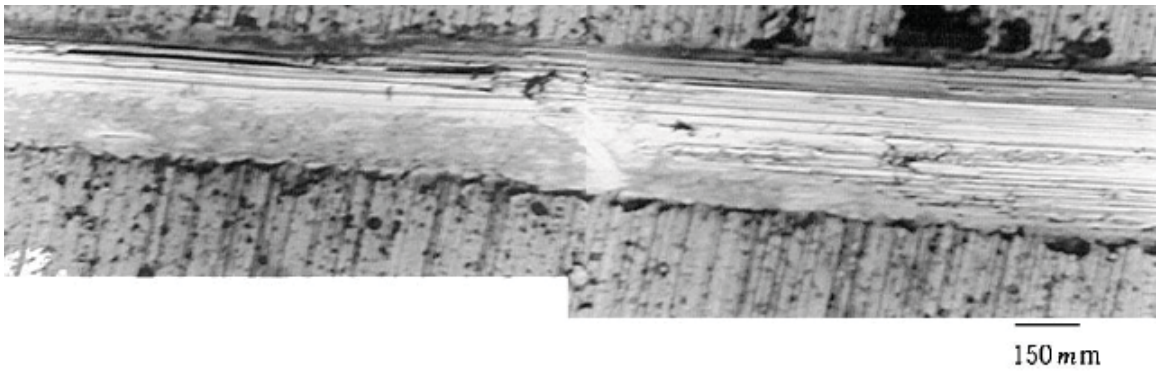

Figure 17. Micrograph showing a wear track cause by a pin on disc contact on Ti(C, N) (19).

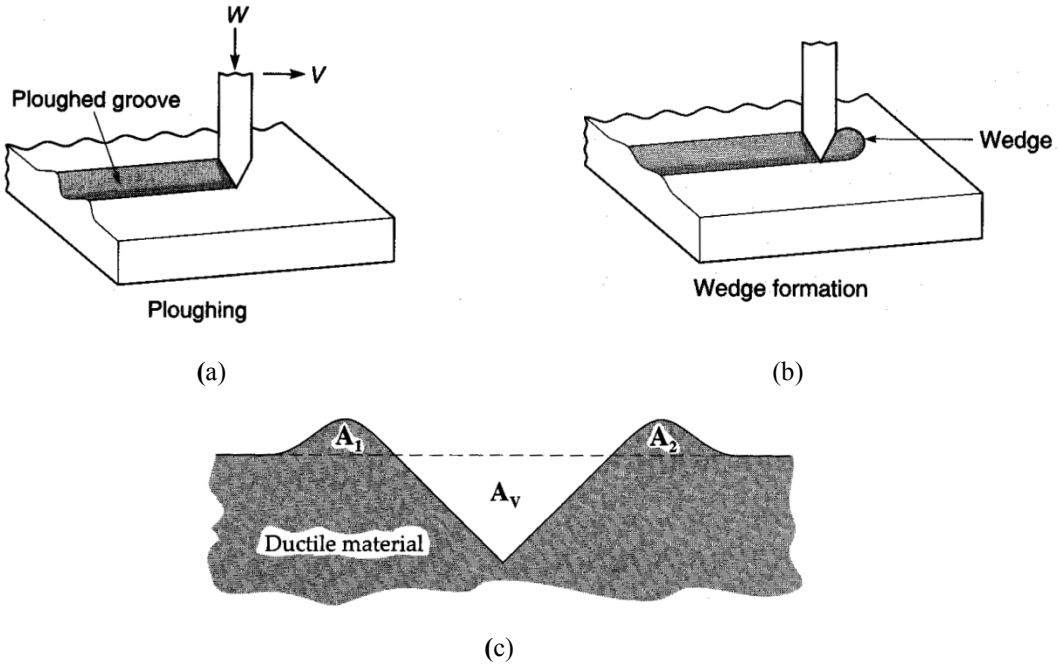

Figure 18. (a) Example of ploughing of a trough in the substrate (12), (b) Formation of a wedge as ploughed material deforms and builds up (12), (c) Formation of edges on ploughed trough (11).

Similar to the ploughing and gouging of fatigue wear, microcutting is where material is removed by the ploughing of a sharp particle through the surface of the material of interest. In the case of microcutting, unlike with the repeated loading scenario, a large portion of the material that is ploughed is removed in the process. The name is derived from the appearance of the gouge and particle that is produced, as they look similar to those produced on a macro scale in industry during the turning of metals by cutting bits. This is an example of extreme and rapid wear, and is not normally present in real world scenarios. Instead, a hybrid of both microcutting and the plastic deformation gouging is most common place. This would produce a wear track where some of the material is removed via microcutting, and the rest is displaced by plastic deformation. A schematic example of a microcutting track, along with a microcutting wear particle, is given in Figure 19 (10-13.16-18).

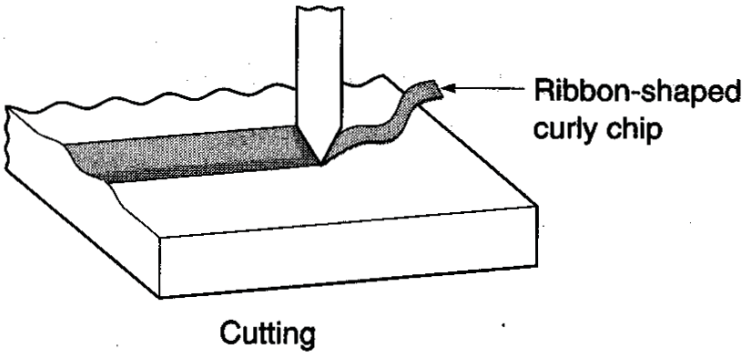

Figure 19. Microcutting wear with a wear particle displayed (12).

Microfracturing is a wear method that produces wear particles by cracking the material of interest in a brittle manner. This normally occurs due to high stresses being applied to the abrasive particles which then transfer those forces to the brittle substrate with their sharp edges. This may occur for ceramics, as well as for metals that form brittle surface layers, such as oxides. As the particles move across the surface of the material, they create cracks which elongate and accumulate as more and more particles contact the surface. These cracks will widen and propagate until particles are released form the material of interest. A schematic representation of the cracking that may be seen is given in Figure 20 (10-13,20,21).

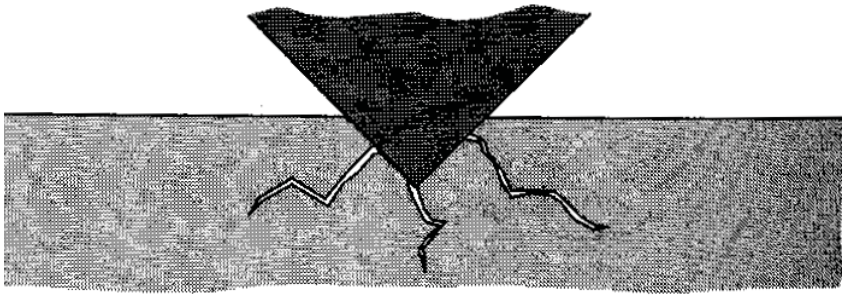

Figure 20. An example of microfracture in brittle materials (11).

The pull-out of individual grains is, as the name implies, where material is removed by the release of individual grains. This would occur when the bonds holding the grains together are weak and may be preferentially disrupted by voids. This would occur instead of crack initiation, taking place on the surface or within the grains themselves. This phenomenon would be more common in ceramics and cermets with

poor adhesion of the binder than it would in metals and polymers. Pull-out will lead to an accelerated wear rate in the presence of large grains, as large amounts of material will be lost with each grain. A schematic representation of this process is given in Figure 21 (10-13,18).

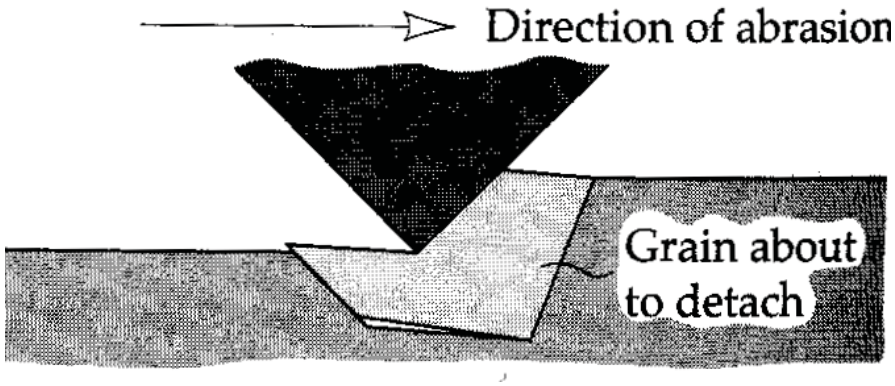

Figure 21. An example of grain pull-out (11).

With the various forms of wear outlined in the previous paragraphs, it is important to know how to prevent abrasive wear. One of the basic methods is to raise the hardness of the material of interest. This method helps to prevent abrasion due to the fact that the particles that are abrading must be approximately ≥ 0.8 than the hardness of the material it is abrading (11). This is a seemingly easy method to prevent wear, but it must be kept in mind that as the hardness increases, the toughness generally decreases. This can then potentially lead to further complications, such as increasing the fracture wear and grain pull-out. As such, a balance must be made between the need for both toughness and hardness in order to control abrasive wear (10-13, 21, 22).

2.4.2 Adhesive Wear

Adhesive wear is any damage to material that occurs due to the adhesion of one material's surface to another. To produce adhesive wear, clean surfaces and close contacts are required. If these conditions are met, the surfaces will adhere to one another, though for varying reasons, depending on whether it is a metal on metal contact, metal on ceramic, or ceramic on ceramic contact. When this occurs, the coefficient of friction tends

to fluctuate while increasing drastically, decreasing mobility and possibly causing the materials to seize (10-13).

When two materials contact one another, it is their asperities that contact, as shown in Figure 14. Provided that nothing intervenes between the two boundaries, metals will form a strong bond by transferring their free electrons from one metal to the other and vice versa, establishing an electron exchange that holds the materials together. If two different metals are adhered, it is theorized that the metal with higher electron density will donate its electrons to the other (11). This is named the "Jellium model". If a metal and a ceramic, or a ceramic and ceramic adhere, it is because of additional reactions that take place between already bonded metal and non-metal ions of one substance to the other. These bonds tend to be weaker than those produced by metal on metal bonding, and as such, the coefficients of friction tend to be lower. However, the bonding forces are strong enough in both cases generally to produce the known phenomenons of asperity junction growth, and the formation of wear particles and transfer films (10-13).

Asperity junction growth is a condition that may occur once asperities have come into contact and adhered under a normal force large enough to plastically deform the asperities. If the bond between the two materials is great enough, the asperities will deform as the materials slide past each other, creating a wider interface over which to distribute both the tangential sliding force and the normal compressive force. It will then require more force to break the bonds between the asperities, and therefore the coefficient of friction will increase. The asperity junction growth along with the redistribution of loads is illustrated schematically in Figure 22 (10-13).

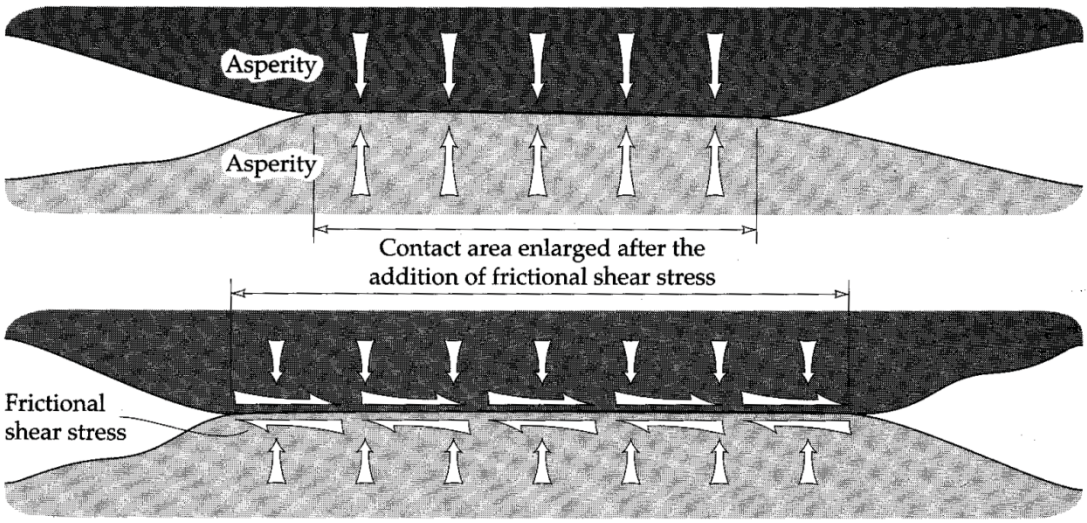

Figure 22. Asperity junction growth as two surfaces in contact move past one another (11).

The formation of wear particles occurs as asperities contact each other during sliding, adhere, and attempt to move past one another. As the two materials in contact are being held together, the asperities cannot simply push over each other, but must essentially move through each other. However, instead of causing abrasion by forcing one asperity through the other, the weaker material forms shear bands that crack once a limiting force is reached. This will create a laminar structured particle that is formed from as many shear bands as were required for there to no longer be an obstruction to motion. This form of wear is more severe for ductile materials, and will deform more, and create greater quantities of wear particles, than brittle materials. This process is illustrated in Figure 23 (10-13, 21, 22).

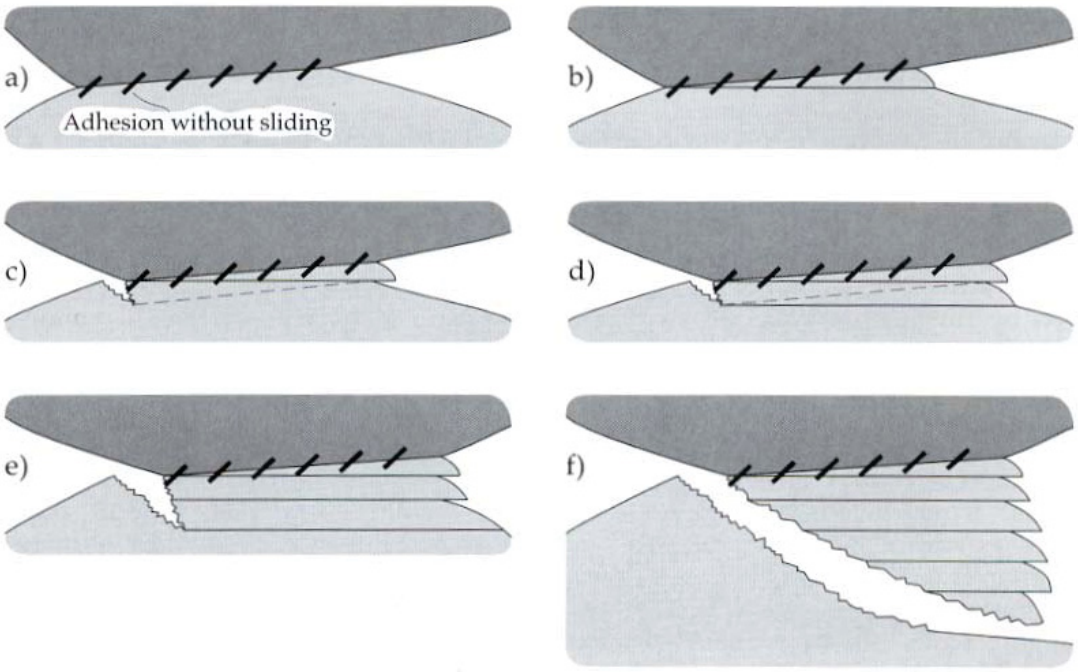

Figure 23. Formation of an adhesive wear particle (11).

Transfer films are, as the name implies, a film of the weaker material that has adhered to the harder material and created a covering film before detaching as a wear particle. The particles that form the transfer films are created via the mechanisms described for the creation of wear particles. However, in this case, the particles remain attached to the surface of the material, and collect. This collection of particles tends to be comprised of wear debris from both materials and will continue to grow, collecting more particles. As it grows, the transfer particle is eventually flattened during sliding and takes on a laminar structure. It is interesting to note that due to the work hardening required to produce the agglomerate of particles, the transfer particles can often be harder than the substrates and may be able to plough through the substrates in a manner similar to that observed in abrasion, except it is much less efficient (10-13, 21, 22).

Due to the complications of seizure, increased friction, transfer particles/films, and extremely high wear rates, adhesion wear should be avoided when possible. Research into how to control adhesion has led to the methods of controlling the sliding surfaces, providing a surface layer that has better adhesion properties, or providing a barrier between the contact surfaces, such as a lubricant. By controlling the sliding surfaces and

choosing the contact materials carefully, the desired adhesion properties may be garnered without any additional processes being required. If this is not possible, forming a surface layer that reduces the adhesion between the materials may also be achieved, such as forming an oxide layer that has poor adhesion qualities as compared to most substrates. Finally, the use of a lubricant may be employed to maintain the distance between surfaces, so as to prevent contact between the materials and stop any adhesion from the beginning (10-13).

2.4.1 Fatigue Wear

Fatigue wear is the loss of material commonly associated with rolling contacts, exemplified with the motion of a bearing, where a surface is repeatedly stressed, eventually forming dislocations that propagate into cracks that will suddenly spall large amounts of material. In this form of wear, it is common to have highly strained surface regions within the material that transition into moderately strained regions where the grains are deformed, so as to be shifted in the direction of sliding due to friction. The strains can build up and produce two different cases of crack propagation (once cases involving lubrication have been eliminated): surface crack initiation, and subsurface crack initiation (10-13).

In surface crack initiation, the cracks nucleate at a defect or weak point at the surface of the material. They then travel down into the bulk following weak planes. The crack may branch into secondary cracks, connect with defects such as voids within the material, or connect with other surface cracks as it propagates through the material until it has reached the surface again. When it has reached the surface, the particle that has become outlined with the crack is released as a wear particle. Due to the deformation of the grains that has already taken place, the cracks tend to propagate more perpendicular to the surface than tangentially, and as such will produce large thin particles. This process is enhanced in materials that are chemically reactive, as the newly exposed crack surface should react quickly and cause a compound to form that will not allow for crack healing due to adhesion to take place. A schematic example of the propagation of a surface initiated crack is given in Figure 24 (10-13, 18, 21, 22).

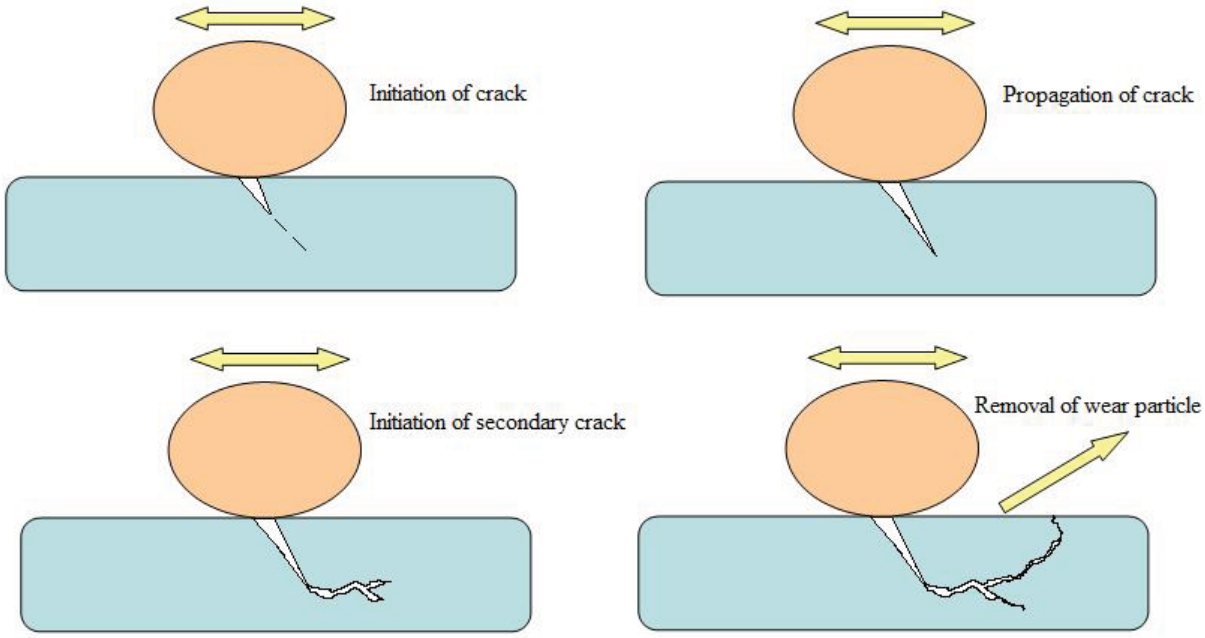

Figure 24. Initiation of surface cracks by fatigue.

In subsurface crack initiation, crack propagation does not initiate at surface defects, but at defects within the bulk, where stress fields are still sufficiently high to promote void formation. The voids form as dislocations pile up in and around defects that promote their growth, such as hard inclusions and holes. The newly formed voids then act to further capture dislocations and grow in size. Due to the triaxial stresses near the surface of the material that inhibited crack growth initially, the cracks that from in the subsurface tend to be confined to grow parallel to the surface and remain below it. However, eventually the crack is able to propagate upwards where it reaches the surface, and allows for a wear particle to be released. This method of producing wear particles has become known as delamination. Since this mechanism is reliant on the presence of inclusions to be initiated, it may be avoided or minimized by using bearing materials that are relatively pure and defect-free. A schematic representation of the propagation of subsurface cracks is shown in Figure 25 (10-13, 18, 21, 22).

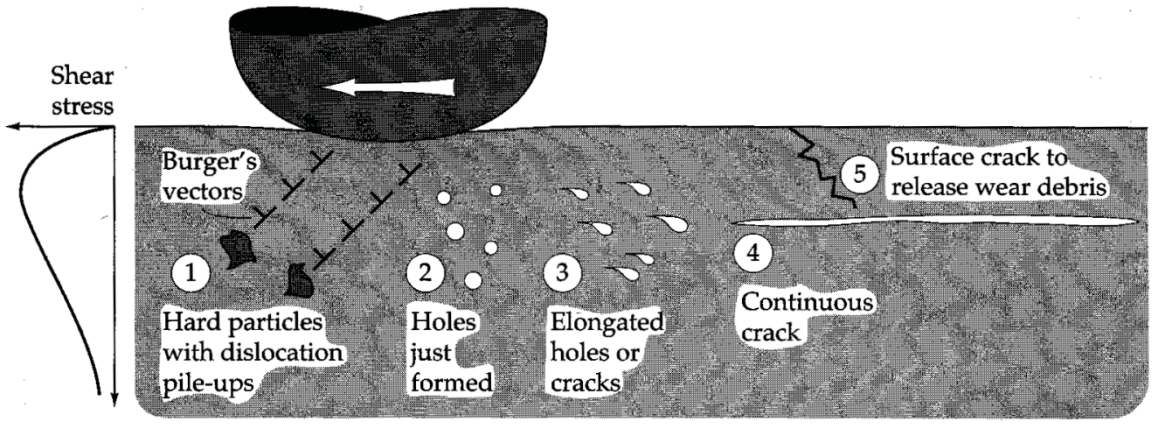

Figure 25. Initiation of subsurface cracks at hard particles (11).

To reduce and/or prevent fatigue wear from occurring, it is important to reduce the friction between sliding materials, increase the hardness, and avoid impurities in the material. By decreasing the friction, the main driving force for fatigue, the stresses caused by deformation during sliding, are reduced. Friction may be reduced in many ways, from applying a lubricant to changing the surface composition or structure of the material, as long as the mechanical properties required for the specific application can be maintained. Increasing the hardness of the material may also help prevent fatigue wear by reducing crack propagation. However, this will also reduce the toughness of the material, which may allow for brittle failure and remove any gain from the increased hardness. Avoiding impurities will ensure that there will be fewer sites for dislocations to migrate to. As such, the dislocations will not pile up in any one area quickly, promoting an increase in fatigue wear resistance (10-13).

2.5 Tribology of Titanium Carbonitride Cermets

The tribological characteristics of titanium carbonitride Ti(C,N) cermets are difficult to predict without thorough testing. When a cermet is being created, it would be optimal to predict the mechanical properties through the use of a simple rule of mixtures. By using the rule of mixtures, the properties of the cermet may potentially be predetermined using a ratio of the properties for each of the constituent parts (according to the mass or volume percent). Unfortunately, this approach tends to only to provide

approximate values to compare with experimental values. The rule of mixtures approach does not accurately predict the outcome when forming cermets, due to the additional concerns that influence the overall behaviour of the composite that are specific to each combination of components, such as wetting, bonding, passivation, chemical reactions, etc.

Fortunately, the mechanical properties of the primary components of Ti(C,N) cermets, the hard ceramic phase, may be estimated via the rules of mixtures. As the solid solution of Ti(C,N) is isomorphous, any amount of carbon or nitrogen may be present in solution and the stoichiometry will remain intact. The information provided in Table 2 and Table 3 give the values that have been obtained for many properties for TiC and TiN, as well as a comparison of generic TiC and Ti(C, N) cermets, respectively. These values allow for the initial estimated values for the presented mechanical properties to be predicted for the hard phase.(2, 7, 15, 23)

The generic term “cermet” has been used to describe the materials in Table 3 because, as previously stated, the properties will vary greatly depending on many factors, including the properties that pertain to wear and tribology. It is still possible however to determine which factors of wear that will be the most prominent under a specific set of tribological conditions. Since Ti(C,N) has high hardness, thermal conductivity and strength, and generally performs well under high wear applications, it has historically been applied as the material for cutting tools. Because of this, although the exact properties that each Ti(C,N) cermet may not be known before testing, it may be assumed that the same forms of wear will be active as in the cases of other cermets in these applications. These include, but are not limited to abrasion, adhesion, and fatigue wear (2, 3, 24).

There are two very distinctive forms of Ti(C,N) cermets that may be differentiated in how they respond to tribological factors, specifically those prepared with Mo_2C additions, and those without. Referring back to Figure 6, the core/rim structure that is formed through the addition of Mo_2C may be observed. Figure 26 provides an image of a Ti(C,N) cermet formed without the core/rim structure. (2, 3, 25-28)

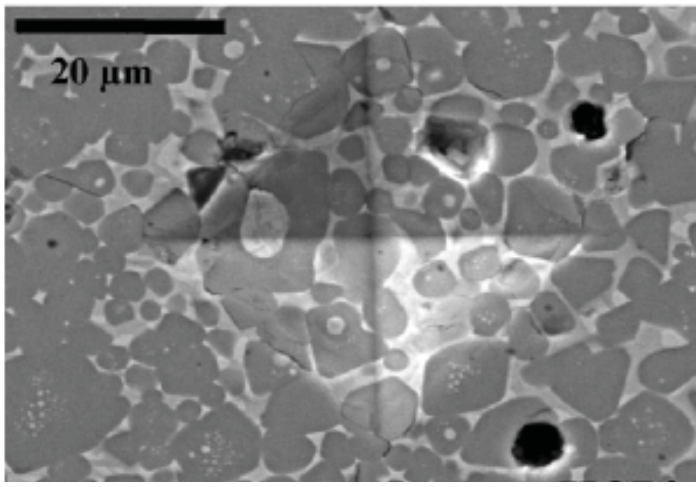

Figure 26. Ti(C, N) cermet without the presence of a Mo_2C derived core/rim structure (29).

The reasoning behind why both microstructures should be treated differently in terms of tribology is due to the effects that the core/rim structure has on the properties of the material. As the core/rim structure forms during sintering, the molybdenum will preferentially form a rim of Mo_2C around the Ti(C,N) core, since it wets extremely well with the binders used with carbides from groups IV_b, V_b, and VI_b of the periodic table, and will dissolve small amounts of titanium. By dissolving the titanium, a chemical bond if formed with the core that, along with the improved wetting with the binder, provides a much stronger bond. This is made evident with the increase of hardness of the cermet. Other benefits provided by this core/rim structure are increased stability of the carbonitride phase, preventing both denitridation and the formation of graphite, and of the retardation of grain growth. These factors tend to produce an increase in the hardness and decrease in the toughness of the material, therefore affecting their tribological response when compared to those without the molybdenum additions. Unfortunately, the limited testing that has been performed to date has included minimal comparison of how the wear mechanisms differ for Ti(C,N) cermets with or without molybdenum additions (2, 3, 25-28).

Abrasion is the wear mechanism of primary concern for Ti(C,N)-based cermets, since their currently most common application in industry is as cutting and finishing tools. It is expected that they should perform well, since they are both hard and tough.

This appears to be the case, as the cermets invariably display the same resilience to direct abrasion from particles as is found with WC-Co alloys (20). Due to the increased particle hardness of Ti(C,N), the abrasive particles in most cases are unable to cut or gouge them and, as such, the bulk material exhibits good abrasion resistance. It is still possible for the binder phase to be preferentially removed by both cutting and gouging. The effectiveness of this wear mechanism would be determined by the bond strength between the hard and soft phase, and the volume ratio of the binder to the hard phase. If there is a good bond between the soft metallic binder and the high modulus ceramic phase(s), the material will be harder to remove. However, this may prove to be a weakness if the bonding is poor. The amount binder volume fraction is an important factor in cermet design because it will change the availability of the binder to be removed. With large amounts of binder, there will be a greater chance for the abrasive particles to contact the soft phase and remove it, while the reverse is true for a low binder fraction.

It has been found that despite the abrasion resistance of Ti(C,N) cermets, deterioration by microfractures, fatigue based abrasion and grain pull-out can still occur. Microfractures are caused when there is a high loading placed onto the abrasive particles, which then allows them to transmit an amplified stress through their sharp contact points as the particles pass over/contact the Ti(C,N) grains. As such the grains may fracture, allowing for cracks to propagate in a brittle manner through the material; this process will eventually cause material loss, as noted earlier. The eventual release of particles from the continuous loading will also cause fatigue wear. This may occur in an intergranular manner, as the microfractures expand over time, or following a transgranular route along the binder phase. Fatigue could then occur in the binding phase as it is contacted repeatedly by particles and work hardened, eventually leading to material loss. This, combined with microcutting and gouging, may lead to the greatly accelerated wear mechanism of grain pull-out. Initially grain pull-out is very difficult to perform on a flat surface, as there would not be enough of a defect to allow a particle sufficient leverage to remove a grain. However, once sufficient bindier phase has been removed, or a large enough intergranular defect has been created, particles may strike the edges of the grain and pull them out. This will increase wear within that region due to the large defect that has now been created. Fortunately, these wear processes do not occur rapidly, and

therefore they allow Ti(C,N) cermets to retain their wear resistances for extended periods of time (11-13, 18-22).

Adhesion wear, in addition to the mechanisms that normally cause wear, may have an additional mechanism present that acts in a slightly different manner than has been previously described for Ti(C,N) cermets. Due to the increased mechanical properties of the Ti(C,N) hard phase, Ti(C,N)-based cermets are generally placed into applications of high stress. The high stresses and increased temperatures that result from the general applications of Ti(C,N) cermets, for example when used as high-speed cutting tools, allows for the binder to soften and be forced out from between the hard phase particles. When this occurs, the extruded binder may be more readily worn and hence removed from the surface. This may cause transfer particles or a transfer film to form. This problem may be compounded as hard phase particles are also potentially removed due to adhesion when the transfer particles are removed. This may cause a much higher wear rate in Ti(C,N) cermets than may have been predicted otherwise (16, 21).

Fatigue wear may also be expected to affect Ti(C,N)-based cermets, as described previously. It has been shown that there is a tendency for the fatigue wear mechanism to initiate subsurface cracks. This is indicated by the delamination of whole grains, as is shown in Figure 27. This form of fatigue wear differs from the fatigue caused by abrasion in that the surface cracks may not be initiated first, and may in fact not be witnessed until the crack has propagated to the extent to allow delamination. Increasing the hardness of the cermet will help prevent this form of fatigue by helping to limit crack propagation, but will reduce the toughness (one of the main advantages of a cermet over a monolithic ceramic). This increase of hardness may be accomplished by using a hard metal for the binding phase, such as molybdenum. (10-13, 18, 19, 21, 22)

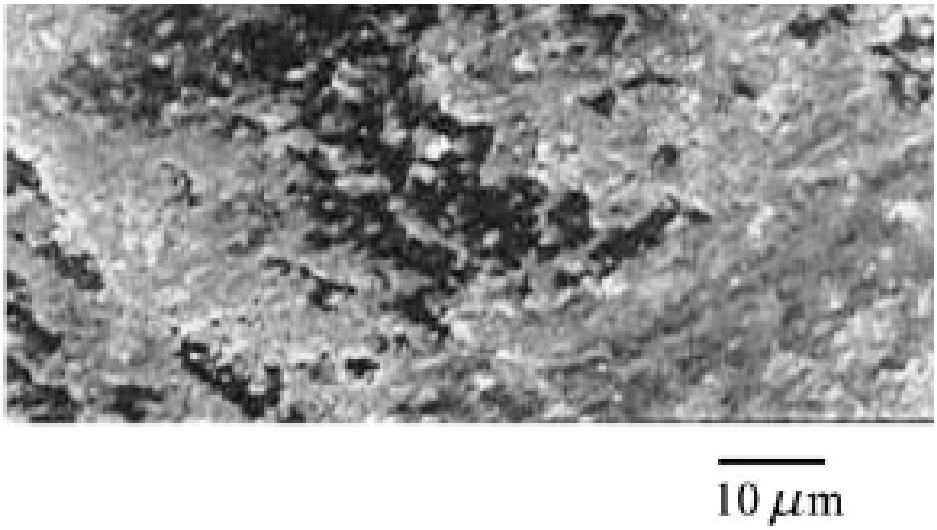

Figure 27. Image taken with a scanning electron microscope of a delamination wear track (19).

2.6 Profilometry

When testing tribological properties of advanced materials, such as cermets, or when performing tests with low amounts of wear, such is common in fretting wear, mass loss measurements, the standard method for the quantification of wear, may become no longer viable. This is due to the limitations of balances which tend to be accurate to the fifth or sixth decimal place, but with maximum loads of up to 100 g (30, 31, 32). With mass losses much smaller than the total loads, close to 10^{-6} of the maximum load, scales will not have a resolution great enough to distinguish between the mass loss and environmental factors, the entrainment of wear debris, and other minute errors. One method to overcome these difficulties is optical profilometry.

Optical profilometry is a non-destructive, non-contact method by which the profile of a surface may be analysed (33). This may be accomplished through several methods detailed in Table 8. Of the devices listed in Table 8, only the stylus profiler contacts the sample, and is included as a common substitute to optical profilometry. Otherwise, the profilometers detail the surface samples using the reflection of light and its diffraction (33, 34).

Table 8. Types of surface measurement devices (30).

Types of surface measurement devices	Stylus profiler	Confocal microscope	Interferometer, laser 3D, white light interferometer
Invasive/not invasive	Invasive but commonly non destructive	Non invasive	Non invasive
Acquisition domain	2D and 3D	3D	3D
Operational mechanism	Contacting tip	Focal plane	Interference of light waves
Resolution	1 nm vertical	10 nm horizontal, 100 nm horizontal	0.1 nm vertical, 500 nm horizontal

As with all measuring techniques, there are inherent flaws and difficulties with this analysis. One primary difficulty is that of surface scattering. Surface scattering induces error by deflecting light away from the sensor, causing areas to either not be imaged or to distort the returned result (33, 34). However, the optical profilometry is still capable of imaging the surface of a sample to a resolution up to 0.1 nm (30, 31). This is done by splitting a beam of light, causing one to strike the surface of the sample and the other to strike an extremely flat reference surface. The beams are then recombined as the light returns to the sensor. The topography of the surface is then determined by the interference induced by the differences in the returning light beams, and measuring the difference in the wavelengths of light.

One drawback to this method is the horizontal resolution of the profilometer. In order to image the surface in a vertical resolution of such accuracy, the focal point that is imaged must be very fine. This links the maximum depth that is possible to be scanned to the maximum area (30, 31, 32). As such, these imaging methods require large quantities of time to be completed. In order to increase the scan rate, the resolution must be decreased. This produces a situation where the accuracy of each test must be weighed against the practicality of test length, especially for large surfaces.

Chapter 3: Materials and Methods

The following chapter is an overview of the materials and experimental methods used throughout this thesis. Only the pertinent properties of the powders used (TiC, Ti($C_{0.7}$,$N_{0.3}$), Ti($C_{0.5}$,$N_{0.5}$), Ti($C_{0.3}$,$N_{0.7}$), and polyvinyl butyral (PVB)) will be presented. The subsequent section will detail sample preparation from milling to polishing. The final section describes the reciprocating test parameters and the analysis of the wear tracks. Analysis is performed using optical profilometry and SEM/EDS. It may be noted that some repetition is present from the papers presented in later chapters. This is unavoidable, as some sections are presented within the papers, but not with the level of detail described here.

3.1 Materials

All powders used throughout testing were commercially attained and will be discussed within this section.

3.1.1 Titanium Carbide and Titanium Carbonitride

Throughout testing, TiC, Ti($C_{0.7}$,$N_{0.3}$), Ti($C_{0.5}$,$N_{0.5}$),and Ti($C_{0.3}$,$N_{0.7}$) were used as the base materials of all samples created. The TiC powders (Lot #PL20125339) were sourced from Pacific Particulate Materials (Vancouver, BC, Canada) while the Ti ($C_{0.7}$,$N_{0.3}$) (Lot #L25809), Ti ($C_{0.5}$,$N_{0.5}$) (Lot #L29865), and Ti ($C_{0.3}$,$N_{0.7}$) (Lot #L25747) powders were attained from Treibacher Industrie AG (Althofen, Austria). Table 9 displays the particle size and densities of each of the powders. Table 10 provide the as received chemical composition for each of the feed powders. The particle sizes, densities and chemical analyses were provided by the manufacturers. The particle sizing for the as received powders were confirmed through the use of SEM. The original feed powders are displayed in Figure 28 in order of increasing nitrogen content from (a) to (d) (TiC to Ti ($C_{0.3}$,$N_{0.7}$)). It may be noted that the particle size distribution for TiC in Figure 28 (a) is much larger than that for the Ti(C,N) powders.

Table 9. Basic properties of TiC and Ti(C,N) powders as provided by the manufacturers.

	Particle Size Before Sintering (µm)	**Density (g/cm^3)**
TiC	1.25 ± 0.53	4.92
$Ti(C_{0.7},N_{0.3})$	2.10 ± 0.57	5.01
$Ti(C_{0.5},N_{0.5})$	1.74 ± 0.49	5.07
$Ti(C_{0.3},N_{0.7})$	1.72 ± 0.49	5.13

Table 10. Compositions of ceramic feed powders, provided by manufacturers.

	Composition (Weight %)								
	Al	Free C	Total C	Ca	Fe	N	O	S	Ti
TiC	-	0.12	19.51	-	0.06	0.05	0.39	-	79.87
$Ti(C_{0.7},N_{0.3})$	< 0.01	0.21	13.28	< 0.01	< 0.03	7.50	0.27	< 0.01	78.68
$Ti(C_{0.5},N_{0.5})$	< 0.01	0.17	10.43	< 0.01	< 0.03	10.89	0.22	< 0.01	78.23
$Ti(C_{0.3},N_{0.7})$	< 0.01	0.02	6.31	< 0.01	< 0.03	15.53	0.37	< 0.01	77.71

(a)

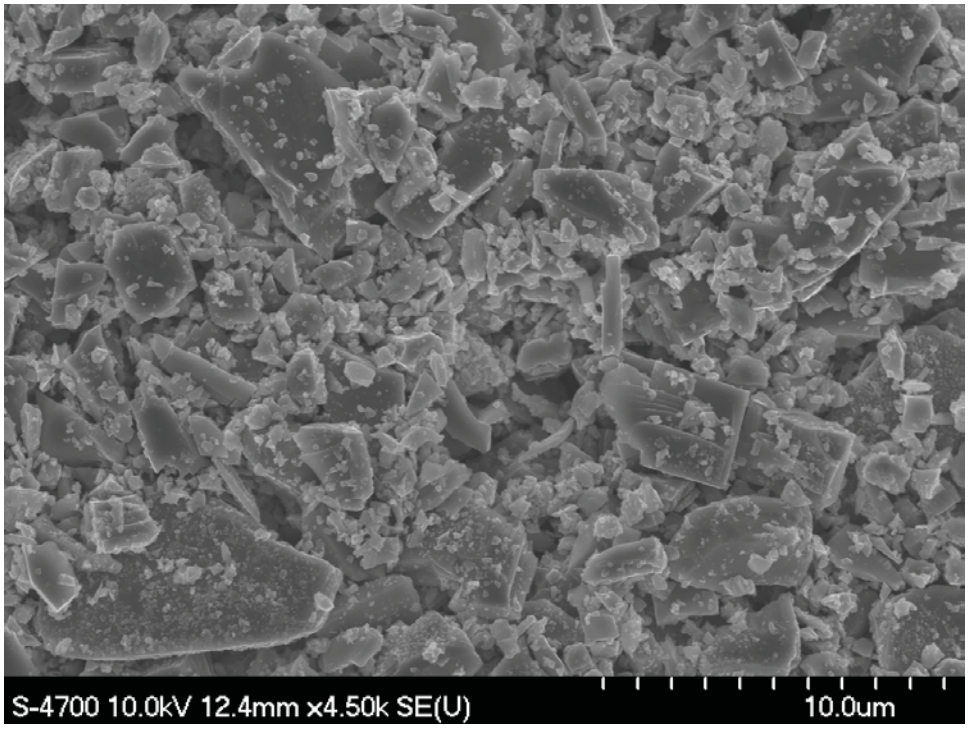

(b)

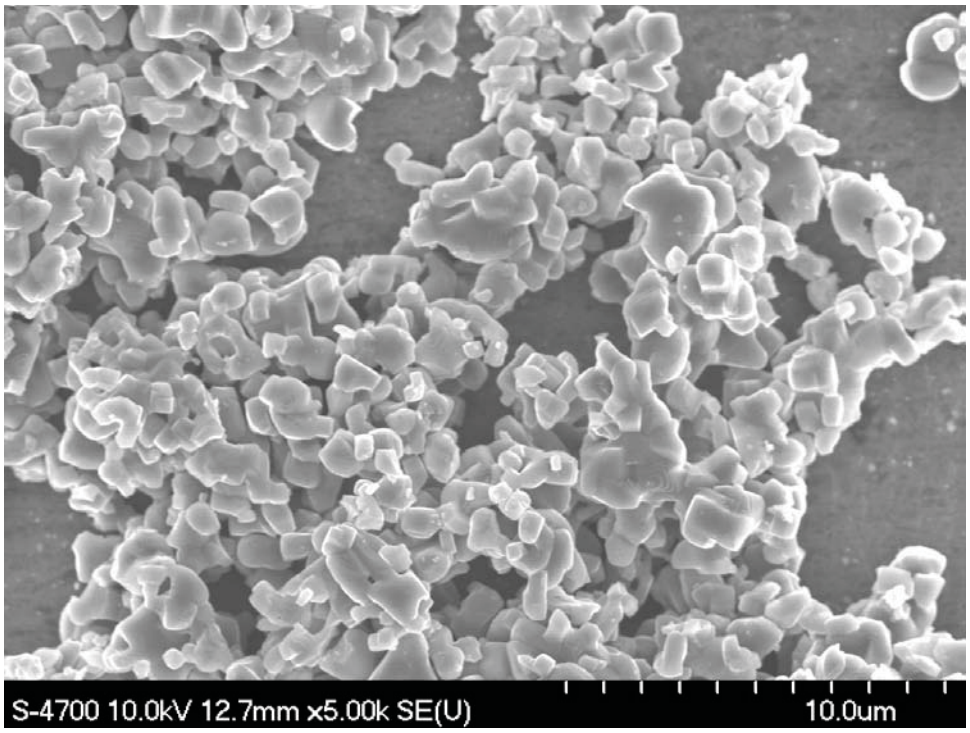
S-4700 10.0kV 12.7mm x5.00k SE(U)
10.0um

(c)

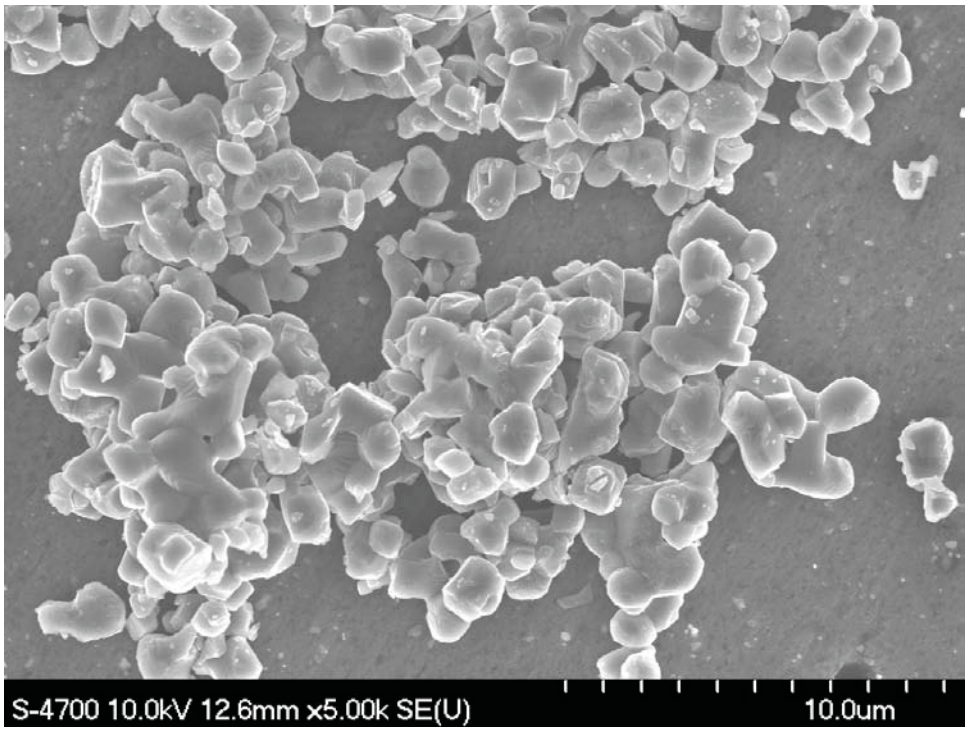
S-4700 10.0kV 12.6mm x5.00k SE(U)
10.0um

(d)

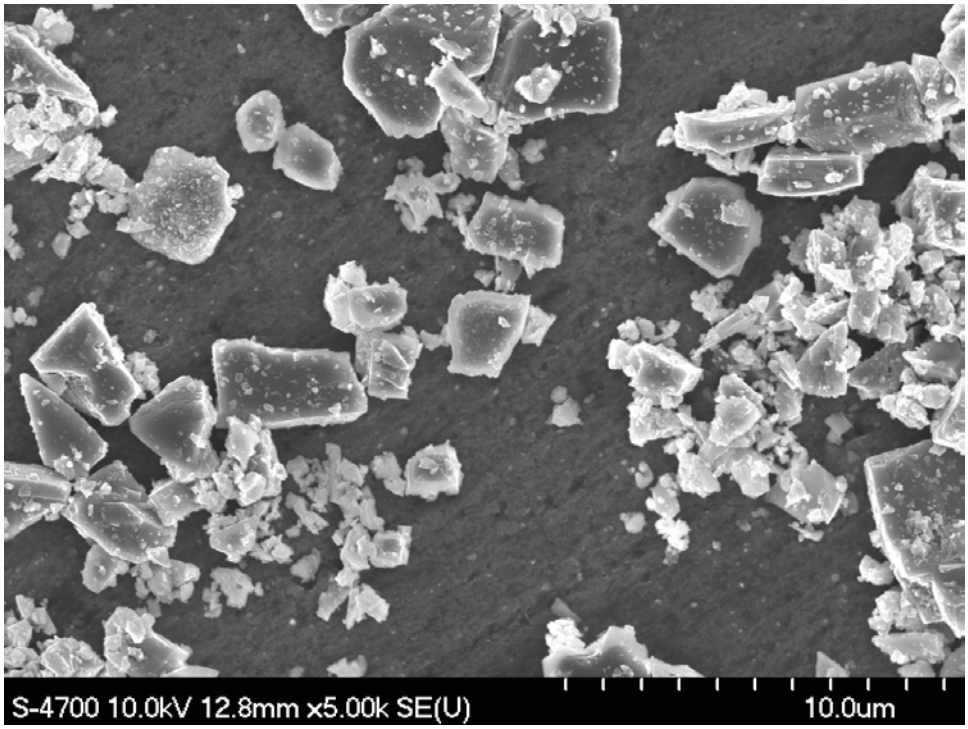

Figure 28. The as received ceramic powders, in order of increasing N content: (a) TiC, (b) $Ti(C_{0.7},N_{0.3})$, (c) $Ti(C_{0.5},N_{0.5})$,and (d) $Ti(C_{0.3},N_{0.7})$.

3.1.2 Nickel Aluminide

Nickel aluminide (Ni_3Al) IC-50 powder (Lot #0412399) was supplied by Ametek Specialty Metal Products (Eighty Four, PA, USA). It is an intermetallic compound formed from nickel and aluminum which has an FCC crystallographic structure. It is known to be ductile and able to retain its strength at increased temperatures, with the yield strength increasing with increasing temperature to a temperature of ~900°C. Table 11 summarizes the basic properties of Ni_3Al. Table 12 displays the alloy composition of the commercially obtained IC-50 Ni_3Al alloy.

Table 11. Basic properties of Ni_3Al.

	Young's Modulus (GPa)	**Yield Strength (MPa)**	**Particle Size (µm)**	**Density (g/cm^3)**
Ni_3Al	179	855	≤ 44	7.6

Table 12. Composition of commercially obtained Ni_3Al IC50 alloy.

	Composition (Weight %)			
	Ni	Al	Zr	B
Ni_3Al	76.9	22.5	0.5	0.1

3.1.3 Compaction Binders

Due to the poor compaction properties, preforms of Ti(C,N) could not be formed without the aid of a binder. In order to create a preform that could survive compaction, 1 wt. % wax binder was to be added to the powders through a ball milling process, described in the next section. It was desirable for the wax to fully dissolve in the milling fluid (200 ml of acetone or 2-propanol). To determine the most applicable wax, a series of solubility tests were conducted using 0.5 g of potential binder agent (polyethylene glycol (PEG 4000 and PEG 10000) from Alfa Aesar (Shore Road, Heysham, Lancs. UK), polyvinyl butyral (PVB) from Solutia Inc., (St. Louis, MO, USA), Poly wax and E2020-T60 from Baker Hughes (Gulf Canada Square, Calgary, AB, Canada), ACumist A-18 from Honeywell (Morristown, NJ, USA), Aqua Poly 215 or MPP-611, from Micro Powders Inc. (Tarrytown, NY, USA)) in 10 ml of solvent. The mixtures were milled and left for 24 hours (imitating the milling process) and were then decanted into drying trays. As may be seen in Table 13, PVB is the only binder to show consistent appreciable solubility.

Table 13. Wax binder solubilities.

	2-Propanol (g)	Acetone (g)
PEG 4000	0.0000	0.0001
PEG 10000	0.0000	0.0000
PVB	0.0357	0.0190
Polywax	0.0000	0.0001
E2020-T60	0.0000	0.0000
ACumist A-18	0.0003	0.0006
Aqua Poly 215	0.0101	0.0006
MPP-611	0.0001	0.0002

Though PVB is more soluble in 2-propanol, the acetone dries appreciably faster, producing a much finer coating along with a fine powder on the drying tray. This was compared to the larger (similar to the initial commercial powder) particles produced with 2-propanol. As such, both PVB and acetone were chosen as the binder and milling fluid, respectively, so as to produce a finer coating. Sieving is conducted after comminution to remove any agglomerates using a 140 mesh stainless steel seive.

3.2 Experimental Procedure

The following section details the methods used to produce the samples and analyse the wear of the cermets.

3.2.1 Sample Preparation

The preparation of tribological testing samples is a multistep process. The following steps outline a breakdown of the process in the simplest form:

- Powder preparation
- Uniaxial pressing
- Isostatic pressing
- Melt infiltration
- Grinding and polishing

The Ti(C,N) powders, as received from the manufacturers, had poor compaction properties, and had to be treated first to allow uniaxial compaction. To prepare the powder mixtures, 54.45 g of Ti(C,N) was combined with 0.55 g of polyvinyl butyral (PVB) binder, ~500 g of tetragonal zirconia polycystal media (TZP or t-ZrO_2) milling media, and ~200 ml of acetone in a 500 ml polypropylene bottle. This mixture is ball milled for 24 hours at 40 rpm, and then poured into a drying pan so that the solvent is allowed to evaporate. After a minimum of 24 hrs of drying time, the powder/wax cake is removed from the pan, broken up using a mortar and pestle, and is then sieved to less than 140 mesh. The powder is now ready for compaction. Due to their better compaction response, the TiC powders do not require this preparation, and no PVB binder is needed.

Once prepared, the powders are uniaxially compacted using a table top press. The three-piece cylindrical die is lubricated on the die walls using steric acid prior to die assembly and filling. For uniaxial compaction ~7.5g of powder is placed into the die, and 12-14 drops of hexane are added to the powder to aid lubrication. After the powder is levelled, it is then compacted at ~46.8 MPa and held at that pressure for 2 min. After the pressure is released, the sample is removed from the die, vacuum sealed in a double layer of plastic, and is then further compacted using cold isostatic pressing (CIPing). The sample is compressed in the CIP at ~220 MPa, with the pressure held for 3 minutes. Following compaction in the isostatic press, the sample is removed from its packaging, and is ready for the melt-infiltration processing stage.

Prior to melt-infiltration, the dimensions and mass of the samples are measured using callipers and a digital balance, to an accuracy of 10^{-3} mm and 10^{-4} g, respectively. The samples are then loaded into alumina crucibles on top of bubble alumina. Nickel aluminide (Ni_3Al) is then added to the top of the Ti(C,N) or TiC preform to be exactly 20, 30 or 40 vol. % of the ceramic powder content (this determination is based on weight and is accurate to ~5 x 10^{-4} g). Once all the samples are prepared with Ni_3Al, they are placed into a furnace and vacuum sintered at a temperature of 1500°C for 1 hr. The heating and cooling rates used are 10°C/min and 25°C/min, respectively, and a dynamic vacuum of ~20 milliTorr is typically achieved at the sintering temperature. Since Ni_3Al melts at ~1440°C, the alloy is allowed to fully melt and infiltrate the sample during the 1 hr hold,

while the wax binder is burned out completely by ~400°C. Thus, a dense cermet sample is formed.

The samples are attached to cylindrical aluminum sample holders using a cyanoacrylate adhesive. Due to an issue with some samples "cupping" slightly, in terms of their shape retention during sintering (increasingly pronounced as nitrogen content increases), grinding and polishing is required to prepare the samples for testing. This is done using a diamond table grinder to obtain a flat sample, followed by sequentially finer diamond grinding and polishing, from 125 μm pads down to 1/4 μm paste.

3.2.2 Reciprocating Wear Testing

Once polished, the samples are tested using the computer controlled Universal Micro-Tribometer (UMT), Multi-Specimen Test System, Center For Tribology, Campbell, CA, USA, shown in Figure 34 (a). Figure 34 (b) depicts the contact and direction for all of the reciprocating tests. The samples are paired with a WC-Co sphere counter-face (McMaster-Carr) which has a diameter of 6.35 mm. Samples are loaded into the wear chamber and the counter-face is lowered into position directly above the specimen. The sphere is then brought into contact and the load is increased until the applied load is achieved and remains constant for 2 seconds. The wear chamber then begins to oscillate perpendicular to the applied load. For all tests, the frequency (20 Hz), stroke length (5.03 mm), and test length (2 hrs) remain constant. The testing was completed using applied loads of 20, 40, 60, and 80 N for all samples. These parameters were chosen for their ability to produce significant wear (detectable both visually without aid and via mass loss using a 0.00001 g resolution balance, determined by mass loss on the lowest applied wear load).

The optical profilometer was used to examine both the general features of the wear tracks and to determine the volumetric wear amount, using a 130 μm "optical" pen. The profilometer is superior to SEM at examining the whole wear area due to its ability to image the complete wear track at once. The wear tracks may also be examined as pseudo three dimensional images, allowing for a comparison of depths. Using the 130 μm pen, only a total depth of 130 μm may be imaged. As such, the samples must be extremely

flat, nearly planar across the surface, to ensure the whole set of wear tracks (between 11 to 16 mm wide) may be imaged.

Two scan settings, high definition and low definition, were used to analyse the samples. The high definition scan used a single area scan with 2 μm steps (for both x and y directions) to analyse the wear tracks and surrounding surface. Due to the large areas to be analysed, these tests require large quantities of time (18-24 hrs). As such, these scans were only performed on a single sample for each cermet series (the 40 vol. % samples). The low definition scans were conducted using an average of three area scans, with 5 μm steps. Less time is required to complete these scans (~9 hrs), allowing this scan to be completed for every sample, maintaining constant variables for the comparisons. The variation in the measured volume between scan types (low and high resolution) is ± 5.1%. This was deemed as being acceptable as this error is equivalent to that generated by the subjective errors introduced by the user. By re-examining the wear data, the error induced by manually selecting the area to be scanned is consistent with that generated between the high and low definition scans.

Chapter 4: Results and Discussion

The following section presents the experimental data produced yet not examined in the following chapter. This includes the examination of the powder materials via XRD, the determination of the densities of the melt-infiltrated samples, and the EDS analysis. As with Chapter 3, there is some repetition noted within this chapter, as the topics presented are mentioned within the papers presented later. This has been kept to a minimum but is unavoidable as this section presents information not present but utilized in the papers.

4.1 Powder Characterization

Although this study was not concentrated on the characterization of the base materials (TiC, Ti($C_{0.7}$,$N_{0.3}$), Ti($C_{0.5}$,$N_{0.5}$), and Ti($C_{0.3}$,$N_{0.7}$)), the base powders for Ti($C_{0.7}$,$N_{0.3}$), Ti($C_{0.5}$,$N_{0.5}$), and Ti($C_{0.3}$,$N_{0.7}$) were examined through the use of x-ray diffraction (XRD) to confirm their compositions and using SEM to determine particle sizing both before and after sintering. TiC and Ni_3Al were examined more thoroughly in a previous study (35), and as such these tests were not repeated. Figure 29 displays the XRD profiles of the Ti(C,N) powders used in this study. Their patterns have been compared to the peaks from the ICCD database with Ti($C_{0.7}$,$N_{0.3}$) (00-042-1489) and Ti_2CN (01-071-6059) when examining the whole patterns, and the ICCD database of TiC (03-065-8805), Ti($C_{0.7}$,$N_{0.3}$) (00-042-1489), Ti_2CN (01-071-6059), and TiN (03-065-5759) when examining the patterns from angles of 35 to 45 degrees, in Figure 30.

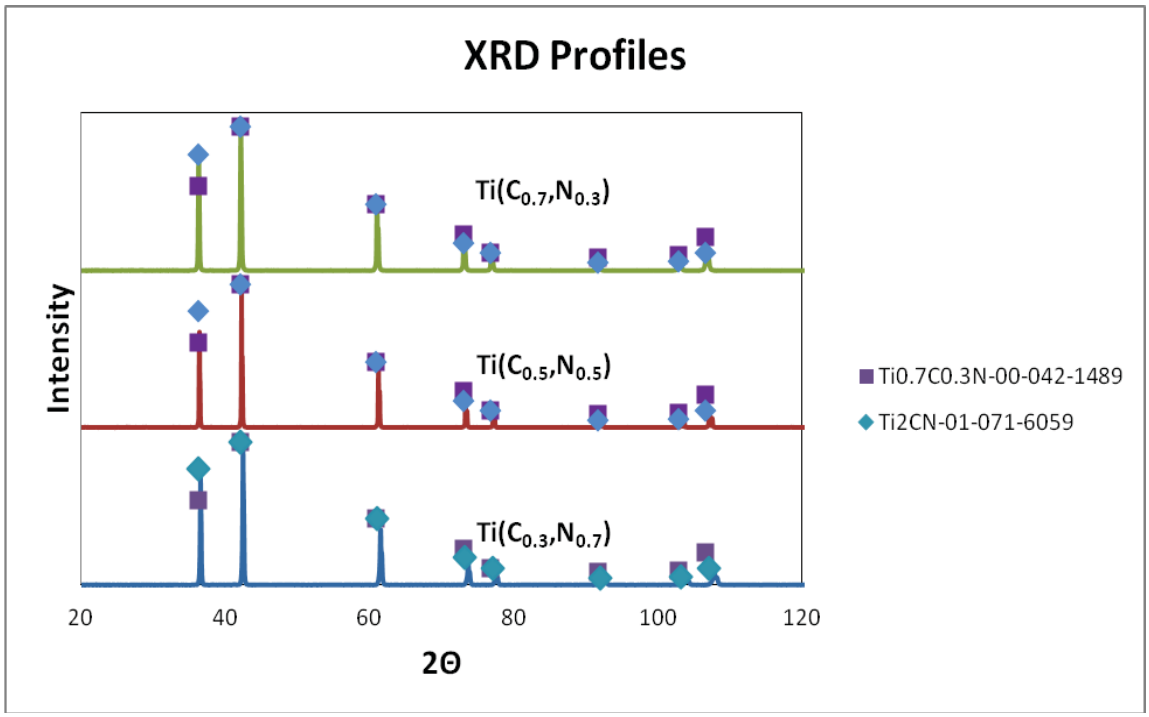

Figure 29. XRD patterns of Ti(C,N) powders.

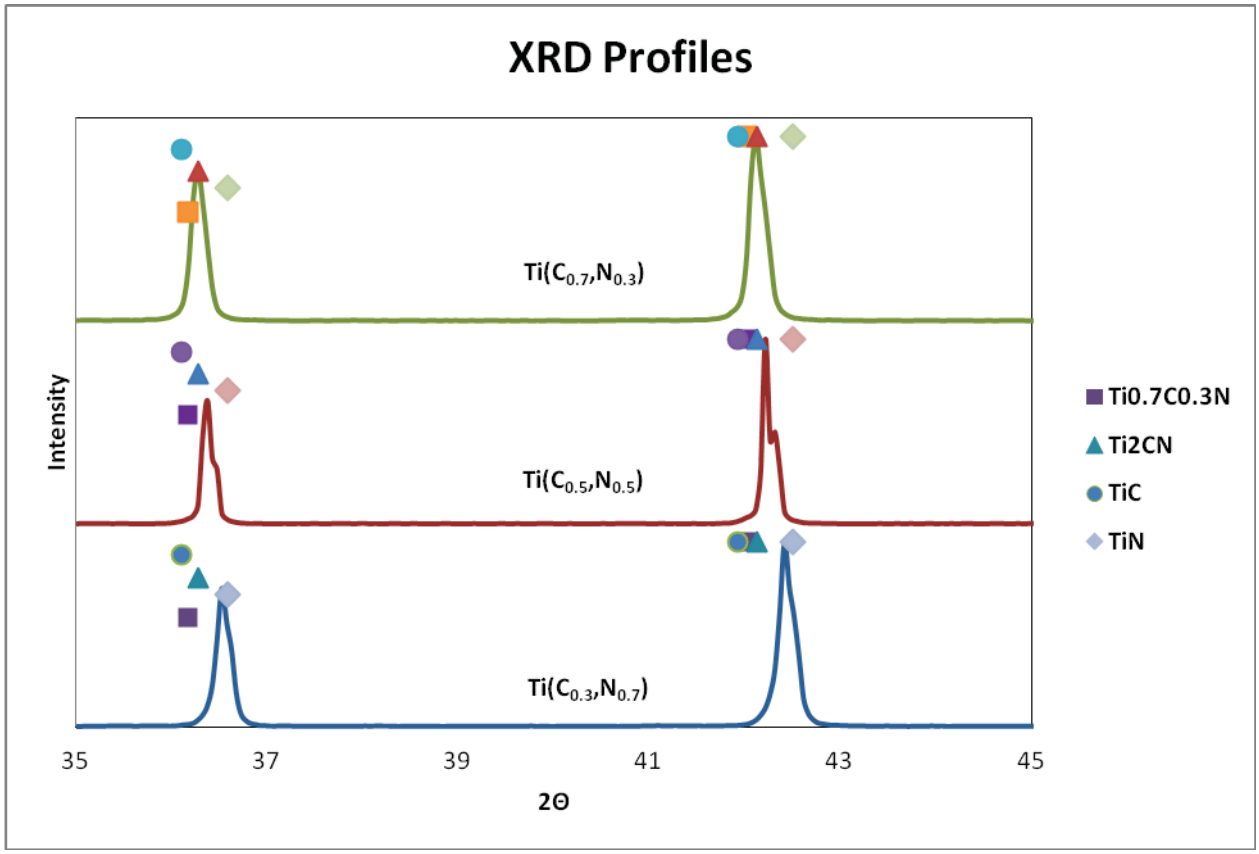

Figure 30. XRD patterns of Ti(C,N) powders from 35-45 degrees.

These results show excellent agreement with the ICCD database. Examining the patterns between the angles of 35 to 45 degrees, it may be seen that the Ti(C,N) powder patterns drift towards the right as the N content is increased. This is to be expected as the crystal structure of the samples are not changing, but are expanding as more N is added. As such, instead of the patterns changing, the patterns drift from behaving like TiC to behaving like TiN. This confirms that the powders received from Treibacher Industrie AG are of the correct crystalline compositions.

Examining the formed samples using SEM, the particle sizing post infiltration were attained using the linear intercept method for all ceramic powders. This was done at 20 vol. % Ni_3Al for TiC to $Ti(C_{0.5},N_{0.5})$ and at 40 vol. % for $Ti(C_{0.3},N_{0.7})$, and is displayed in Table 14. The discrepancy in binder content is due to $Ti(C_{0.3},N_{0.7})$ only being successfully produced at 40 vol. %. An example of the cross section for each finished cermet at 20 vol. % for TiC to $Ti(C_{0.5},N_{0.5})$ and at 40 vol. % for $Ti(C_{0.3},N_{0.7})$ are given in Figure 31 (a) to (d) in order of increasing N content, from TiC to $Ti(C_{0.3},N_{0.7})$.

Table 14. After Infiltration particle size.

	After Infiltration Particle Size (µm)
TiC	3.61 ± 2.07
$Ti(C_{0.7},N_{0.3})$	2.16 ± 0.93
$Ti(C_{0.5},N_{0.5})$	2.07 ± 0.95
$Ti(C_{0.3},N_{0.7})$	2.11 ± 0.90

(a)

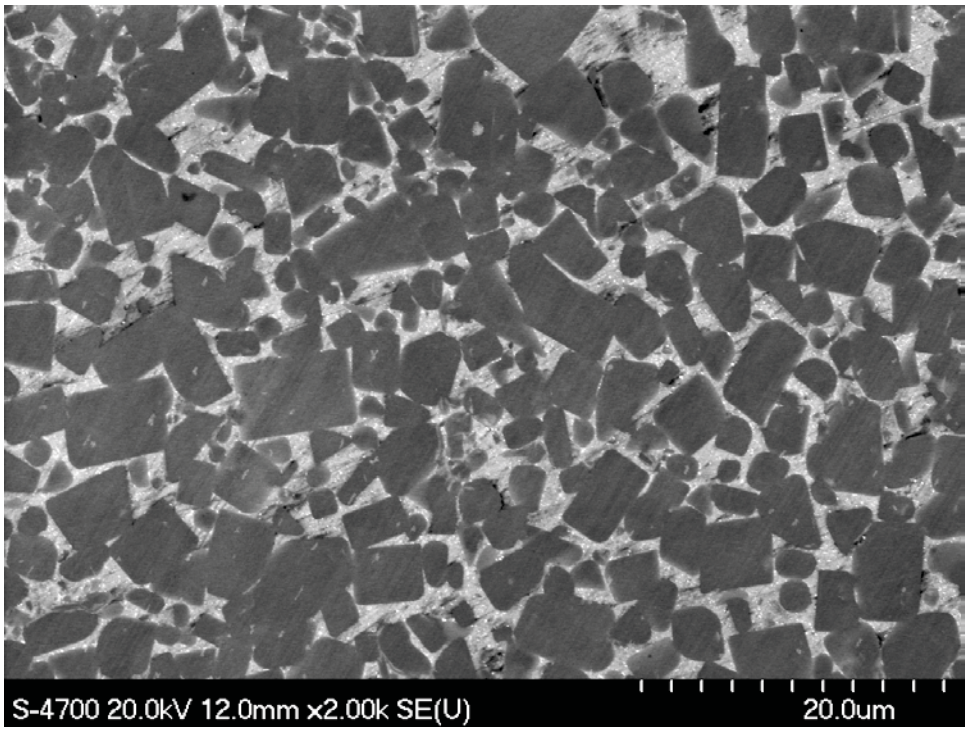
S-4700 20.0kV 12.0mm x2.00k SE(U)
20.0um

(b)

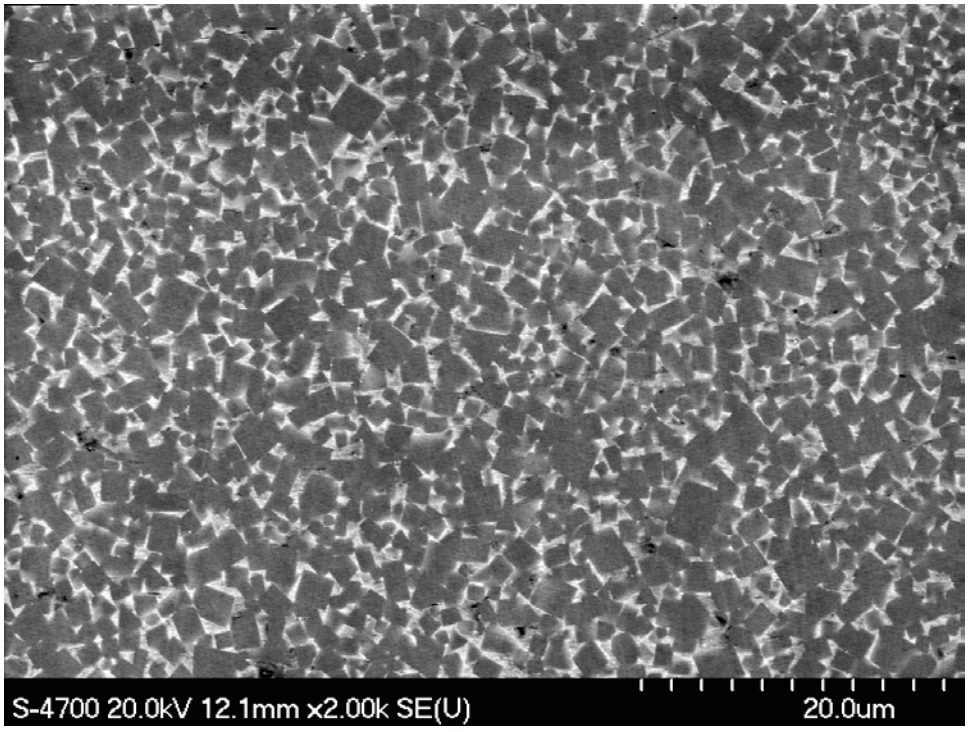
S-4700 20.0kV 12.1mm x2.00k SE(U)
20.0um

(c)

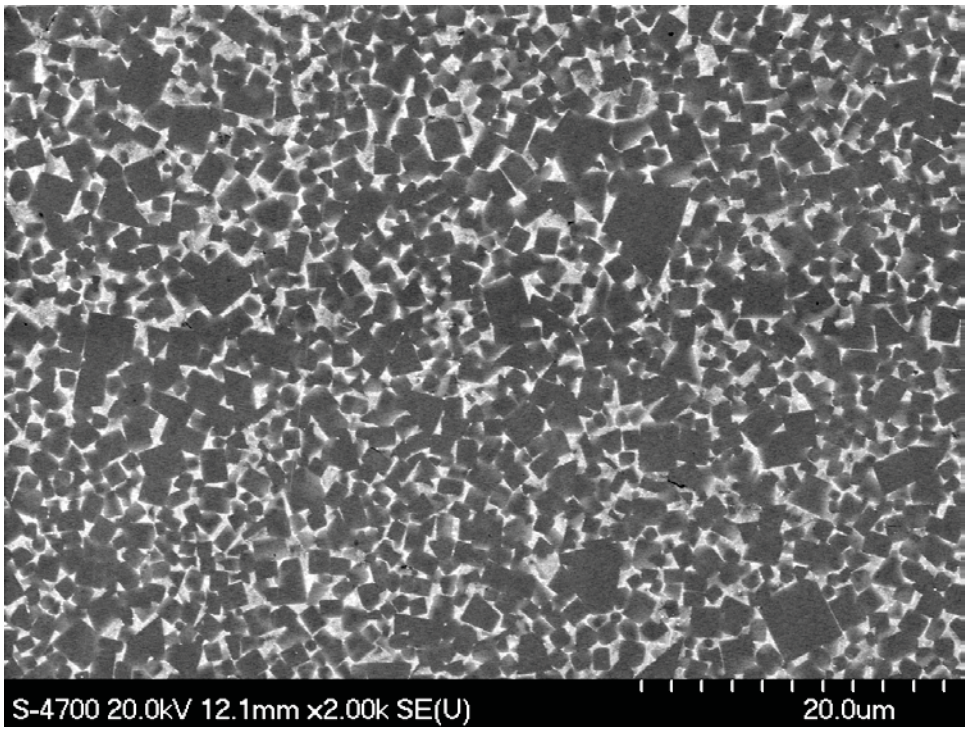

(d)

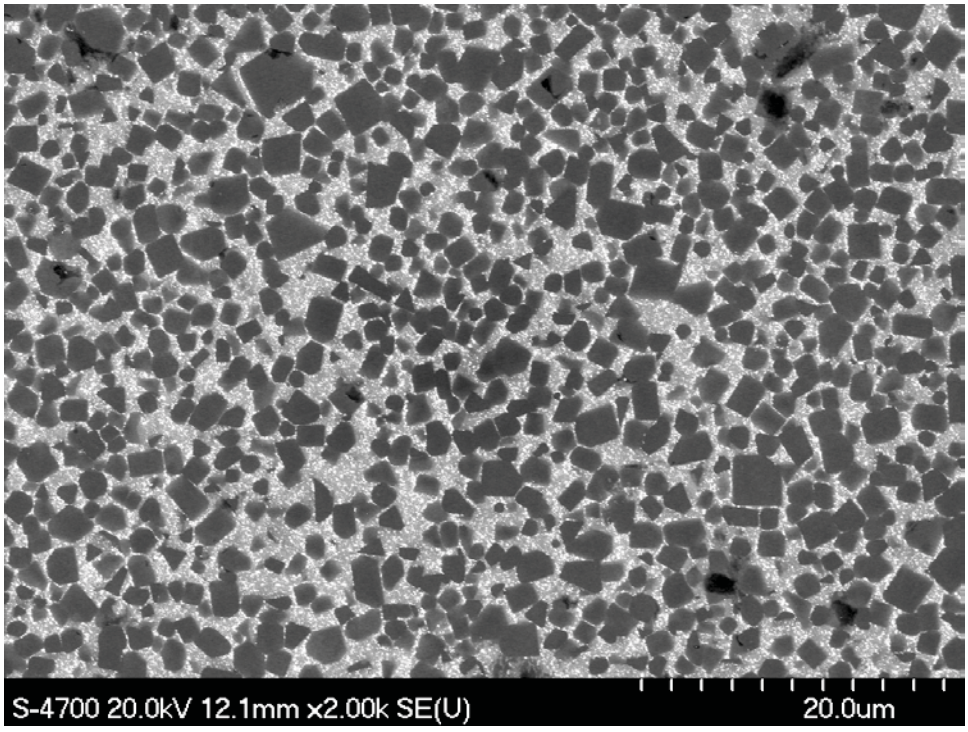

Figure 31. Cross section of finished cermets, in order of increasing N content: (a) TiC, (b) $Ti(C_{0.7},N_{0.3})$, (c) $Ti(C_{0.5},N_{0.5})$,and (d) $Ti(C_{0.3},N_{0.7})$.

4.2 Density Measurements

The sintered densities of all successfully melt-infiltrated samples were measured using the Archimedes principle, through immersion in water at room temperature. Figure 32 displays the average relative densities of each of the successful samples, by binder content.

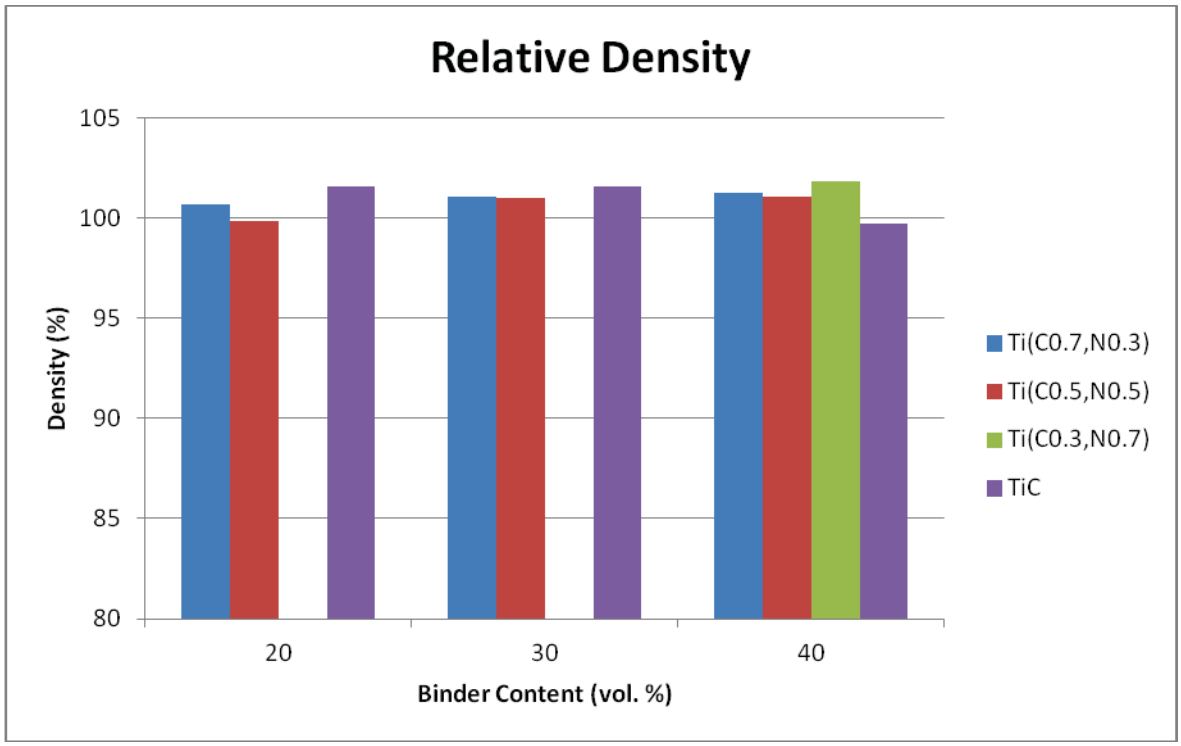

Figure 32. The relative densities of all successfully melt-infiltrated samples.

It may be observed that all densities are in excess of 99 % of theoretical. Additionally, it is clear that an error exists which causes the samples to appear more dense than the theoretical density. It is believed that this trend is due to the fact that the density of the Ni_3Al –IC50 used for experimentation is not of the expected stoichiometry (having greater quantities of Ni and B). As such, the samples appear to be more dense than predicted.

4.3 Energy-dispersive X-ray Spectroscopy

Energy-dispersive x-ray spectroscopy (EDS) is a powerful tool for the examination of samples when conducting SEM. EDS allows for the composition of areas or specific points within an SEM image to be examined and identified. This is a required feature when examining the tribology of a sample as it allows for the identification of various components and the explanation of assorted wear phenomenon. This includes, but is not limited to, the identification of tribolayers, specific wear debris, determination of material transfer to a surface, and oxidation. Table 15 demonstrates the composition of the end of the wear track for TiC-Ni_3Al at 40 vol. % and an applied load of 80 N. Figure 33 displays the SEM image of the end of the wear track and the EDS analysis, depicting the corresponding amounts of Ti, W, and O and their position in the wear track.

Table 15. Composition determined from an area scan of the end of the wear track in TiC-Ni3Al, with 40 vol. % binder and an applied load of 80 N.

Element	App Conc.	Intensity Corrn.	Weight %	Atomic %
C K	17.83	0.4754	7.29	17.03
O K	71.96	0.4841	28.9	50.68
Al K	8.74	0.5714	2.97	3.09
Ti K	109.94	0.8866	24.11	14.12
Ni L	81.64	0.5363	29.6	14.14
W M	23.96	0.6116	7.62	1.16
Totals			100.49	100.22

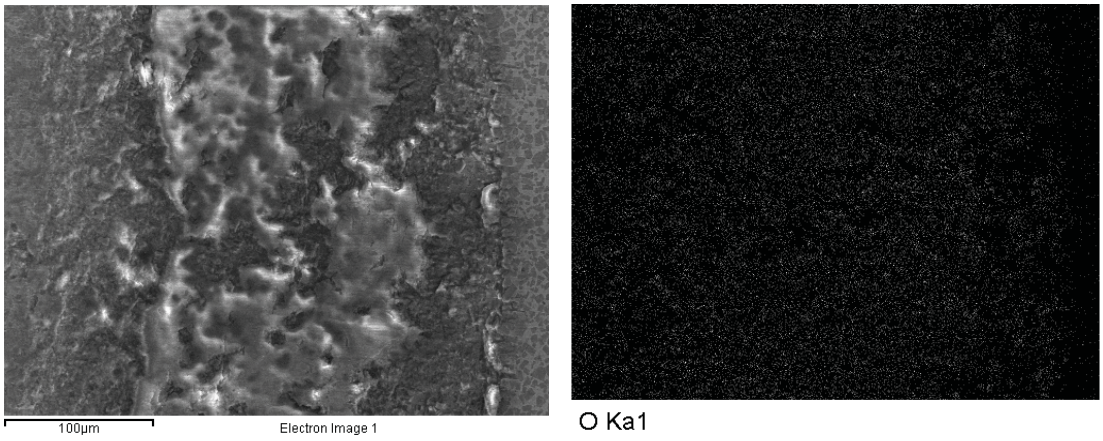

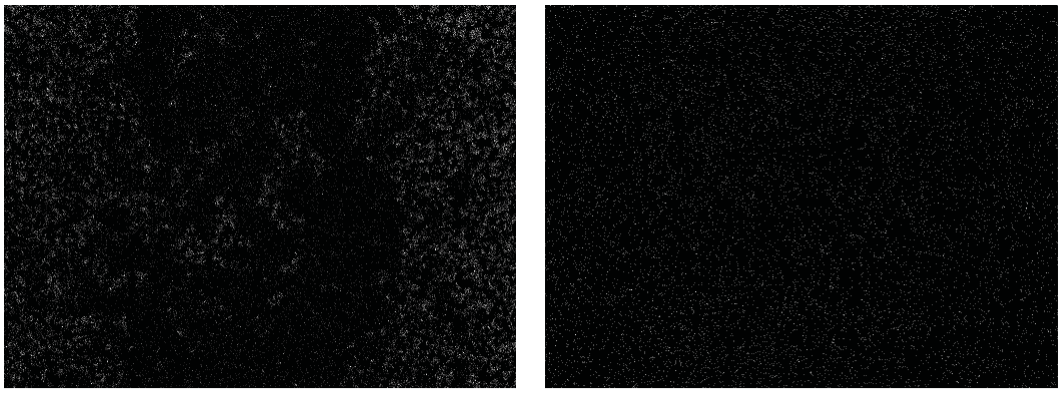

Figure 33. EDS analysis of the end of the wear track for TiC-Ni_3Al at 40 vol. % binder and an applied load of 80N.

This data shows that the tribolayer formed is depleted of titanium, and high in oxygen. Tungsten may be observed as being evenly distributed throughout the wear track. These results, as well as the observations obtained through SEM, optical profilometry, and additional EDS demonstrate that the wear mechanisms are a combination of 2 and 3-body wear, adhesion, and fretting. The evenly distributed particles of W indicate that the counter-face is being worn and that the wear debris is becoming trapped and embedded within the wear track. The large quantities of oxygen indicate the formation of an oxide layer consisting to a large degree of binder (indicated by the depletion of Ti, but high quantities of Ni and O). The wear mechanisms that cause this phenomenon are explained within the papers found in the following sections.

Chapter 5: The Reciprocating Wear Behaviour of TiC-Ni_3Al Cermets

S. Buchholz, Z.N. Farhat, G.J. Kipouros and K.P. Plucknett*
Dalhousie University, Materials Engineering Program, Department of Process Engineering and Applied Science, 1360 Barrington St., Halifax, Nova Scotia, CANADA

5.1 Abstract

TiC-based cermets have become more popular as a replacement to traditional WC-Co 'hardmetals' due to their superior mechanical properties at elevated temperatures, improved corrosion resistance and significantly lower mass. The current study assesses the reciprocating wear response of TiC-Ni_3Al cermets fabricated by melt infiltration, with Ni_3Al binder contents ranging from 20 to 40 vol. %. Wear testing was performed using a ball-on-flat geometry, with a WC-Co sphere used as the counter-face material. It is demonstrated that the cermets are affected by similar wear mechanisms for each of the binder contents, but displayed the lowest wear when prepared with 30 vol. % Ni_3Al. Additionally, the 40 vol. % samples displayed a clear transitional behaviour, with an improved wear resistance comparable to the 30 vol. % samples at low applied loads, but a degraded wear response comparable to the 20 vol. % samples at high applied loads.

5.2 Introduction

Advanced, wear resistant materials have received considerable attention due to their importance in reducing production and maintenance costs in many applications [1-3]. In recent years titanium carbide (TiC) based cermets have become more prominent, due to their improved capabilities when compared to more traditional and widely used tungsten carbide (WC) based'hardmetals', such as those prepared with cobalt binders (WC-Co) [3]. TiC based cermets have several superior properties when compared to those of WC, such as increased hardness and toughness, improved corrosion resistance, as well as a lower mass (the density of WC is ~3 times that of TiC) [4]. These properties, in addition to TiC cermets generally having a lower fabrication cost than WC, could lead to TiC-based cermets replacing WC for many applications.

The desired properties of the cermet are controlled through the addition of metallic binders, including alloys of Ni, Fe, or Co [5-8]. Each alloy will bring specific benefits to the cermet, such as improving the sintering response, increasing toughness, enhancing resistance to corrosion and chemical attack, increasing thermal conductivity, and/or improving thermal shock resistance. Many of these properties may also be customised for use at elevated temperatures, for example by utilising ductile intermetallic alloys such as Ni_3Al (which actually exhibits an increasing yield strength with temperature, up to ~900°C) [6,9,10]. These cermets then offer a further benefit over WC-Co, as that system is known to exhibit poor elevated temperature strength and oxidation resistance [11]. Additionally, other carbides may be added to TiC-based cermets, such as WC, TaC, and Mo_2C so as to improve the sintering behaviour, as well as properties like hardness and/or fracture toughness [12,13]. Although it is often perceived that the presence of additional carbides is indispensible, there can be unwanted side effects, such as the reduced toughness when adding Mo_2C, that have led researchers to look for ways to improve the alloying additions without the addition of carbides [1,12,13].

Generally, cermets are used in applications where their tribological properties are of great importance, such as high-speed cutting tools. As a consequence, considerable research has been conducted within this field to determine how TiC-based cermets withstand various forms of wear and their associated damage mechanisms. Of specific importance are fretting and/or reciprocating wear, as this type of contact motion is very common and can often produce severe wear degradation. Fretting wear occurs in situations where there is low amplitude oscillatory sliding motion between two surfaces in contact [9,13-19]; typically fretting wear is referred to in instances were the sliding displacement is small (i.e. less than 500 μm) [13]. This normally produces damage from both 2 and 3-body wear modes; the surface impinging the test sample both gouges the material and traps the debris between both surfaces. This is a common form of damage for bearings, and is often simulated using a ball-on-flat test. In the present work fretting-type tests were performed, only using a longer sliding distance which is subsequently referred to as reciprocating wear.

5.3 Materials and Methods

5.3.1 Sample Preparation and Characterisation

The TiC-Ni_3Al samples used for wear testing were fabricated using a simple melt-infiltration technique, documented in detail in prior publications [8,20]. The TiC powder (Grade TiC-2012, Pacific Particulate Materials, Vancouver, BC, Canada) had a manufacturer quoted a mean particle size of ~1.3 μm, which was confirmed through subsequent particle size analysis [21]. Pellets were prepared using 7.5 g of TiC, uniaxially compacted at a pressure of ~67 MPa, after which they were bagged and further compacted by cold isostatic pressing at ~220 MPa. For melt-infiltration the samples were weighed, and placed onto a layer of bubble alumina within a closed alumina crucible. A known amount of -325 mesh Ni_3Al powder (Alloy IC-50, Ametek, Eighty Four, PA, USA) was placed onto the TiC samples, corresponding with a desired volume fraction of the metallic binder. The crucibles were placed into a vacuum furnace, which was evacuated to less than 20 milliTorr, heated to 1500°C at a rate of 10ºC/min, and then held at this temperature for 1hr, followed by cooling to room temperature at a nominal rate of

25ºC/min. Typically the furnace maintained a vacuum level of less than 20 milliTorr during the 1 hr hold period. Using this method, samples TiC cernets were fabricated with 20, 30, and 40 volume percent of Ni_3Al.

After sintering the samples were ground flat on one face using a diamond surface grinder. They were then attached to cylindrical aluminum sample holders for polishing, using a cyanoacrylate adhesive and ground and polished through successively finer grades of diamond (starting from a 125 μm diamond pad and finishing with 0.25 μm diamond paste), to achieve a 'mirror-like' surface finish for subsequent evaluation.

The sintered densities of the melt-infiltrated samples were measured following Archimedes' principle, through immersion in water at room temperature. The microstructure of the cermets after melt-infiltration was determined using a field emission scanning electron microscope (SEM; Model S-4700, Hitachi High Technologies, Tokyo, Japan).

The hardness and indentation fracture resistance of the TiC-based cermets was determined using a Vicker's hardness tester with loads of 1 kg and 50 kg, respectively. The indentation fracture resistance was calculated using the approach of developed by Anstis *et al* [22, 23]. The hardness and indentation fracture resistance were determined from an average of 9 indentations to ensure that the properties of the whole sample are represented, with hardness testing following ASTM practice [24].

5.3.2 Reciprocating Wear Test Procedure

To conduct the reciprocating wear tests, the samples were loaded into a computer controlled Universal Micro-Tribometer (UMT; Multi-Specimen Test System, Center For Tribology, Campbell, CA, USA), shown in Figure 34. The TiC-Ni_3Al samples were tested in pairing with a WC-Co sphere counter-face (McMaster-Carr), with a diameter of 6.35 mm. The WC-Co sphere was brought into contact with the sample and the applied load increased until the desired level is reached and remained stable for 2 seconds. For the

present study, applied contact loads of 20 N, 40 N, 60 N, or 80 N were used. The lower platform, supporting the sample being tested, then oscillates at a frequency of 20 Hz, for a total period of 2 hours, with an amplitude (track length) of 5.03 mm. This simulates ~14.5 km of contact with a material of comparable hardness, and was chosen as the test parameter expected to produce significant wear (i.e. any wear detectable both visually without aid and via mass loss using a 0.00001 g resolution balance, as determined by the mass loss on the lowest applied wear load). After testing, any loose and easily removed wear debris was collected for further analysis.

(a)

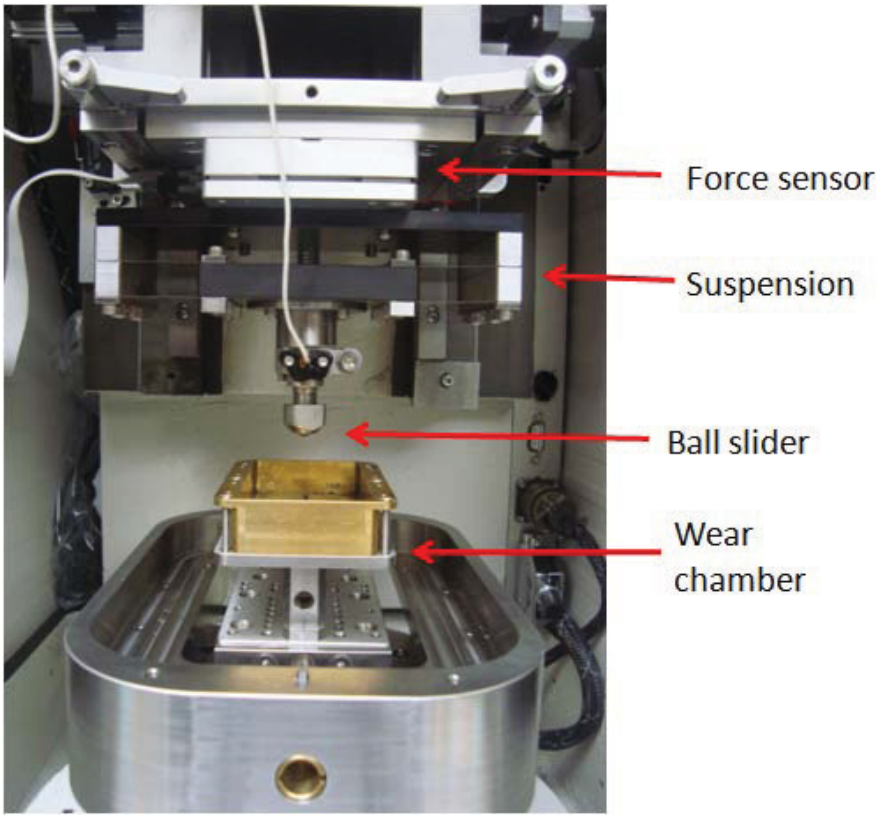

(b)

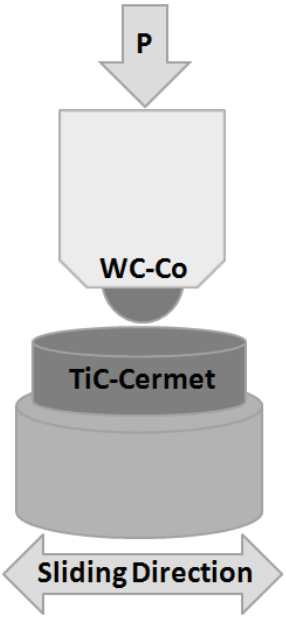

Figure 34. (a) The computer controlled Universal Micro-Tribometer (UMT), Multi-Specimen Test System. (b) A representation of the contact and motion of the ball slider and test sample.

Following wear testing, each sample was characterised using optical profilometry (NANOVEA, Micro Photonics Inc., Irvine, CA 92618, USA) and SEM to determine the wear response. The optical profilometer was used to examine the general features of the whole wear track and to determine the volumetric wear amount, using a 130 μm "optical pen". Two instrument settings were used to analyse the wear tracks and the surrounding surface, namely low definition (5 μm steps) and high definition analysis (2 μm steps). Due to the relatively large areas to be scanned (~10 mm^2), the high definition setting requires significant time (~24 hrs) to perform a single area scan. Consequently, high definition scans were restricted to TiC with 40 vol. % Ni_3Al only. An essentially equivalent level of scan accuracy could be achieved with the low definition analysis, when conducted using an average of 3 area scans, which resulted in a significant decrease in analysis time (~9 hrs per three scan series). The volumetric analysis was consequently conducted for *every* sample using the lower definition scan procedure. The microstructural features of the wear tracks were also examined using SEM. Energy-dispersive x-ray spectroscopy (EDS) was conducted using the SEM to assess the wear track composition, including chemical evaluation of any tribolayer formed. EDS was also used to determine if there was any transfer of the WC-Co counter-face ball material to the wear track surface.

5.4 Results and Discussion

5.4.1 Cermet Hardness and Indentation Fracture Resistance

After melt-infiltration the TiC-Ni_3Al cermets consistently exhibited densities in excess of 99 % of theoretical. Figure 35 demonstrates the typical microstructures observed for the TiC-based cermets prepared with 20 and 40 vol. % Ni_3Al, revealing a relatively fine grain structure of TiC within the continuous Ni_3Al metallic binder phase. The mean TiC grain size was determined to be ~2 μm using the lineal intercept method (for the 20 vol. % Ni_3Al composite), although larger isolated grains are also occasionally noted (e.g. Figure 35(a)).

(a)

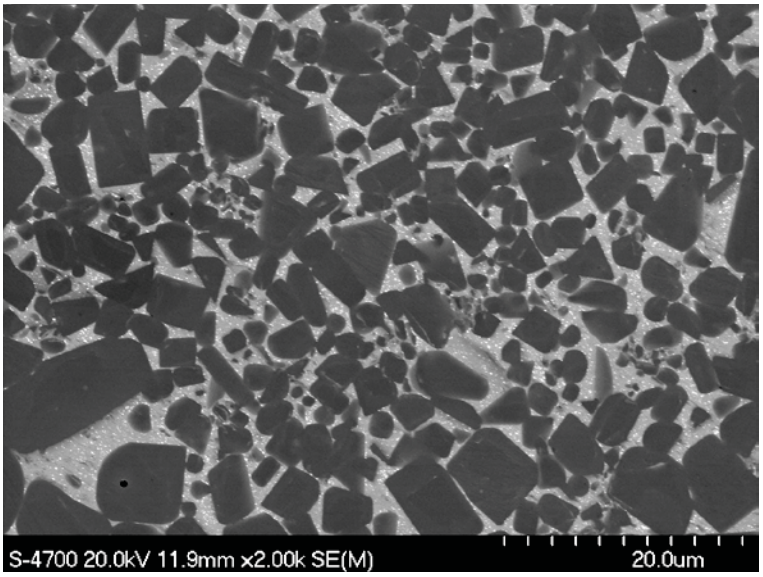

(b)

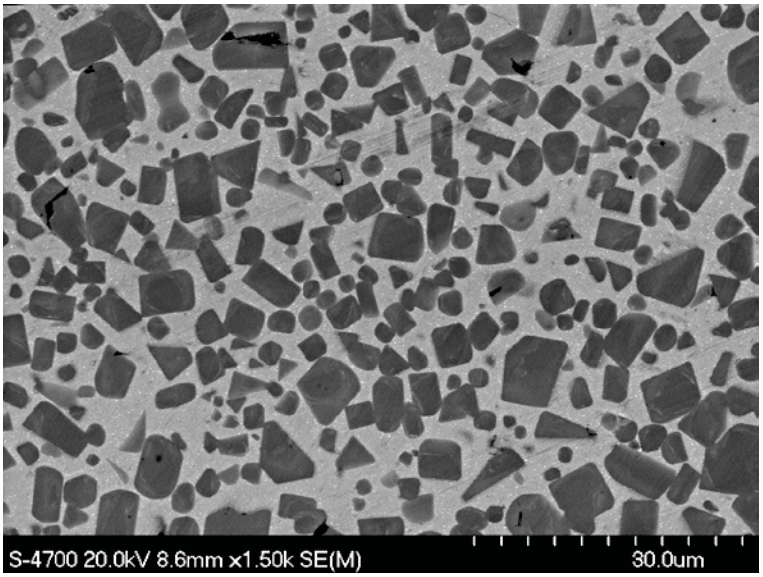

Figure 35. The typical microstructure of TiC-Ni_3Al cermets with binder contents of (a) 20 vol. % and (b) 40 vol. %.

The Vicker's hardness and indentation fracture resistance of the TiC-Ni_3Al cermets are presented in Table 16. The hardness is seen to decrease in an essentially linear manner with increasing Ni_3Al binder content, mirroring the predicted composite elastic modulus

(estimated using a simple rule of mixtures [21]), shown in Table 16. This linear response confirms the general simple rule of mixtures behaviour of selected properties of these materials. It is also apparent that the indentation fracture resistance increases in a nominally linear manner, as a function of binder content. (Table 16). It is clear that the indentation fracture resistance shows the opposite trend to the composite hardness. A comparison of the fracture resistance as a function of hardness is given in Figure 36. This type of reciprocal response is typical of cermet materials, and again can be related to the respective elastic properties of the two phases present. The elastic modulus data highlights the effects of increasing Ni_3Al content in a manner similar to the hardness. In combination, the decreasing hardness and increasing toughness could ultimately be used to subsequently customise the cermet properties for a specific application.

Table 16. Elastic modulus, hardness, and indentation fracture resistance, for TiC-Ni_3Al at binder contents of 20, 30, and 40 vol. %.

Ni_3Al Content (vol. %)	Elastic Modulus (GPa)	Hardness (HV1)	Indentation Fracture Resistance ($MPa.m^{1/2}$)
20	401	1844.9 ± 129.1	12.38 ± 1.14
30	374	1473.1 ± 83.6	16.49 ± 2.21
40	347	1138.1 ± 44.0	19.32 ± 1.44

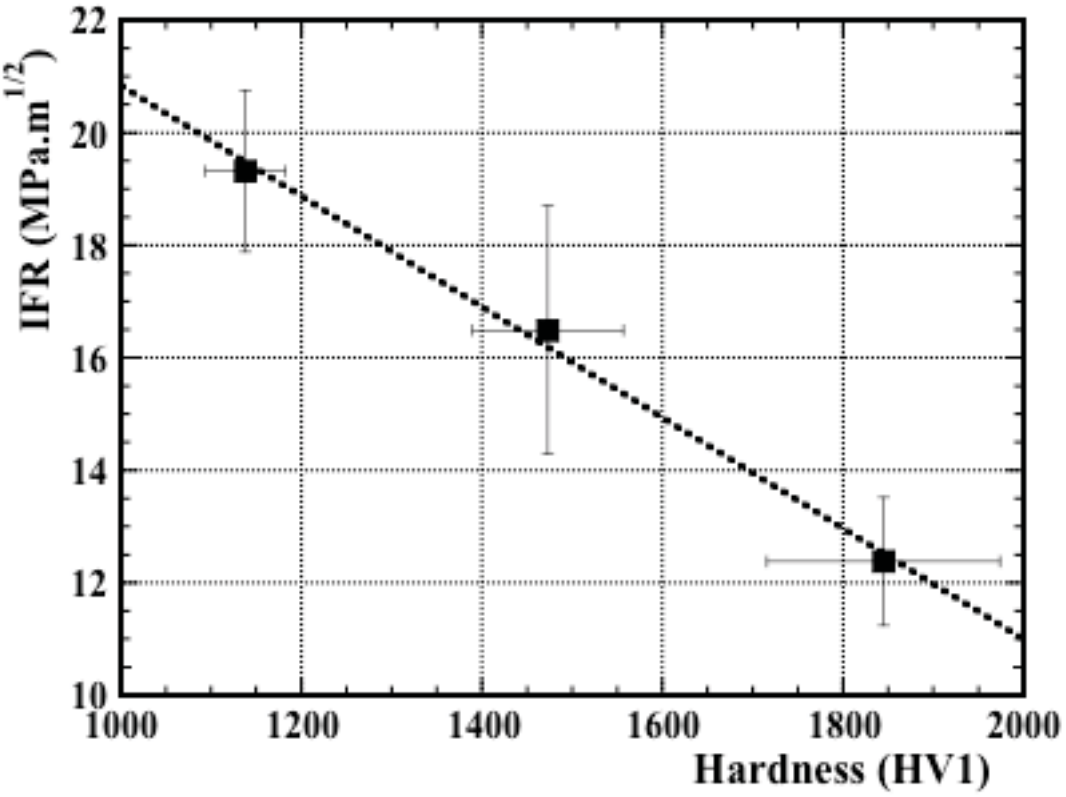

Figure 36. Indentation fracture resistance (IFR; 50 kg load) vs. hardness (1 kg load) for TiC prepared with 20, 30 and 40 vol. % Ni_3Al.

The Vicker's hardness and indentation fracture resistance can potentially provide some information relating to the most likely forms of wear that will occur. Spalling and grain removal are common wear mechanisms for cermets, since the most wear resistant component of the cermets are the ceramic particles. As the particles are impacted, both the hardness and fracture resistance will help determine if cracks will initiate in the ceramic particles and if these cracks will propagate through the particle, or result in interfacial debonding and failure through the metallic binder. The hardness and fracture resistance may also be used in conjunction with the wear data to determine for what applications the cermet may be suited.

3.2 *Reciprocating wear behaviour*

The reciprocating wear response of the TiC-Ni_3Al samples was tested using 20, 40, 60, and 80 N loads, following the procedure described previously. Figure 37 demonstrates the

volumetric wear loss recorded as a function of both binder content and applied load, determined from three-dimensional profilometry measurements. It is consistently observed that the wear loss increases with applied load. Interestingly, the intermediate composition, prepared with 30 vol. % Ni_3Al shows the lowest recorded material loss, for all loads examined.

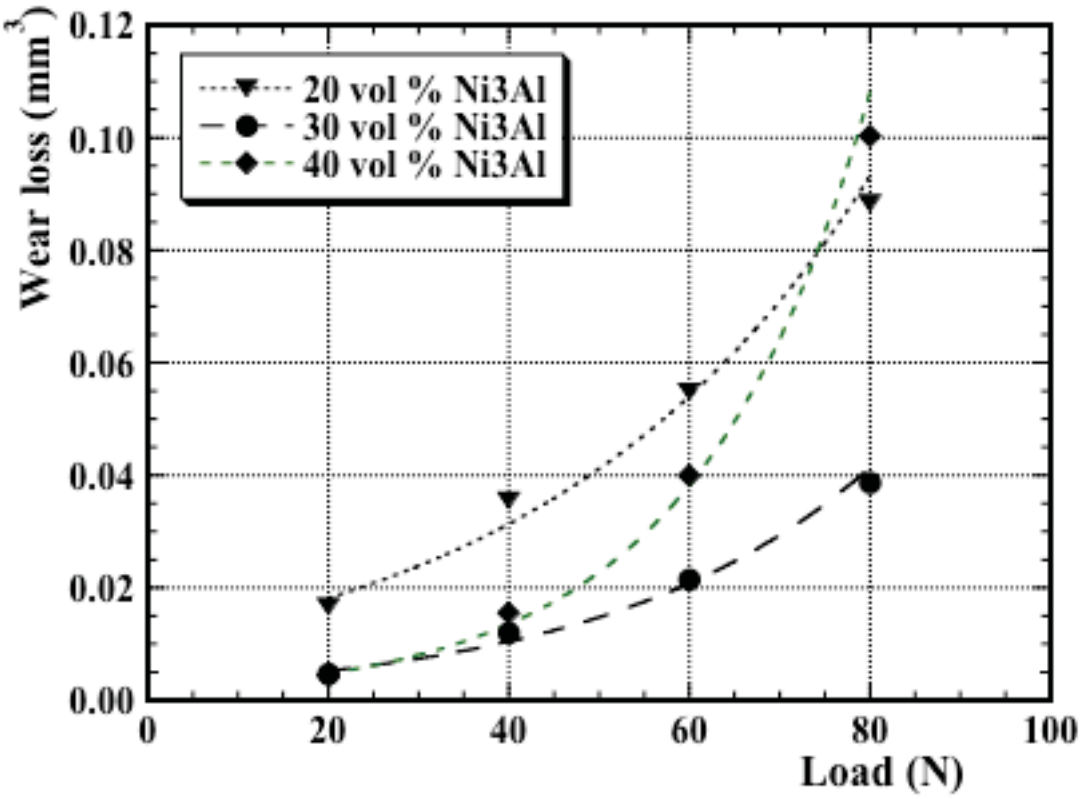

Figure 37. The effects of applied load and Ni_3Al binder content upon the material loss during reciprocating wear testing (2 hour testing duration).

The coefficient of friction (COF) was also analysed during the reciprocating wear tests. The UMT is able to accurately determine the COF for each data point (resolution of ~5 mN), as well as being able to determine the average COF for the whole wear test. The results of the mean COF for each combination of binder content and applied load is presented in Figure 38. It is apparent that the COF remains essentially consistent for each of the cermets examined, and also is largely independent of applied load. The small variances in the COF may be caused by macroscopic microstructural details in the

material, such as processing voids, spalling, or other damage [14,16,17,25,26]. This information is of particular importance as it may be used to help determine the nature of the wear that is occurring. If the COF were to change abruptly, during the test, or begin at one value and gradually shift to plateau at another, the COF can point to where a transition may occur between 2- and 3-body wear mechanisms [2,16,27]. Since there is no clearly defined transition within the measured data, the COF cannot be used in the present example to infer the wear mechanism for each wear test. However, the COF may be used in this instance to indicate that all of the samples, at each of the four loads, are nominally affected by the same or similar wear mechanisms.

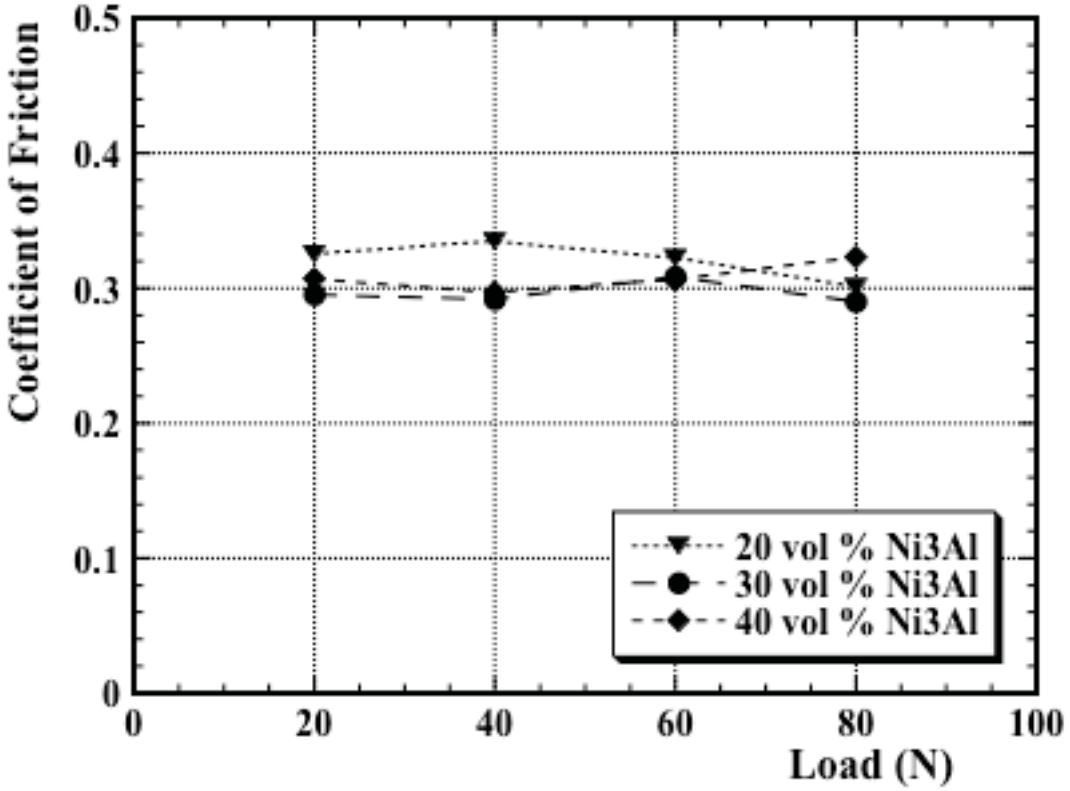

Figure 38. The mean COF of TiC-based cermets as a function of Ni_3Al binder content and applied load.

The trend made visible by the wear loss data, shown in Figure 37, that the extent of wear decreases from 20 to 30 vol. % Ni_3Al, and then increases for 40 vol. % Ni_3Al can potentially be explained from the hardness and indentation fracture resistance

observations presented in Table 16. It has previously been demonstrated for similar TiC-Ni_3Al cermets that the contiguity, a measure of the carbide-carbide grain contacts, decreases with increasing binder content [8]. The hardness and indentation fracture resistance data indicate that, for the lowest binder contents, the cermets will fail in a nominally brittle fashion, resulting in grain cracking and pull out [28]. This allows for large amounts of wear to occur rapidly, as cracks form and portions of material may be removed. Increasing the fracture resistance, through increasing binder volume fraction, promotes a transition from a predominantly brittle fracture mechanism to one that is more ductile. This would potentially decrease the extent of wear occurring by allowing an increasing amount of plastic deformation during loading. Additionally, the binder may suffer from a form of "extrusion", caused by the localised compressive compaction of the cermet, forcing the binder upwards between the ceramic particles and allowing the binder to be preferentially removed [16,29-32]. In general, this will allow for additional wear mechanisms, such as adhesive wear and the formation of tribolayers, to occur, which are known to slow the wear process. However, as the binder content is increased to 40 vol. %, the wear rate again increases, as the cermet wears in a manner more like the metallic binder than the ceramic matrix. Although this would allow for further ductility, the cermet will also suffer from a decreased hardness, thereby decreasing the resistance to wear. It is notable that the highest binder content samples exhibit a far greater sensitivity to the applied load than the 20 and 30 vol. % Ni_3Al cermets, in support of this argument.

To determine the causes of the wear associated with each of the applied loads and Ni_3Al binder contents, the individual wear tracks were imaged using both the optical profilometer and the SEM. Optical profilometry is able to better contrast the macroscopic details of the wear track and the changes in depth than imaging with the SEM. Figures 39 demonstrates typical images that were captured using the profilometer, in both a pseudo three dimensional (a) and cross-sectional view (b). A clear comparison can be obtained of the evolution of the wear tracks with applied load, confirming the increasing mass loss with load.

(a)

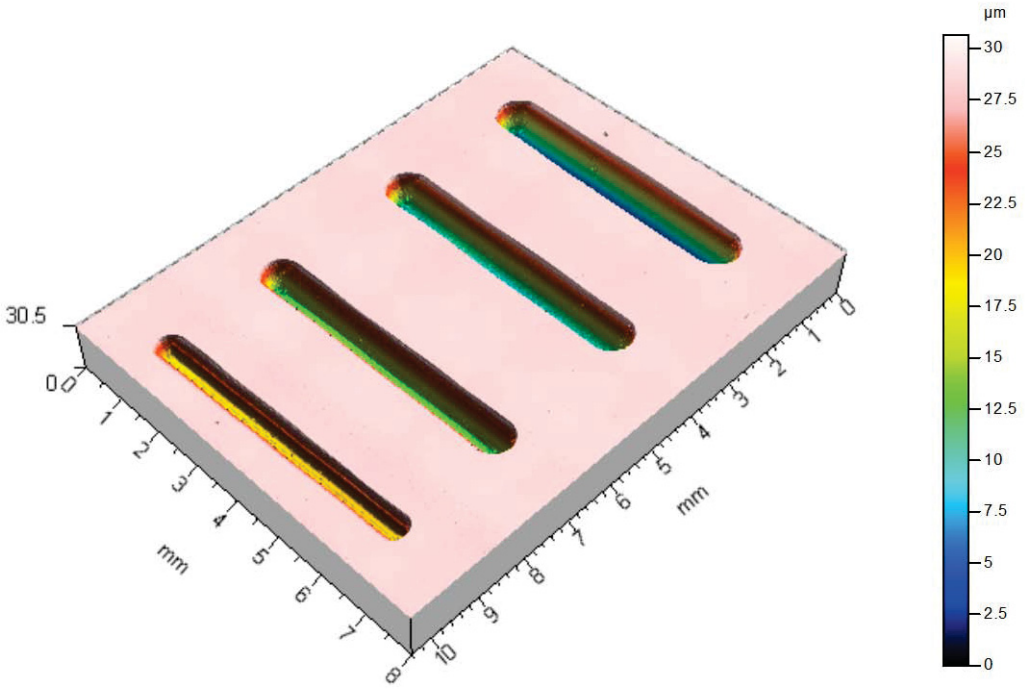

(b)

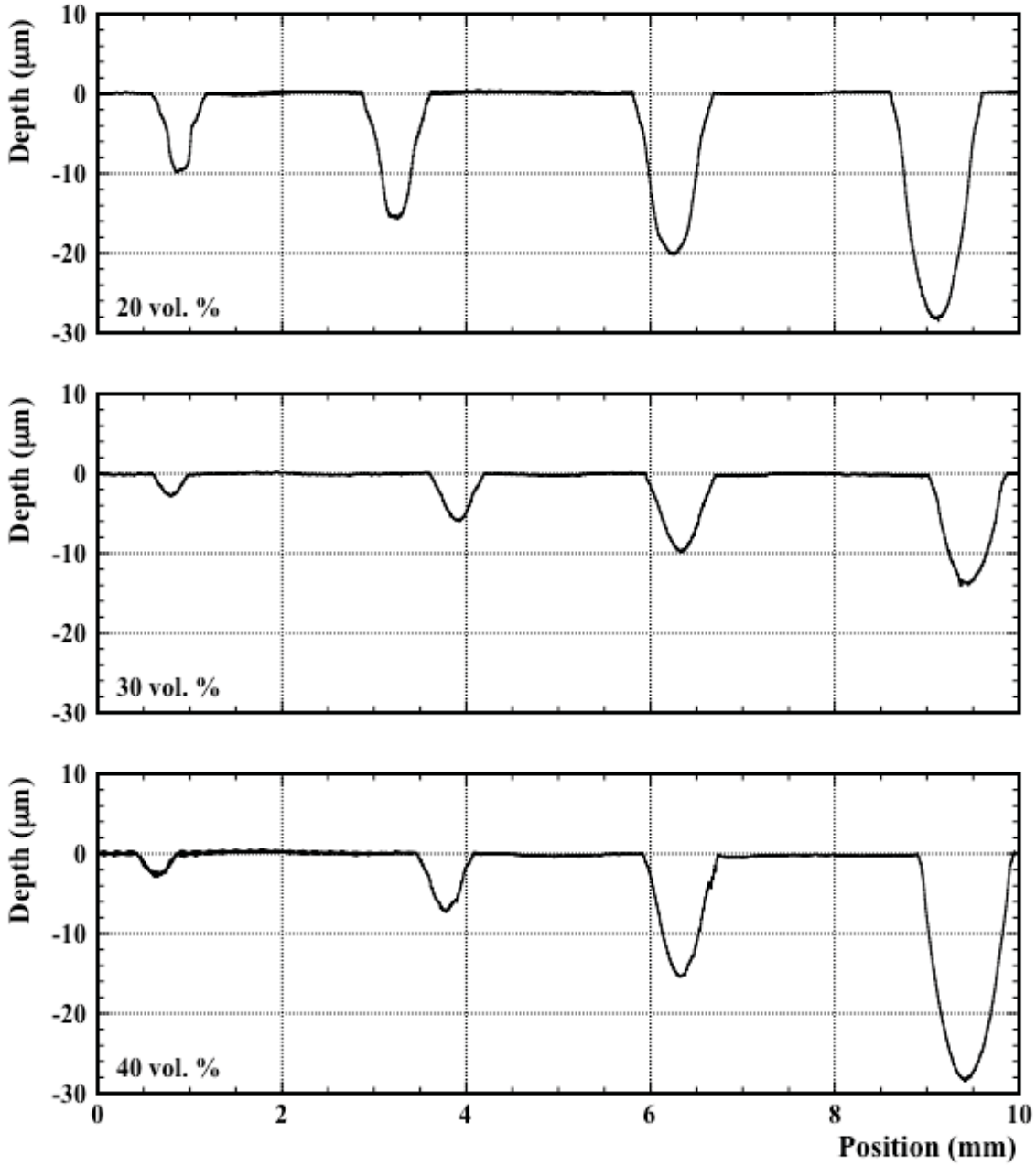

Figure 39. (a) Psuedo three-dimensional profilometry image of the wear tracks obtained for TiC-based cermets with 20 vol. % Ni_3Al binder (left to right: applied loads of 20 to 80 N, with a total wear track length of 5.3 mm). (b) Optical profilometer cross-sectional profiles of the wear track generated at loads of 20 to 80 N (left to right), for TiC with 20, 30 and 40 vol. % Ni_3Al.

The difference in wear resistance may be clearly observed by comparing the depths of the wear tracks (Figure 39b). Based on these observations, the 20 vol. % TiC-Ni_3Al sample has lost the most material from each of its tests, while the 30 vol.% sample lost the least, in accordance with the volumetric data presented in Figure 37. The profilometry may also be used to allow detailed examination of wear tracks individually, as shown in Figure 40. Examining the 60 N load track for TiC prepared with 40 vol. % Ni_3Al sample, particular wear traits may be observed. At the ends of the wear tracks there is some evidence of the wear debris and/or material from the sample being pushed out of the wear track. Ploughing and cutting are also visible, especially along the centre of the track, and continuing for its full length. The removal of small sections of material is also observed throughout the wear track, appearing as black dots or slight indentations. This damage is indicative of grain removal/pull out and potentially spalling, wear mechanisms that are commonly observed with cermets [31].

(a)

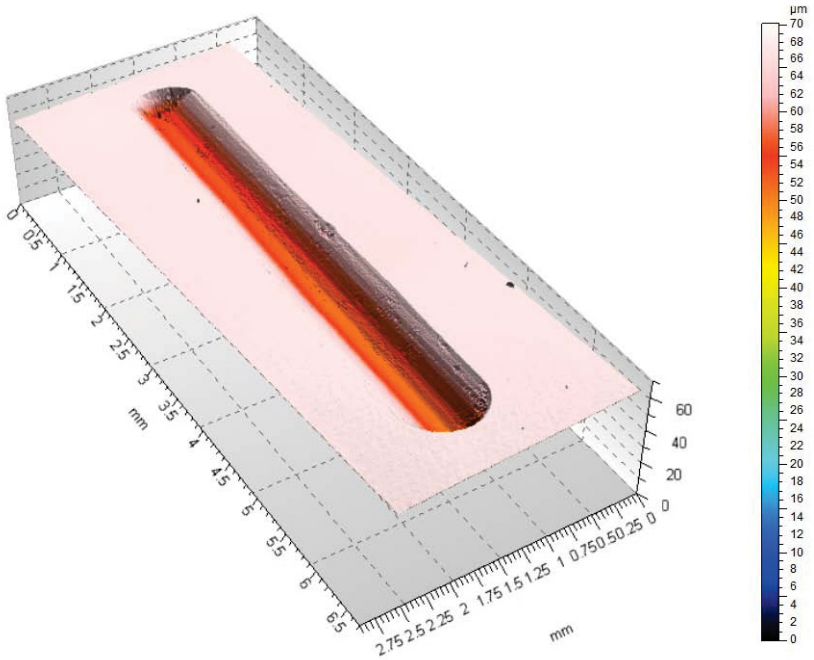

(b)

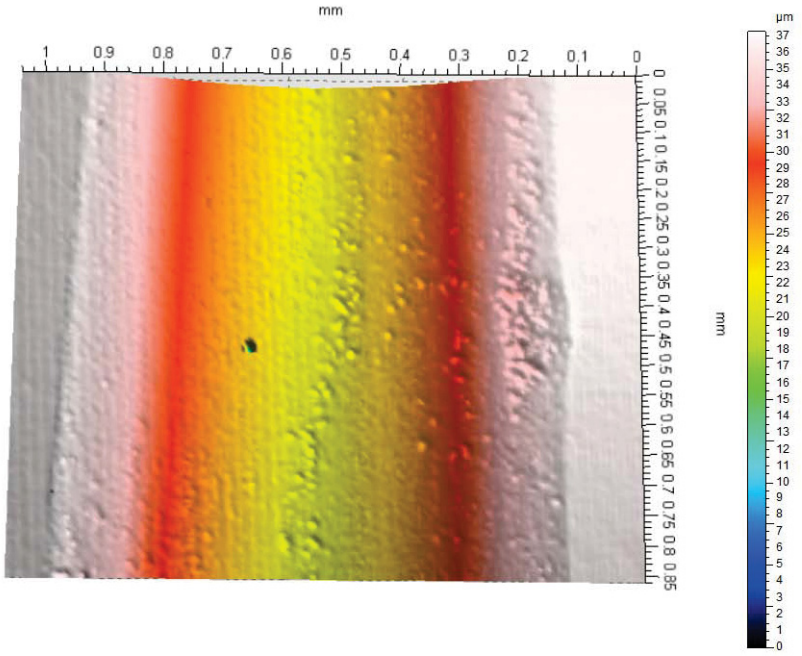

Figure 40. Three-dimensional analyses of an individual wear track (a) and a selected wear feature within the track (b). TiC prepared with 40 vol. % Ni_3Al tested at an applied load of 60 N.

To investigate these wear mechanisms more closely, the samples were examined using the SEM, with associated compositional analysis performed using EDS. Figure 41 displays micrographs of the ends of wear tracks obtained for 40 vol. % Ni_3Al samples, at applied loads of 20 and 40 N. The transition from the wear track to the undeformed material is clear, with no significant evidence of material 'uplift' outside of the wear region itself. The build up of debris within the wear track is also apparent, and it can be seen that the amount of debris increases with increasing load. The ends of the wear tracks change significantly in two ways, an increase of the build up ploughed material and the more obvious presence of a tribolayer. The ploughed material at the ends of the wear track indicates a combination of 2- and 3-body abrasive wear. In general, 2-body wear is associated with the cutting and ploughing of material, as well as the uplift and deposition

of material at both the sides and the ends of wear tracks [28-30]. The presence of material deposited at the end of the wear track would indicate 2-body wear, but the lack of a significant raised lip at the ends of the wear track would indicate 3-body wear, which is also confirmed to be essentially absent at the sides of the wear tracks (Figure 42). The combination of both mechanisms points to abrasive wear, although the presence of the tribolayer also indicates a simultaneous mechanism of adhesive wear. Higher magnification imaging demonstrates that the debris is being incorporated into a tribolayer, or film. At even higher loads the extent of the tribolayer can be seen to increase (Figure 43), and the tribolayer itself is now showing clear signs of charging within the electron beam of the SEM, hinting at a composition that is electrically insulating in its characteristics.

(a) (b)

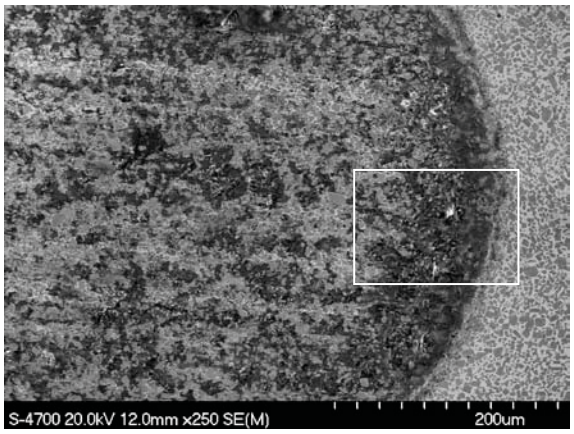

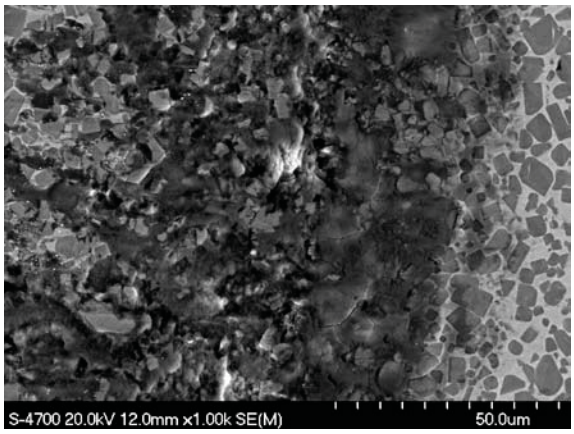

(c) (d)

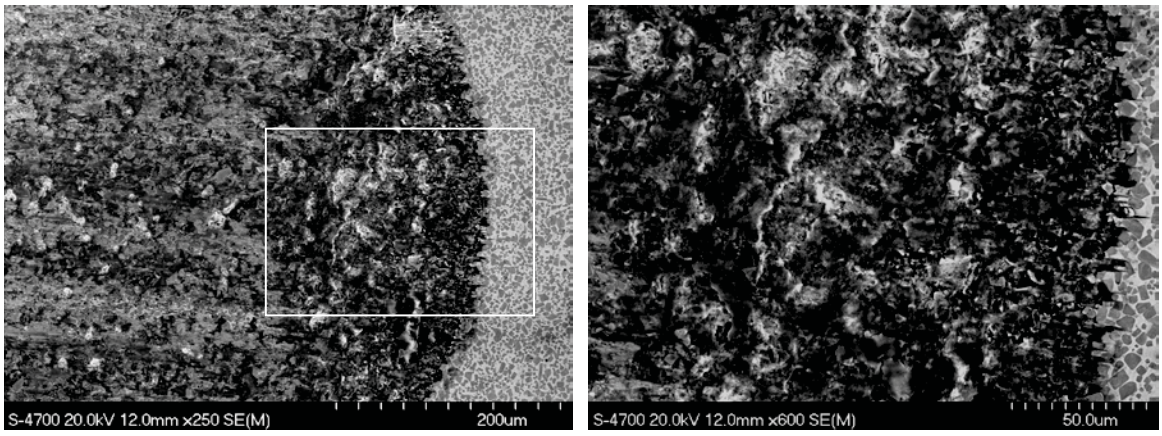

Figure 41. SEM images of the ends of wear tracks formed in TiC with 40 vol. % Ni_3Al binder at (a,b) 20 N and (c,d) 40 N. The images show the low magnification structure (a,c) and higher magnification images of the inset regions, showing the tribofilm formed near the end of the respective wear tracks (b,d).

(a)

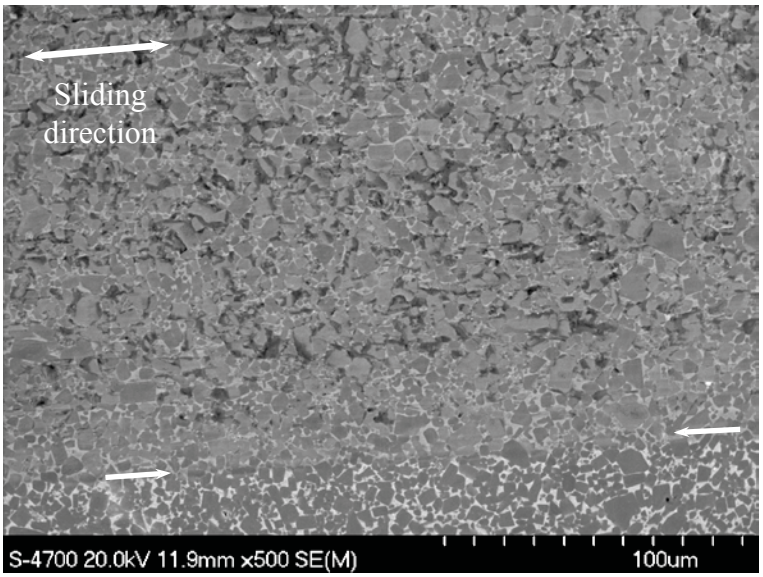

(b)

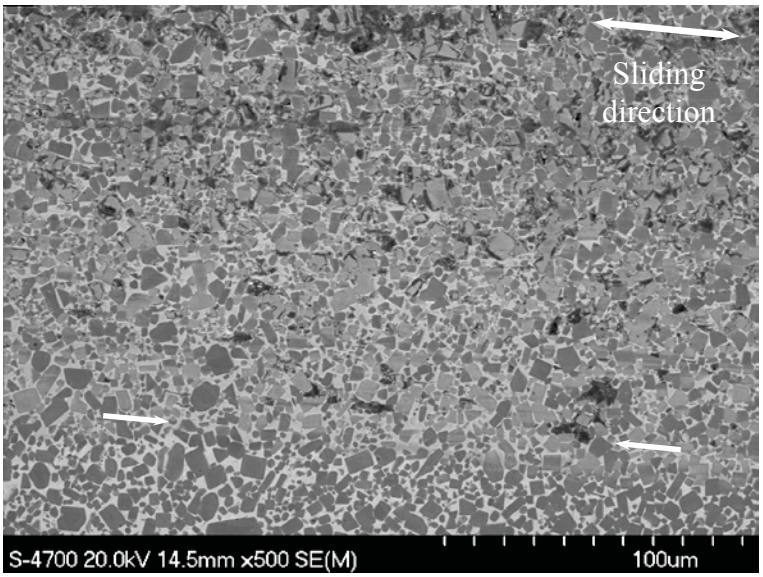

Figure 42. SEM images of the edges of wear tracks (arrowed), demonstrating the general absence of material up-lift or damage outside of the wear zone (lower region of micrograph); TiC prepared with (a) 20 vol. % Ni_3Al and (b) 30 vol. % Ni_3Al. Samples were both tested at an applied load of 40 N.

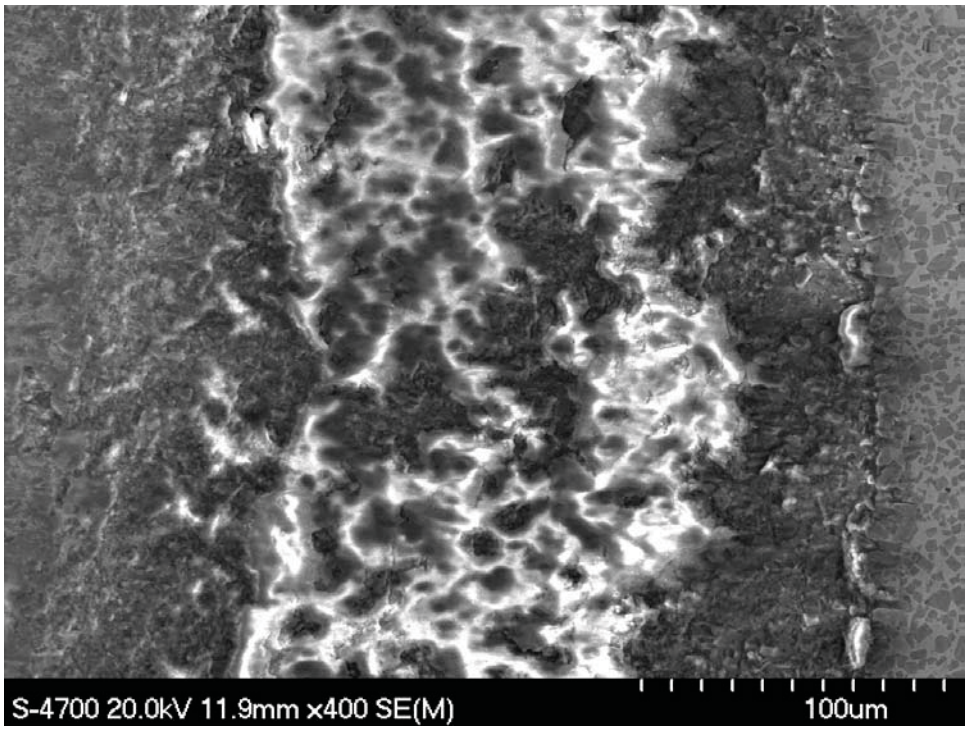

Figure 43. SEM image of the oxide-rich tribolayer build-up at the end of the wear track in a TiC-40 vol. % Ni_3Al sample. Charging artifacts are apparent due to the electrically insulating characteristics of the oxide film.

As noted previously, it is apparent that the extent and amount of the tribolayer increases with applied load. EDS analysis indicates that the layer is comprised primarily of oxides, formed in part from the removed binder (i.e. Ni and Al), but which also contains large quantities of Ti, and trace amounts of W from the WC-Co counter-face sphere (Figure 44). The amount of oxide generated in the tribolayer within the wear track increases with both applied load and binder content, and was consistently greater than 40 at. % at the higher applied loads, which indicates that the majority of cationic species are now chemically bound with oxygen. The mean W content of the example in Figure 44 is relatively low, at ~1 at. %. However, at higher loads the W content reached levels of ~4-5 at. % within the tribolayer, demonstrating measurable wear of the WC counter-face sphere. It is notable that the cermets prepared with Ni_3Al binders show excellent high temperature strength retention [33], in comparison to WC-Co [11], with the Ni_3Al exhibiting both excellent resistance to oxidation and an increasing yield strength with temperature [34]. Ni_3Al is known to form a passive Al_2O_3-based protective scale during

elevated temperature oxidation, and in fact essentially all of the elemental constituents (with the exception of C) can be expected to exhibit passivating oxide surface layers, even at room temperature [35]. The oxide nature of this film also confirms the electrically insulating characteristics observed in Figure 42. Consequently, the extensive oxide formation within the tribolayer can be anticipated to arise either through significant heat build-up during testing, resulting in oxidation, or through the constant creation of new exposed surfaces (or more likely a combination of the two). This is a typical occurrence in fretting/reciprocating type wear scenarios.

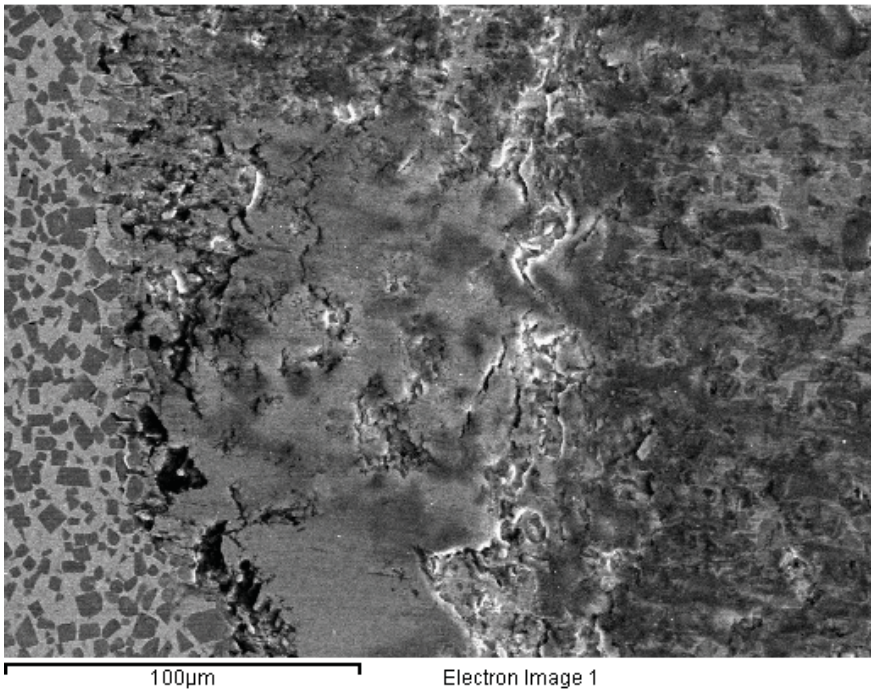

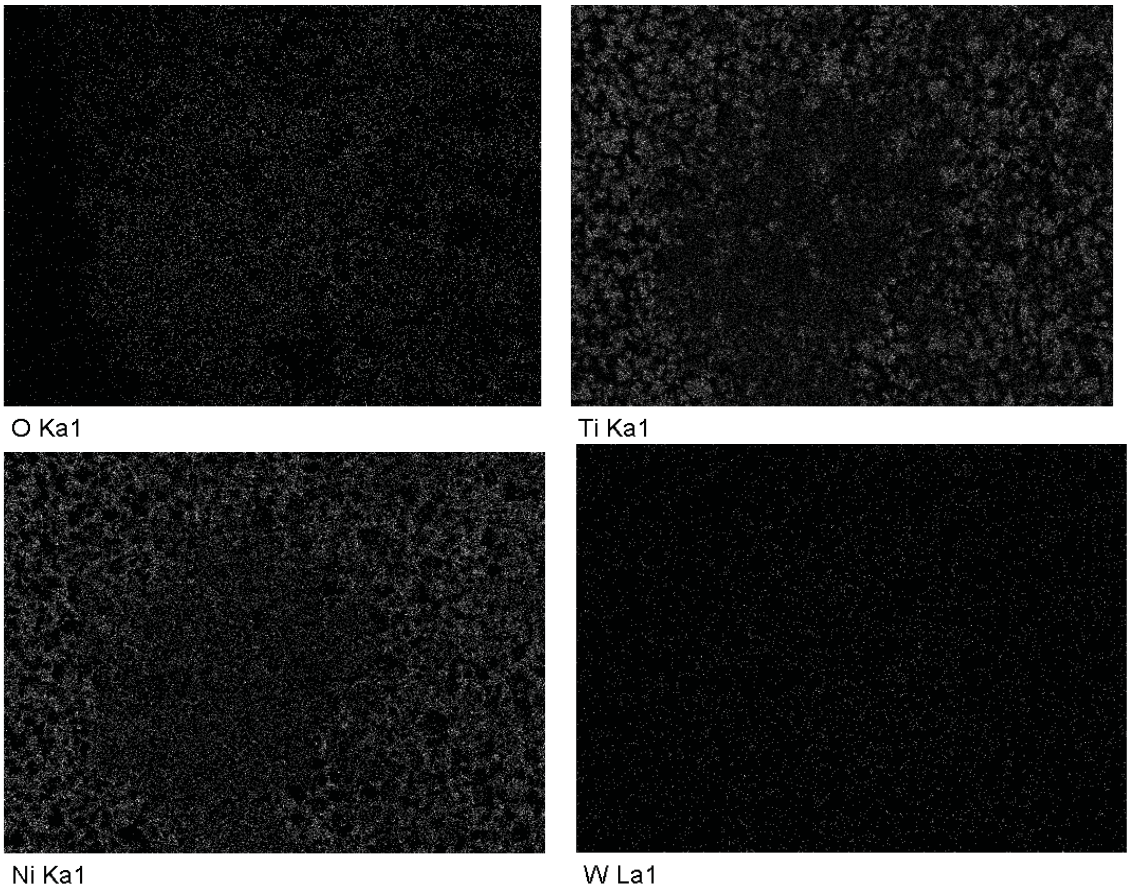

Figure 44. EDS maps of O, Ti, Ni and W in and near the ends of a wear track. TiC prepared with 40 vol. % Ni_3Al and tested at an applied load of 60 N.

Based on the EDS analysis, the oxide constituents of the tribolayer are expected to be a primary portion of the tribolayer. During the compression and abrasion of the cermet, the metallic binder is observed to be removed preferentially, as seen in Figure 45 (region A). As the loose binder is removed, the ductile metallic debris passes over the surface of the wear track repeatedly, either as an adhered layer or as loose debris in a 3-body wear mode. The TiC and WC particles and related fragments are then able to become embedded in the oxidising, loose binder and become part of the tribolayer. The continuing repetition of the rolling and sliding motion present during reciprocal wear, in a 3-body scenario, can allow for a nearly homogenous mixture of the constituents to be generated within the tribolayer. Evidence for this is found in the consistent chemical composition determined by EDS analysis.

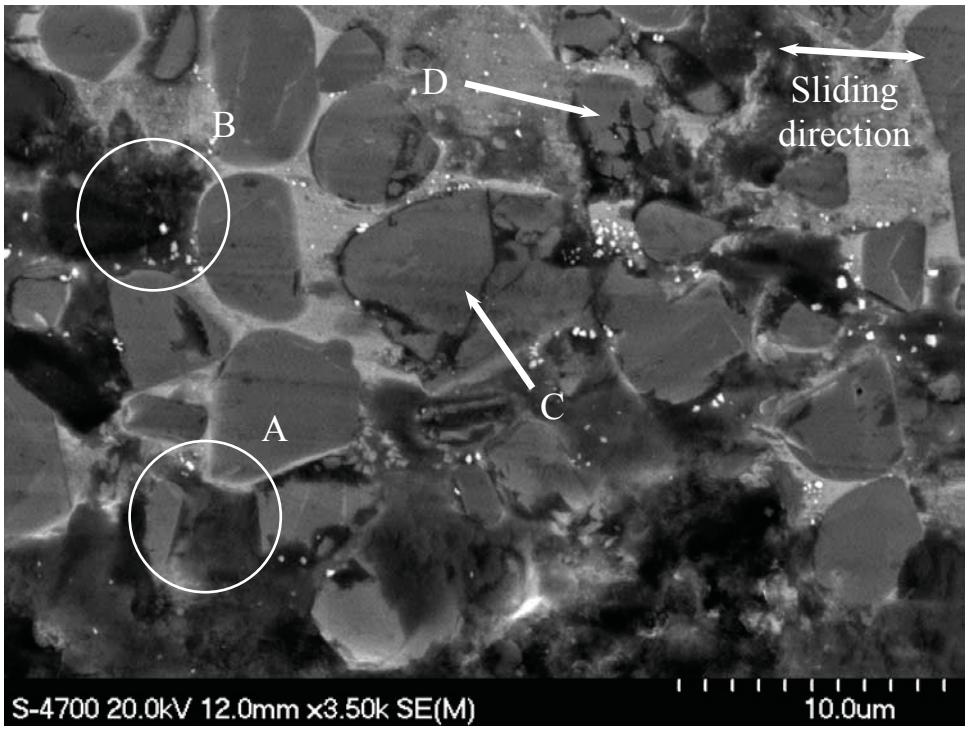

Figure 45. A SEM micrograph displaying wear features for TiC prepared with 20 vol. % Ni_3Al binder, with an applied load of 20 N for the reciprocating wear test.

Regions C and D in Figure 45 display the clear abrasion of TiC particles, which are retained in place within the sub-surface binder. It can be observed that as the ceramic particles are abraded, they may either be fully removed, as highlighted in the darkened area within B, or the particles may fracture. The fractures initiate at irregularities on the particles and cut though the particle, ending at the tough binder, and creates fine debris that will then likely be incorporated into the tribolayer. This occurs repeatedly until either the whole grain is removed, or the ceramic particle breaks up into smaller pieces that are also removed. This can be seen in the apparent fragmentation of the particle highlighted in region D of Figure 45. It is clear that the cracks generally run perpendicular to the sliding direction, with the mechanism causing the fractures being repeated Hertzian-type loading of the particle [3,36]. These observations are typical of fatigue wear behaviour in brittle materials.

5.5 Conclusions

TiC-based cermets with Ni_3Al binder contents between 20 and 40 vol. % were successfully fabricated and evaluated for their reciprocating wear response, using a ball-on-flat configuration with WC-Co counter-face spheres. Hardness and indentation fracture resistance testing were conducted on the TiC cermets, and it was determined that with increasing Ni_3Al binder content the hardness decreases while the resistance to indentation fracture increases. It was determined for each composition that as the reciprocating wear load was increased the wear volume, and hence the extent of wear, also increased. This behaviour was confirmed using an optical profilometer and SEM imaging. Although all three cermet compositions follow the same general trend with increasing load, the volumetric wear remains the highest for materials with 20 vol. % binder and lowest for those prepared with 30 vol. % Ni_3Al. It is notable that samples prepared with the highest Ni_3Al binder content (i.e. 40 vol. %) actually exhibit a clear and smooth transition in their behaviour. At low loads the wear response is comparable to the more wear resistant 30 vol. % samples, while at high loads it is comparable to the low binder content samples.

Through observations garnered from optical profilometry and SEM/EDS, it was determined that the cermets (at each load and binder content) suffered abrasive wear as the primary degradation mechanism. This wear took the form of preferential binder removal, together with grain fracture and pull-out, arising from a form of fatigue induced by Hertzian loading. This occurred as a combination of 2 and 3-body wear, causing the debris that formed to accumulate at both ends of the wear track but without causing significant uplift around the edges of the wear track. As the load increased there was a noticeable increase in the formation of an additional tribolayer, which was generated from an aggregation of the binder, and fine TiC and WC particle fragments. EDS analysis also showed that the tribolayer has a high oxygen content, typical of fretting/reciprocating wear.

5.6 Acknowledgements

This study was supported by Petroleum Research Atlantic Canada (PRAC) and the Natural Sciences and Engineering Research Council of Canada (NSERC). The support of the Canada Foundation for Innovation (CFI), the Atlantic Innovation Fund (AIF), and other partners who helped fund the Facilities for Materials Characterisation, managed by the Dalhousie University Institute for Materials Research, are also gratefully acknowledged. The authors would also like to thank Brad Collier for his assistance during the initial stages of this study and Dean Grijm for technical assistance.

5.7 References

1. Zhang SY. Titanium carbonitride-based cermets: Processes and properties. Materials Science and Engineering A. 1993;163(1):141.
2. Zhang S. Material development of titanium carbonitride-based cermets for machining application. Key Engineering Materials. 1998;138:521.
3. Liu HY, Huang JH, Yin CF, Zhang JG, Lin GB. Microstructure and properties of TiC–Fe cermet coatings by reactive flame spraying using asphalt as carbonaceous precursor. Ceramics International. 2007 7;33(5):827-35.
4. Ettmayer P, Kolaska H, Dreyer K. Effect of the sintering atmosphere on the properties of cermets. Powder Metallurgy International. 1991;23(4):224.
5. Kwon WT, Park JS, Kang S. Effect of group IV elements on the cutting characteristics of Ti(C,N) cermet tools and reliability analysis Journal of Materials Processing Technology. 2005;166(1):9.
6. Wang J, Liu J, Feng Y, Ye J, Tu M. Effect of NbC on the microstructure and sinterability of $Ti(C_{0.7},N_{0.3})$-based cermets. International Journal of Refractory Metals and Hard Materials. 2009;27(3):549.
7. Zhang H, Yan J, Zhang X, Tang S. Properties of titanium carbonitride matrix cermets. International Journal of Refractory Metals and Hard Materials. 2006;24(3):236.
8. Plucknett KP, Becher PF. Processing and microstructure development of titanium carbide-nickel aluminide composites prepared by melt infiltration/sintering (MIS). Journal of the American Ceramic Society. 2001;84(1):55.
9. Asthana R, Kumar A, Dahotre NB. Materials Processing and Manufacturing Science. Butterworth-Heinemann; 2006.
10. Bowen P, Bonjour C, Carry C, Gonseth D, Hofmann H, Mari D, Mulone R, Streit P. Novel alumina titanium-carbonitride nickel composites. JOM. 1995;47(11):56.
11. Acchar W, Gomes UU, Kaysser WA, Goring J. Strength degradation of a tungsten carbide-cobalt composite at elevated temperatures. Materials Characterization. 1999;43:27–32.

12. Ying L, Jin Y, Yu H, Ye J. Ultrafine (Ti, M)(C, N)-based cermets with optimal mechanical properties. International Journal of Refractory Metals and Hard Materials. 2011;29(1):104-7.
13. Manoj Kumar BV, Basu B. Fretting wear properties of TiCN-Ni cermets: Influence of load and secondary carbide addition. Metallurgical and Materials Transactions A. 2008;39(3):539.
14. Bunshah RF, editor. Handbook of Hard Coatings. William Andrew Publishing/Noyes.; 2001.
15. Harper CA, editor. Handbok of Plastics, Elastomers, and Composites. Fourth Edition ed. McGraw-Hill Companies, Inc., McGRAW-HILL; 2002.
16. Stachowiak GW, and Batchelor AW. Engineering Tribology. 3rd ed. Amsterdam: Elsevier Butterworth-Heinemann; 2005.
17. Czichos H. Tribology: A Systems Approach to the Science and Technology of Friction, Lubrication, and Wear. Amsterdam ; New York : Elsevier Scientific Pub. Co. ; New York: distributors for the U.S. and Canada, Elsevier North Holland; 1978.
18. Smith EH. Mechanical Engineer's Reference Book. 12th ed. Oxford, England; Boston: Butterworth Heinemann; 1998.
19. Powers MT, Lavernia EJ, Groza JR, Shackelford JF, editors. Materials Processing Handbook. CRC Press; 2007.
20. Collier RB, Plucknett KP. Spherical indentation damage in TiC-Ni_3Al composites. International Journal of Refractory Metals and Hard Materials. 2012;30(1):188-95.
21. Collier RB, Plucknett KP. A comparison of anionic and cationic polyelectrolytes for the aqueous colloidal processing of titanium carbide ceramics. International Journal of Refractory Metals and Hard Materials. 2011;29(2):298-305.
22. Anstis GR, Chantikul P, Lawn BR, Marshall DB. A critical evaluation of indentation techniques for measuring fracture toughness. I. direct crack measurements. Journal of the American Ceramic Society. 1981;64(9):533-8.
23. Yount HJ. Hardness and fracture toughness of heat-treated advanced ceramic materials for use as fuel coating and inert matrix material in advanced reactors. MSc dissertation, University of Wisconsin-Madison; 2006.

24. ASTM standard C1327; 2008; Standard test method for Vicker's indentation hardness of advanced ceramics; ASTM International; West Conshohocken, PA, 2008; DOI: 10.1520/C0033-03; www.astm.org.
25. Bhushan B. Introduction to tribology. New York: John Wiley & Sons; 2002.
26. Chen H, Hutchings IM. Abrasive wear resistance of plasma-sprayed tungsten carbide-cobalt coatings. Surface and Coatings Technology. 1998;107(2):106-14.
27. Yeong Y, Lin JF, Ai CF. Correlation between three-body wear and tribological characteristics of titanium nitride, titanium carbonitride and titanium carbide coatings. Wear. 1997;208(1):147.
28. Pirso J, Viljus M, Juhani K, Letunovitš S. Two-body dry abrasive wear of cermets. Wear. 2009 1/5;266(1-2):21-9.
29. Guu YY, Lin JF, Ai C. The tribological characteristics of titanium carbonitride coatings prepared by cathodic-arc ion plating technique. Thin Solid Films. 1996 10/30;287(1-2):16-24.
30. Guu Y, Lin JF. Analysis of wear behaviour of titanium carbonitride coatings. Wear. 1997;210(1-2):245.
31. Wei C, Lin JF, Jiang TH, Ai CF. Tribological characteristics of titanium nitride and titanium carbonitride multilayer films. Part II. the effect of coating sequence on tribological properties. Thin Solid Films. 2001;381(1):104.
32. Wei C, Lin JF, Jiang TH, Ai CF. Tribological characteristics of titanium nitride and titanium carbonitride multilayer films. Part I. the effect of coating sequence on material and mechanical properties. Thin Solid Films. 2001;381(1):94.
33. Plucknett KP, Becher PF, Waters SB. Flexure strength of melt-infiltration-processed titanium carbide/nickel aluminide composites. Journal of the American Ceramic Society.1998;81:1839–44.
34. Dimiduk DM. Dislocation structures and anomalous flow in $L1_2$ compounds. Journal de Physique III. 1991;1:1025-53.
35. Choi SC, Cho HJ, Kim YJ, LeeDB. High-temperature oxidation behavior of pure Ni_3Al. Oxidation of Metals. 1996;46:51-72.
36. Fischer Cripps AC, Collins RE. The probability of Hertzian fracture. Journal of Materials Science. 1994;29(8):2216-30.

Chapter 6: Reciprocating Wear Response of Ti(C,N)-Ni_3Al Cermets

S. Buchholz, Z.N. Farhat, G.J. Kipouros and K.P. Plucknett*
Dalhousie University, Materials Engineering Program, Department of Process Engineering and Applied Science, 1360 Barrington St., Halifax, Nova Scotia, CANADA

6.1 Abstract

Ti(C,N)-based cermets have received significant attention due to their enhanced mechanical properties at elevated temperatures, low mass, and increased chemical stability, when compared to WC-Co 'hardmetals'. These properties have been found to be superior in many cases to traditional 'hardmetal' replacements, such as TiC-Ni. The current study focuses on Ti(C,N)-Ni_3Al cermets formed through melt infiltration (with binder contents ranging from 20 to 40 vol. % Ni_3Al). Comparison is made with TiC-Ni_3Al cermets using an identical binder alloy. The reciprocating ball-on-flat wear properties of the cermets was evaluated as a function of applied load (using a WC-Co counter-face), together with the composite hardness and indentation fracture resistance. It is shown that nitrogen content negatively affects infiltration, resulting in non-infiltrated areas within low binder content cermets, which decreases the indentation fracture resistance and hardness. This problem can be largely mitigated by increasing binder content. When comparing fully infiltrated cermets, increasing nitrogen content decreases hardness and increases toughness, while all Ti(C,N) cermets outperform TiC (at 40 vol. % binder). Reciprocating wear increased with increasing load, and typically was the most severe for the lowest binder contents. A combination of wear mechanisms were apparent, including both abrasive and adhesive wear, with the formation of an oxide tribolayer containing components from both the tested cermets and the WC-Co counter-face.

Keywords: Ceramic-metal composites, abrasive wear, adhesive wear, hardness, fracture resistance, melt-infiltration

*Author for correspondence (kevin.plucknett@dal.ca)

6.2 Introduction

High performance, wear resistant ceramic-metal composites, or cermets, have received considerable attention due to their potential to reduce operational damage accumulated in sliding and contact wear scenarios, therefore reducing in-service costs. Titanium carbonitride, Ti(C,N), cermets have been the focus of considerable research due to their enhanced mechanical properties when compared to traditional tungsten carbide-cobalt (WC-Co) 'hardmetals' and more recent, lightweight titanium carbide (TiC) cermets.[1-4] In general, Ti(C,N)-cermets have higher hardness and, hot hardness, greater chemical resistance and toughness, and improved wear resistance when compared with WC 'hardmetals.[5] Cermets developed with Ti(C,N) are also much lighter than WC (Ti(C,N) is ~3 times less dense than WC),[4,6] and are less costly to produce. In addition, WC-Co exhibits severe property degradation above ~500ºC.[7] As a consequence, Ti(C,N)-cermets may be considered as a viable replacement for WC in applications such as high speed cutting applications, where WC-Co suffers from chemical degradation, chipping, softening, and high wear rates.[8]

However, Ti(C,N) can suffer from both carburisation and denitrification during formation. This has led research to focus on cermets containing transition metal carbide additions (e.g. Mo_2C, WC, TaC, etc.), owing to their ability to improve sintering, by forming a core-rim carbide structure that increases wetting and chemical bonding between the ceramic phases and the metallic binder, while decreasing carburization and denitrification.[6,9-11] As a consequence, carbide additions are often thought of as being indispensable to the formation of Ti(C,N)-cermets.[1,2,12] However, increased wetting and bonding generally comes with a performance cost of reduced toughness. This typically arises due to an increase in hardness, which may concurrently reduce the fracture resistance to the point where the cermet is no longer useful in the desired application. This has led to interest in pre-sinter solid solutions (PSSS), where alloyed Ti(C,N) is formed before sintering with the metallic binder phase. Through this method, carburization and denitrification may be accounted for prior to the addition of the

binder.[1,2,12] This allows for cermets of superior mechanical properties to be formed, often equalling cermets with carbide additions in hardness, while exceeding them in toughness.

The desired properties of the cermets are also controlled through the addition of metallic binders, such as alloys of Ni, Fe, and Co.[5,6,9,10,13-15] Each alloying addition can bring performance benefits to the cermet, such as increased ductility, hardness, corrosion resistance, thermal conductivity, and/or thermal shock resistance. Ni_3Al is of particular interest because of its high yield strength which actually increases up to ~900°C. [16] This anomalous yielding response is also evident when cermets are developed utilising Ni_3Al binders, with strength increasing up to ~1,000°C.[17] An additional benefit is that Ni_3Al forms an Al_2O_3-based passivating layer during elevated temperature oxidation,[18] further protecting the material from chemical attack. As a consequence, there is a significant potential improvement over WC-Co 'hardmetals', as this system is known to exhibit poor elevated temperature strength and oxidation resistance.[7]

Generally, cermets are used in applications where their tribological properties are of great importance, such as high-speed cutting tools, seals, etc. As a result of this, significant research has been conducted within this field to determine how TiC and Ti(C,N)-cermets withstand various forms of wear, and their associated damage mechanisms. Of specific importance are abrasion and fretting wear, as these are both very common mechanisms, and often produces severe wear degradation. In particular, abrasive wear occurs when two surfaces in contact move relative to each other. Similarly, fretting wear occurs in situations where there is a low amplitude oscillatory sliding motion between two surfaces in contact.[19-21] Abrasive and fretting wear both normally produce damage from 2 and 3-body wear modes; the surface impinging the test sample gouges the material while trapping debris between both surfaces. This is a common form of damage for bearings, and is often simulated using a ball-on-flat test. Several tribological studies have focused on these phenomena in Ti(C,N)-based cermets.[11,14,22,23]

In the present work a family of novel Ti(C,N) cermets, utilising ductile Ni_3Al intermetallic binders, have been developed and evaluated using a ball-on-flat

reciprocating wear tester, with a WC-Co counterface sphere. Comparison is made between cermets with various C:N ratios, as well as pure TiC, using Ni_3Al binder contents from 20 to 40 vol. %.

6.3 Materials and Methods

6.3.1 Sample Preparation

The samples were prepared using a melt infiltration technique that is documented in prior publications.[24,25] Samples were prepared using three Ti(C,N) powder compositions, namely $Ti(C_{0.7},N_{0.3})$ (lot #L25809; D_{50} = 2.10 μm), $Ti(C_{0.5},N_{0.5})$ (lot #L29865; D_{50} = 1.74 μm) and $Ti(C_{0.3},N_{0.7})$ (lot #L25747; D_{50} = 1.72 μm), all sourced from Treibacher Industrie AG (Althofen, Austria). For comparison, TiC powder (Grade 2012; lot #PL20125339; D50 = 1.25 μm) was obtained from Pacific Particulate Materials (Vancouver, BC, Canada). The Ti(C,N) powders were prepared with 1 wt. % wax binder (polyvinyl butyral (PVB)) addition through ball milling, to aid compaction response. Pellets were produced by using 7.5 g of either set of powders, followed by uniaxial compaction at a pressure of ~67 MPa. The samples are then bagged and further compacted by cold isostatic pressing at ~220 MPa. The samples are then weighed, and placed into an alumina crucible on a layer of bubble alumina. The Ni_3Al infiltrant was used in powder form (-325 mesh, Ni_3Al alloy IC-50; Ametek, Eighty Four, PA, USA), and is placed onto the samples to meet the desired volume fraction of binder (20, 30, or 40 vol. %). The loaded crucibles were then placed into a vacuum furnace and evacuated to ~20 milliTorr. Sintering was conducted at 1500°C for 1hr, with heating and cooling rates of 10 and 25C/min, respectively. Typically, a vacuum level of ~20 milliTorr, or better, is maintained at the sintering temperature. Using this method, samples consisting of $Ti(C_{0.7},N_{0.3})$, $Ti(C_{0.5},N_{0.5})$, $Ti(C_{0.3},N_{0.7})$ and pure TiC were prepared with 20, 30, and 40 vol. % of Ni_3Al.

The sintered densities were measured following Archimedes' principle, by the immersion in water at room temperature. Cermet microstructure was characterised using a field emission scanning electron microscope (SEM; Model S-4700, Hitachi High

Technologies, Tokyo, Japan). The mean grain size was determined using the linear intercept method,[26] with a factor of 1.56 applied to correct for grain sectioning.

The hardnesses and indentation fracture resistance for the Ti(C,N) and TiC cermets were determined using a Vicker's hardness tester, with applied loads of 1 kg and 50 kg, respectively. The indentation fracture resistance was calculated using the methods developed by Anstis *et al*,[27] while hardness was determined using standard ASTM procedures.[28] Hardness and fracture resistance were both determined from the mean of 9 indentations.

6.3.2 Reciprocating Wear Test Procedure

Reciprocating wear testing is conducted using a computer controlled Universal Micro-Tribometer (UMT) (Multi-Specimen Test System, Center For Tribology, Campbell, CA, USA). The samples are paired with a 6.35 mm diameter WC-Co sphere counter-face (McMaster-Carr), placed into the wear chamber and secured. The contact sphere is then lowered into position slightly above the area where the wear test is to be conducted. The sphere is brought into contact with the specimen surface and the load is increased until the desired level is reached and maintained for 2 seconds. The applied loads used for this study vary between 20 N, 40 N, 60 N, and 80 N. The lower platform, which supports the specimen, then oscillates at 20 Hz for a period of 2 hours, with an amplitude (track length) of 5.03 mm. The reciprocating tests simulate ~14.5 km of total contact distance with a material of comparable hardness. Further details regarding the reciprocating wear procedure can be found in a prior publication.[29]

Detailed examination of the wear tracks was performed using optical profilometry (Model PS50, Nanovea, Irvine, CA 92618, USA) in combination with SEM in order to determine the cermet wear characteristics. The optical profilometer is used to observe the features of the whole wear track using a 130μm optical "pen", to determine the volumetric wear loss as well as to examine macro and microscopic details, effectively through the generation of a three-dimensional map. Two operational settings were analysed in the present work, the first is termed "high definition" (involving a single area scan with 2 μm steps) while

the second is termed “low definition” (an average of three area scans with 5 μm steps) in comparison. As the areas to be scanned are relatively large (~10 mm^2), the individual high definition scans require ~24hrs, and as such was only used on a single specimen for each cermet series. The low definition scan series (i.e. three averaged scans) required significantly less time (~9 hrs) and was consequently performed on every sample. Comparison of these two approaches resulted in a maximum wear volume deviation of ~5 %. The wear tracks were also examined using the SEM, with energy-dispersive x-ray spectroscopy (EDS) applied to assess the composition of components of the wear track, including a chemical evaluation of any tribolayers that were formed.

6.4 Results and Discussion

6.4.1 Hardness and Indentation Fracture Resistance

Melt infiltration was successfully achieved for Ni_3Al binder contents between 20 and 40 vol. % . However, uninfiltrated regions were visible in samples prepared with the lower binder contents in combination with the highest nitrogen content (i.e. $Ti(C_{0.3},N_{0.7})$. Similar observations have been previously made using alternate binders for Ti(C,N) cermets.[6,12] Tentatively, this response can be attributed to an increase in the melt contact angle with increasing N content in Ti(C,N), as noted in a previous study.[30] This phenomenon may be counteracted in part by increasing the binder content in the samples, but remains an important factor. Due to the relatively poor sintering and the resultant expected poor mechanical properties, the 20 and 30 vol. % samples for $Ti(C_{0.3},N_{0.7})$ were not tested further.

However, all remaining samples were able to be successfully evaluated for hardness, fracture resistance, and tribological properties, and they were found to have sintered densities consistently in excess of 99 % of theoretical. Figure 46 highlights the typically fine grain structure that is retained with the Ti(C,N) and TiC cermets, within the continuous Ni_3Al metallic binder phase. Figure 47 displays the slightly decreased infiltration and apparent residual porosity using a pseudo three dimensional image, obtained using optical profilometry, for $Ti(C_{0.5},N_{0.5})$ prepared with 20 vol. % Ni_3Al. Mean grain sizes of selected examined cermets, determined using the lineal intercept

method, are presented in Table 17. It is apparent that fine grain sizes are retained after melt-infiltration, especially for the N containing Ti(C,N) materials, which show only minimal increase in grain size relative to the original manufacturer specifications.

(a)

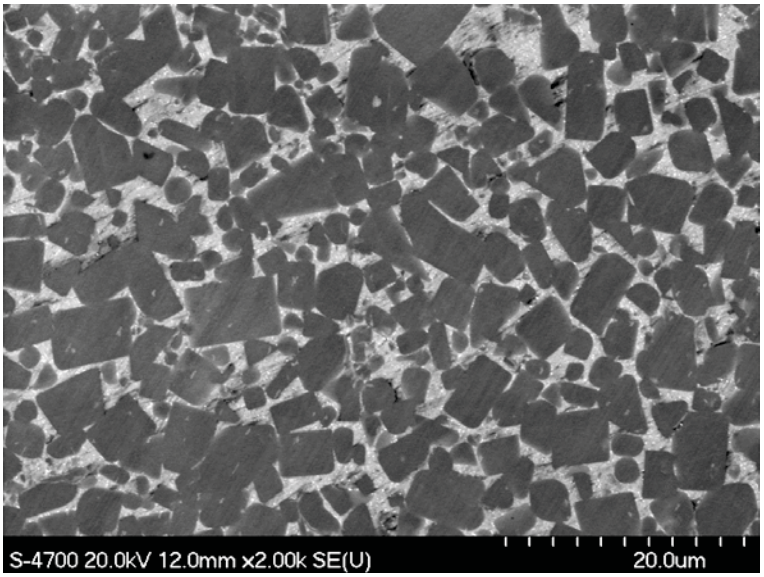

(b)

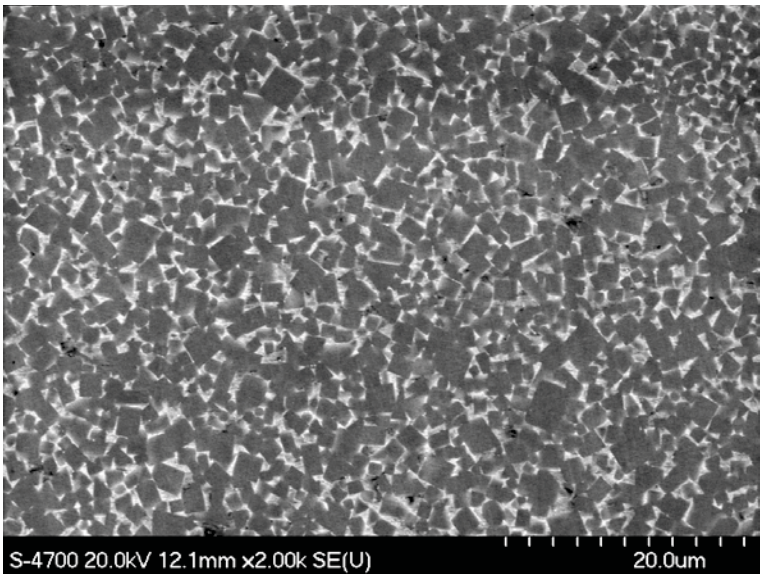

(c)

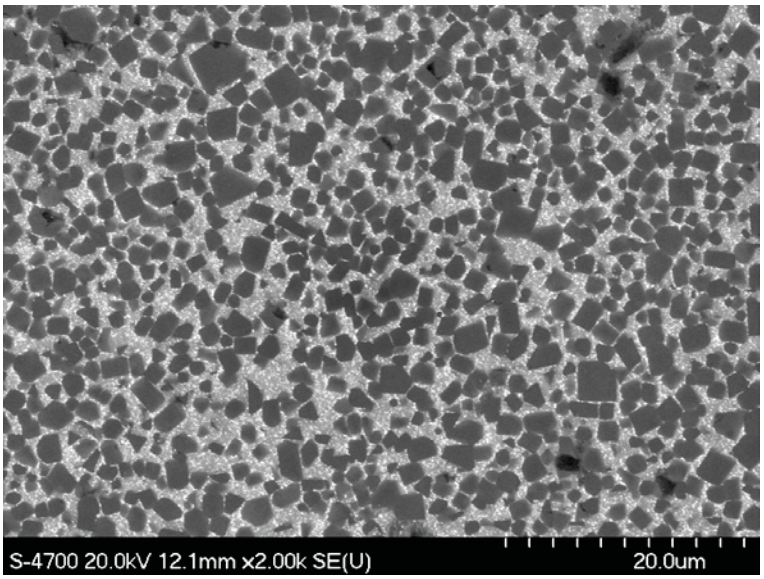

Figure 46. The typical microstructures for (a) TiC with 20 vol. % Ni_3Al, (b) $Ti(C_{0.7},N_{0.3})$ with 20 vol. % Ni_3Al and (c) $Ti(C_{0.3},N_{0.7})$ with 40 vol. % Ni_3Al.

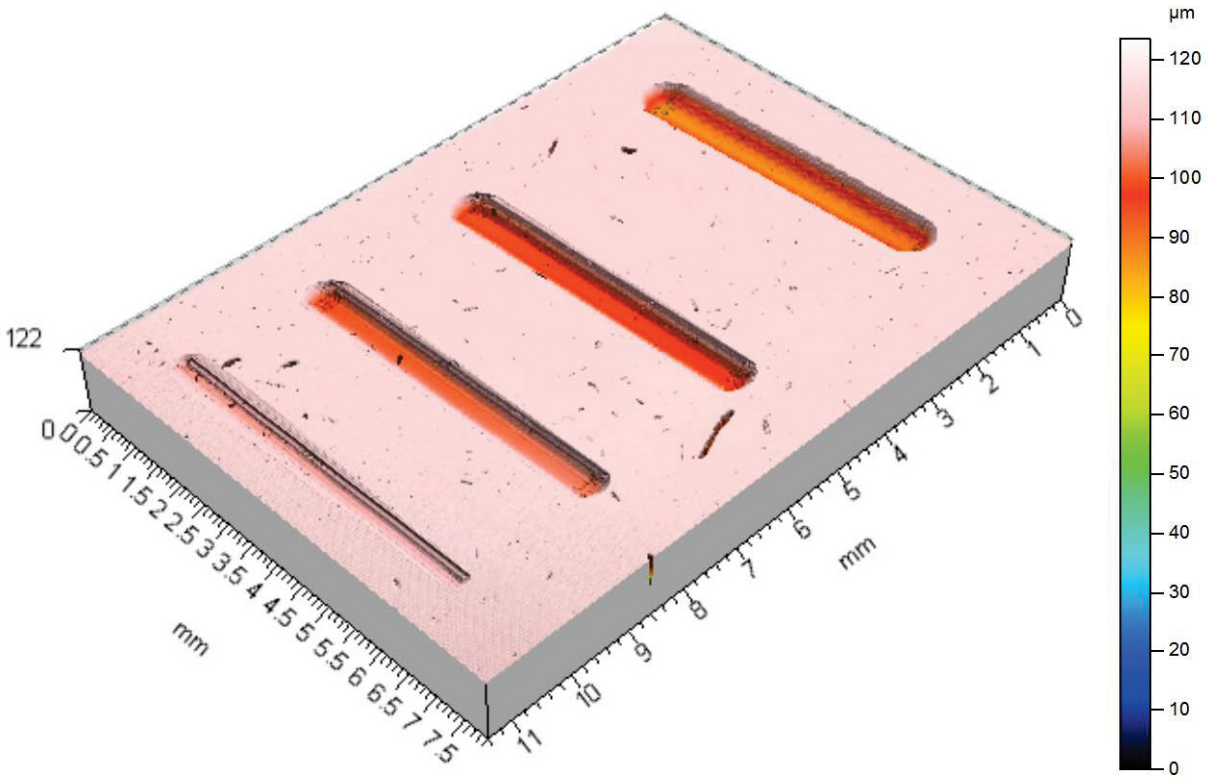

Figure 47. A pseudo three-dimensional wear profile map of $Ti(C_{0.5},N_{0.5})$-Ni_3Al cermets with a binder content of 20 vol. %. The measured wear tracks are for applied loads of 20, 40, 60 and 80 N (left to right).

Table 17. Post melt-infiltration processing grain size measurements for selected samples.

	Ni_3Al content (vol. %)	**Post infiltration grain size (µm)**
TiC	20	3.61 ± 2.07
$Ti(C_{0.7},N_{0.3})$	20	2.16 ± 0.93
$Ti(C_{0.5},N_{0.5})$	20	2.07 ± 0.95
$Ti(C_{0.3},N_{0.7})$	40	2.11 ± 0.90

When testing the various cermets, it is important to characterise and compare them by both the C:N ratio of the carbonitride and the binder content, so as to determine their respective effects. However, the apparent change in the sintering characteristics of the samples with high N contents may disrupt this process by reducing the hardness of the

cermets artificially through the introduction of voids that can be expected to adversely affect the tribological characteristics.[12,31]

The Vicker's hardness and indentation fracture resistance of the Ti(C,N)-Ni_3Al and TiC-Ni_3Al cermets are presented in Table 18. The hardness for all of the cermets is seen to be decreasing in an essentially linear manner with increasing binder content, while the indentation fracture resistance displays a reciprocal response. The Young's modulus of each of the Ti(C,N) and TiC composites was estimated through a simple rule of mixtures, based on values found in literature.[1,2,25] The values for each cermet, as well as those determined experimentally for hardness and indentation fracture resistance, are given in Table 18. The observed trend for hardness mirrors that of the predicted elastic moduli, confirming that the cermets follow a simple rule of mixtures behaviour. As a consequence of this combination of decreasing hardness and increasing toughness, the cermets can be tailored for specific applications.

Table 18. Young's Modulus, hardness, and indentation fracture resistance, for TiC-Ni_3Al and Ti(C,N)-Ni_3Al at binder contents of 20, 30, and 40 vol. %.

		Ni_3Al Content (vol. %)		
		20	**30**	**40**
TiC	**Young's Modulus (GPa)**	401.0	374.0	347.0
	Hardness (HV1)	1844.9 ± 129.1	1473.1 ±83.6	1138.1 ± 44.0
	Indentation Fracture Resistance ($MPa.m^{1/2}$)	12.38 ± 1.14	16.49 ± 2.21	19.32 ± 1.44
$Ti(C_{0.7},N_{0.3})$	**Young's Modulus (GPa)**	409.4	380.6	351.8
	Hardness (HV1)	1791.1 ± 68.2	1572.7 ± 71.6	1491.0 ± 58.8
	Indentation Fracture Resistance ($MPa.m^{1/2}$)	10.39 ± 1.65	17.10 ± 2.70	19.48 ± 1.35
$Ti(C_{0.5},N_{0.5})$	**Young's Modulus (GPa)**	439.8	407.2	374.6
	Hardness (HV1)	1760.8 ± 103.0	1540.7 ± 62.6	1361.2 ± 111.8
	Indentation Fracture Resistance ($MPa.m^{1/2}$)	7.64 ± 0.85	14.60 ± 2.46	20.45 ± 0.86
$Ti(C_{0.3},N_{0.7})$	**Young's Modulus (GPa)**	470.2	433.8	397.4
	Hardness (HV1)	-	-	1256.8 ± 85.2
	Indentation Fracture Resistance ($MPa.m^{1/2}$)	-	-	20.85 ± 0.88

The Vicker's hardness and indentation fracture resistance of the cermets may also potentially be used to predict their tribological behaviour, while providing a quantitative method with which to compare the materials. Cermets are often susceptible to both spalling and grain removal, due to the high hardness and wear resistance of the ceramic phase.[19,22,23,31,32-34] In combination, the hardness and the fracture resistance of the cermet will help determine if cracks will initiate in, and propagate though, the ceramic particle or

will result in debonding of the interface between phases. The hardness vs. facture resistance response for each cermet, at each of the binder contents (20 vol. % to the left and 40 vol. % to the right) is presented in Figure 48.

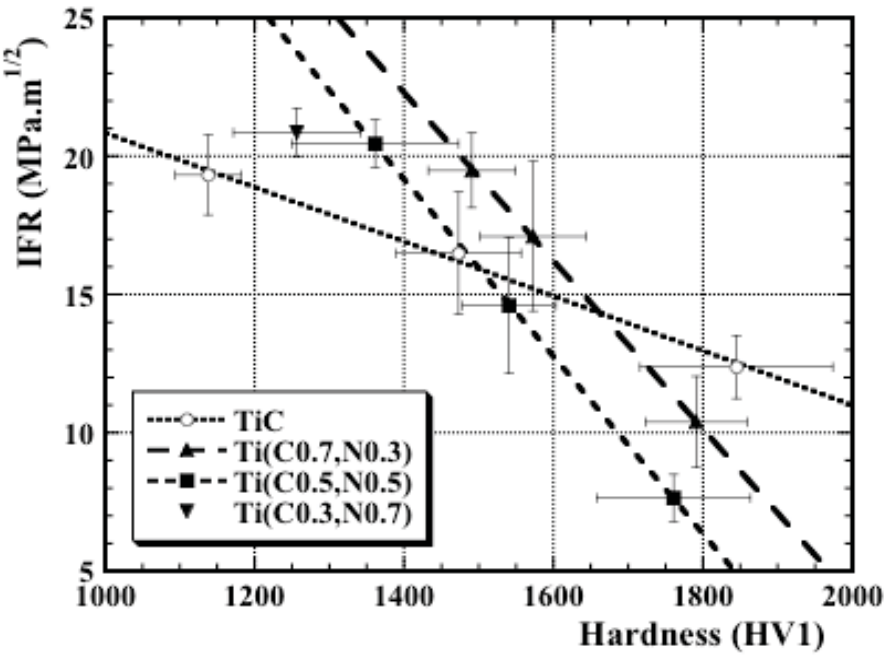

Figure 48. Vicker's hardness (1 kg load) vs. indentation fracture resistance (50 kg load), from 20 to 40 vol. % Ni_3Al binder (left to right).

Figure 48 demonstrates two clear trends in terms of the TiC and Ti(C,N) cermets. Following Table 18, samples of Ti(C,N) should become progressively tougher as the nitrogen content increases. However, the apparent trend indicates that the Ti(C,N) samples are initially less tough than TiC, and are toughened more through the addition of the binder than TiC. The discrepancy in toughness may potentially be explained by the presence of uninfiltrated regions within the sample. These regions would tend to have decreased hardness and fracture resistance, and may act as brittle crack initiation sites.[6] These sites, while individually small, decrease the overall toughness of the samples as they allow easy paths for crack growth. It is observed that the cermets, when viewed generally, give the expected trend of an increase in fracture resistance and a decrease in hardness as the binder content is raised. This is predicted to occur through the use of the

rule of mixtures used to estimate the Young's modulus and hardnesses of each cermet, as greater quantities of the soft, ductile metal matrix is added. Additionally, the cermets are predicted to increase in fracture resistance as the nitrogen content is increased.[1] Ti(C,N) cermets that are processed through the PSSS route tend to increase in fracture resistance, while maintaining or even increasing in hardness.[2] However, as may be seen, although the hardness remains comparable to that of TiC, the fracture resistance does not follow the expected trend. This follows the visual evidence of porosity already demonstrated in Figure 47.

Since the porosity acts as a stress raiser and potential crack initiation site, the greater the volume of porosity, the lower the hardness and fracture resistance. However, the degree to which each property is affected by the porosity need not be the same, as it appears fracture resistance is affected to a greater extent than hardness. The trends seen in Figure 48 displays this effect, as the Ti(C,N) cermets tend to have similar hardnesses but lower fracture resistance when compared to pure TiC. This is exemplified by the 20 vol. % samples (the first data point in each trend line). By the rule of mixtures, $Ti(C_{0.5},N_{0.5})$ should be the most ductile of the cermets, yet testing indicates it is the least. At 20 vol. % the $Ti(C_{0.5},N_{0.5})$ samples have the largest residual porosity, decreasing the effectiveness of the binder addition. Since an increased binder content decreases the porosity, the trend of the Ti(C,N) cermets first being less resistant than TiC and later more resistant to fracture may be explained though the decrease in porosity.

6.4.2 Reciprocating Wear Behaviour

For the reciprocating wear analysis, each of the TiC-Ni_3Al and Ti(C,N)-Ni_3Al samples were tested with applied loads of 20 N, 40 N, 60 N, and 80 N, with a WC-Co counter-face sphere, utilising the test conditions outlined previously. Figure 49 demonstrates the wear rate for each of the examined samples, as a function of Ni_3Al binder content and applied load; the wear rate data in this instance is generated through the use of three-dimensional optical profilometry measurements. A consistently observed trend with these measurements is that the wear loss increases in a nominally exponential manner, as the applied load is increased. Additionally, it may be seen that the intermediate composition

(30 vol. % Ni_3Al) is the most resistant to damage for the highest C containing cermets (i.e. TiC and $Ti(C_{0.7},N_{0.3})$). Conversely, the highest Ni_3Al containing compositions (i.e. 40 vol.%) are the generally most wear resistant for the higher N containing cermets (i.e. $Ti(C_{0.5},N_{0.5})$ and $Ti(C_{0.3},N_{0.7})$), where densification is the most dependent upon binder volume fraction, as shown in Figure 50. However, this effect is subtle, and highlights the generally consistent wear response regardless of the C:N ratio.

(a)

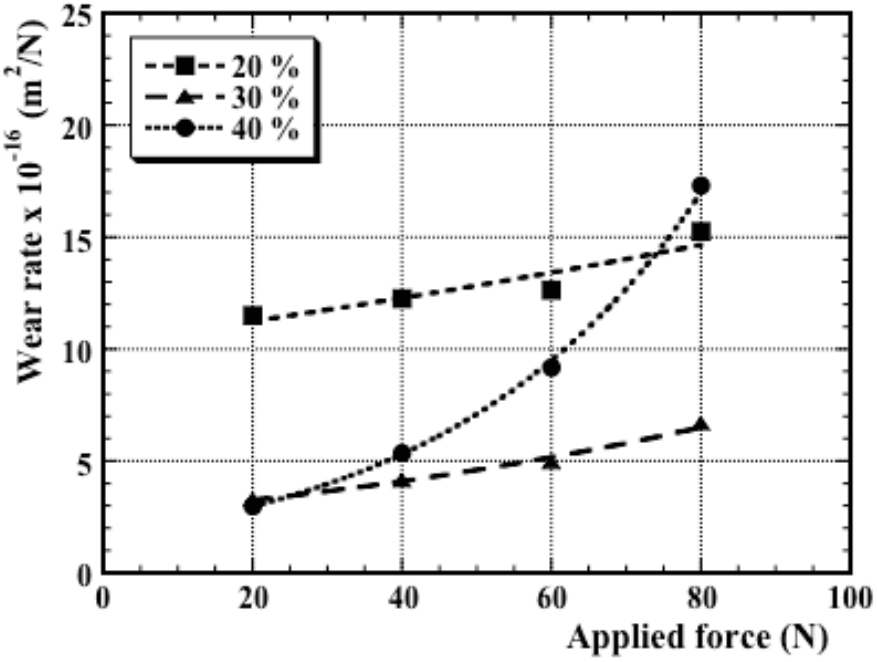

(b)

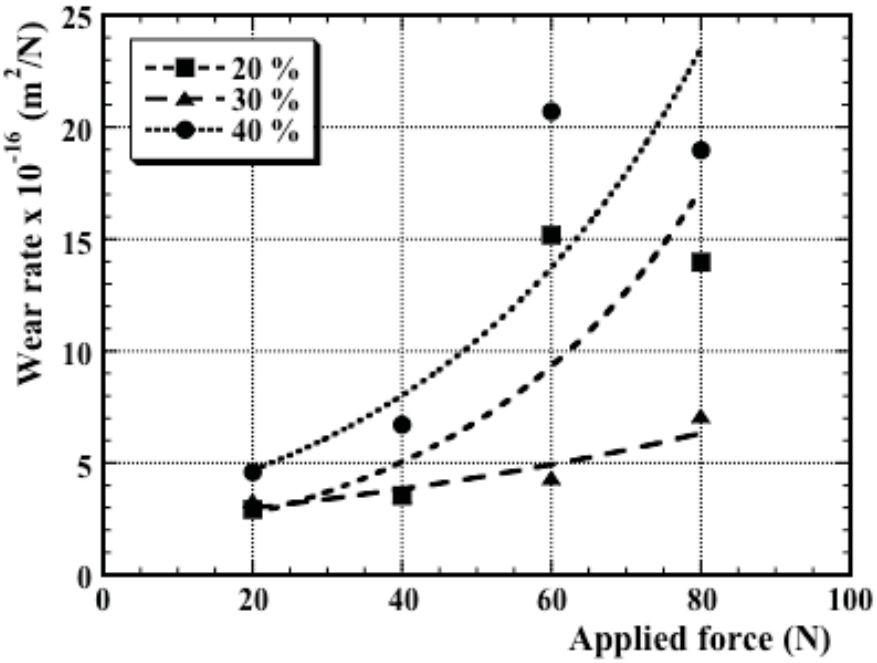
20 %
30 %
40 %
Wear rate x 10^-16 (m^2/N)
Applied force (N)
0
5
10
15
20
25
0
20
40
60
80
100

(c)

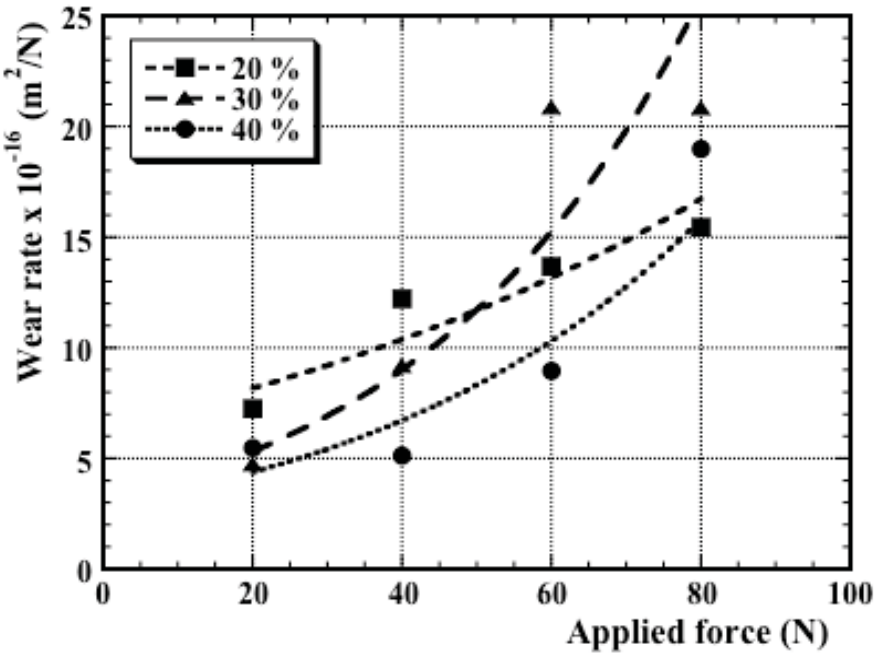
20 %
30 %
40 %
Wear rate x 10^-16 (m^2/N)
Applied force (N)
0
5
10
15
20
25
0
20
40
60
80
100

(d)

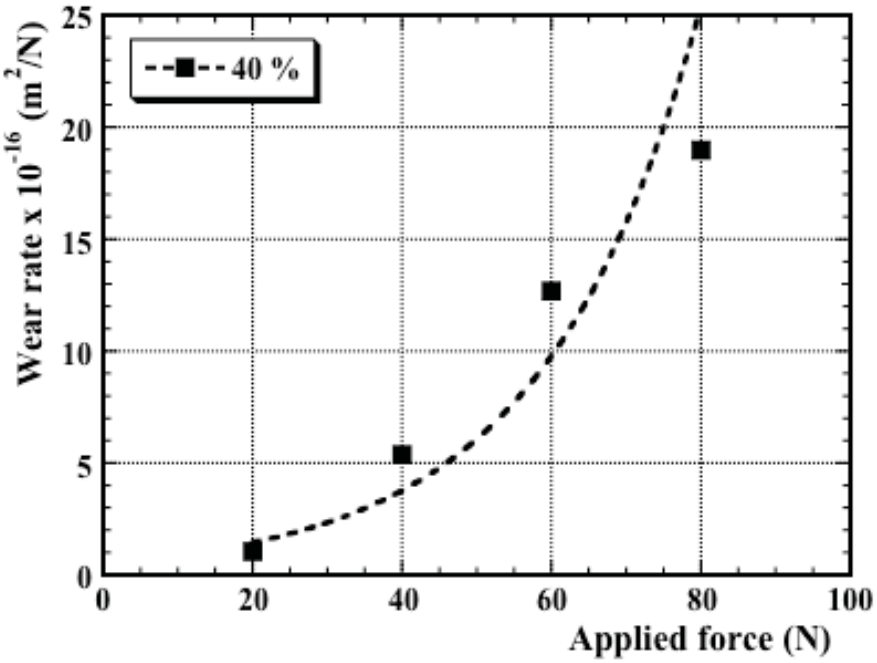

Figure 49. The effects of load and Ni_3Al binder content upon the reciprocating specific wear rate for cermets prepared with: (a) TiC, (b) $Ti(C_{0.7},N_{0.3})$, (c) $Ti(C_{0.5},N_{0.5})$, and (d) $Ti(C_{0.3},N_{0.7})$.

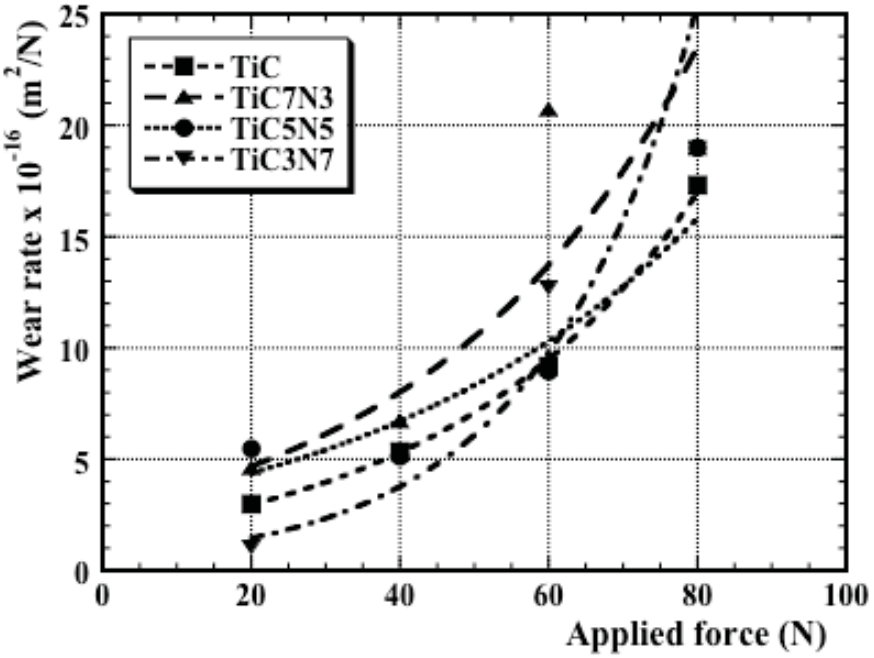

Figure 50. The effects of nitrogen content on the reciprocal wear rate for TiC to $Ti(C_{0.3},N_{0.7})$-Ni_3Al with 40 vol % Ni_3Al.

The coefficient of friction (COF) was assessed during the reciprocating wear tests using the UMT wear tester. The UMT is able to accurately determine the COF for every data point (with a resolution of ~5 mN), as well as determine the mean COF for the entire test. The results of the mean COF for each of the cermets, at binder contents of 20 and 40 vol. % are presented for each applied load in Figure 51.

(a)

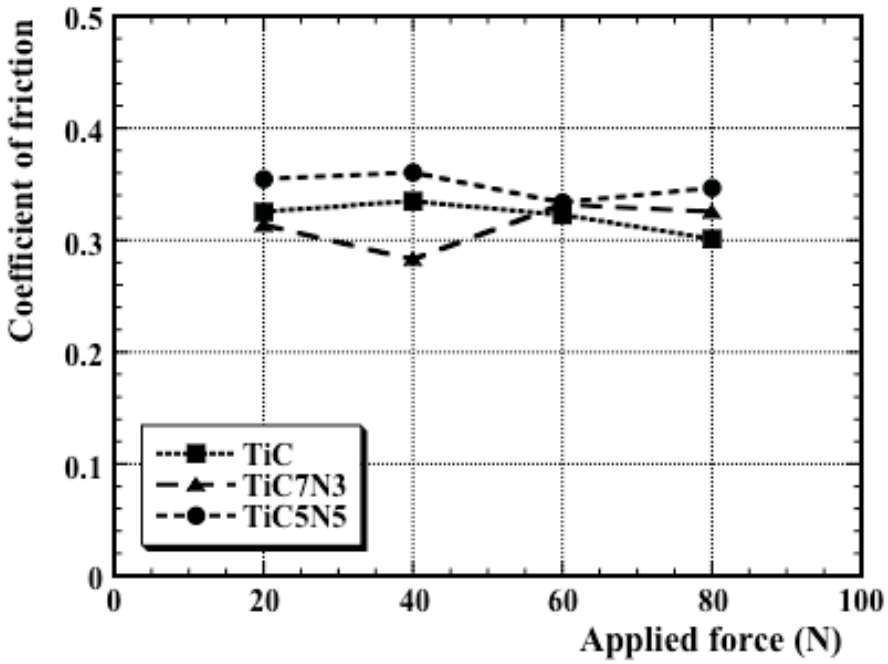

(b)

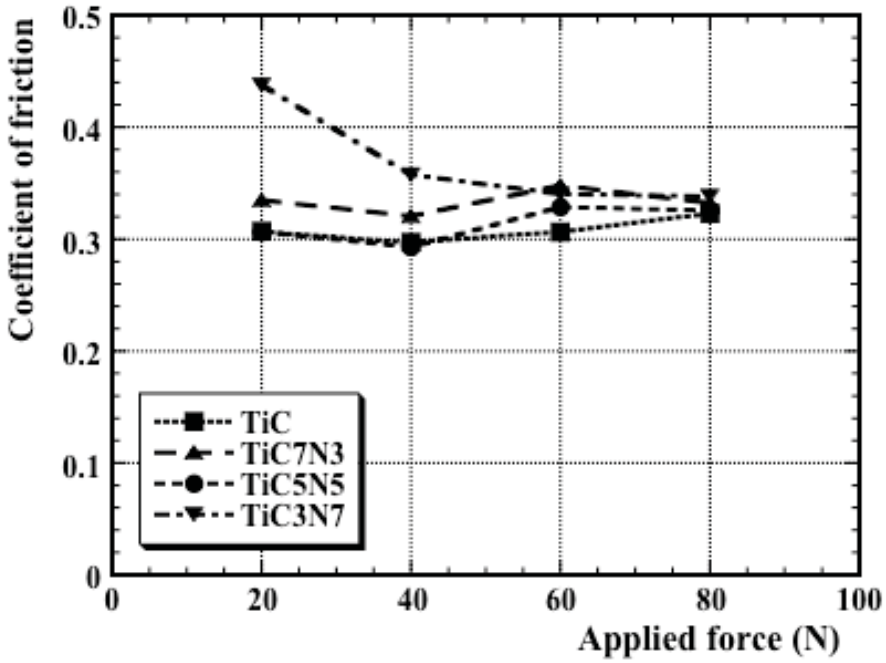

Figure 51. The mean COF of TiC and Ti(C,N) cermets as a function of applied load, for samples prepared with (a) 20 vol. % Ni_3Al and (b) 40 vol. % Ni_3Al.

It is apparent from Figure 51 that the COF remains essentially constant for all the samples, with a mean COF of 0.325 ± 0.028 determined. This response is regardless of the ceramic matrix used (i.e. C:N ratio), the Ni_3Al binder content, or the applied load during the wear tests. The small variances in the COF may be attributed to macroscopic inconsistencies in the samples (e.g. small, poorly infiltrated regions), spalling, or other damage. This information is important because it may indicate a shift in the wear mechanisms. Abrupt changes of the COF may indicate the wear mechanism is changing, or that macroscopic damage is being generated, such as spalling, or simply that macrostructural variation in the material is being exposed, such as encountering a pore.[19,35-37] A more gradual shift in the COF could indicate that a transition from 2-body to 3-body wear is occurring, or an abrasive dominant to adhesion dominant wear mechanism, such as the formation and gradual thickening of a tribolayer. As the COF data remains relatively constant for all of the reciprocating tests performed in the present work, the data cannot point toward any specific wear mechanism.[35,36,38] However, it may

still be used to infer that each of the TiC- and Ti(C,N)-Ni_3Al compositions are affected by essentially the same wear mechanisms at each load, and at each binder content.

The general trends observed in Figures 49 and 50, that the extent of wear decreases from 20 to 30 vol. % Ni_3Al for both TiC and $Ti(C_{0.7},N_{0.3})$ and then increases to 40 vol.%, and the decreasing wear from 20 to 40 vol.% Ni_3Al for $Ti(C_{0.5},N_{0.5})$ and $Ti(C_{0.3},N_{0.7})$ may be explained in part through the hardness and indentation fracture resistance data presented in Table 18, in combination with the observed sintering response of each composition. It has been previously demonstrated for TiC-Ni_3Al cermets that as the binder content is increased, the contiguity, a measure of the carbide-carbide grain contact, decreases.[24] For the TiC-Ni_3Al samples, the hardness and indentation fracture data of Table 18 indicates that at the lowest binder content (20 vol. %) the samples will act in a mostly brittle manner, failing largely due to grain cracking and pull out.[39] This may allow for large volumes of wear to occur rapidly, as the grains fracture and are then removed. As the binder content increases to 30vol. %, the wear mechanisms will reflect the transition from nominally brittle behaviour to a more ductile composite material. This may, in fact, decrease the total wear as the amount of plastic deformation increases. In terms of the wear mechanisms operating, the ductile Ni_3Al binder may exhibit a form of "plastic extrusion", where the binder is forced out from between the ceramic particles, due to the high compressive stress, and is then preferentially removed. This is known to introduce additional wear mechanisms including adhesive wear, with the concurrent formation of a tribolayer, which can coat both of the surfaces in contact.[39-43] This tribolayer, a combination of binder and wear debris (from the ceramic particles and WC sphere), lowers the wear rate by introducing an intermediate layer. As the binder content is increased to 40 vol. %, the properties of the cermets transition to favour those of the metallic binder, causing the cermets to become even more ductile in their response. Although this would indicate an increase in the volume of tribolayer, the samples also suffer from a greatly reduced hardness, resulting in greater wear amounts.

The TiC-Ni_3Al cermets are fully infiltrated for each of the three binder volumes, with densities in excess of 99% of theoretical, and as such they may be used as a guide for

predicting the behaviour of the Ti(C,N)-Ni_3Al cermets. This performance guideline is accurate for Ti($C_{0.7}$,$N_{0.3}$)-Ni_3Al, as seen in Figure 49(b), as the densification behaviour is comparable to the TiC-based cermets. However, there is an apparent deviation from this response for both the Ti($C_{0.5}$,$N_{0.5}$) and Ti($C_{0.3}$,$N_{0.7}$)-based cermets. This may be explained by the sintering response of these compositions, and in particular the homogeneity of the samples. As previously indicated, as the nitrogen content is increased the homogeneity of infiltration process decreases, resulting in small areas of porosity and lower levels of densification. These resulting uninfiltrated areas can then decrease the toughness of the samples because these sites allow a more easy path for crack growth and brittle fracture. As such, though the Ti($C_{0.5}$,$N_{0.5}$) and Ti($C_{0.3}$,$N_{0.7}$) cermets may essentially follow the same trend as TiC-Ni_3Al, full strengthening will not occur until full and uniform infiltration can be achieved.

In order to determine the causes of the wear associated with each of the ceramics, the applied loads, and the Ni_3Al binder content, the individual wear tracks have been imaged using both optical profilometry and SEM. The use of the optical profilometer allows quantification of changes in depth and also allows accurate resolution of the macroscopic details of the wear tracks. As previously demonstrated in Figure 47, the pseudo three dimensional images typically generated through the use of the optical profilometer can be used to highlight wear track features. Figure 52 depicts a typical cross-sectional wear track view that can be obtained using the optical profilometer. These cross sections allow for a clear comparison of the evolution of the wear tracks that are obtained, as a function of applied load, for TiC, Ti($C_{0.7}$,$N_{0.3}$), and Ti($C_{0.5}$,$N_{0.5}$) cermets prepared with 20 vol. % Ni_3Al.

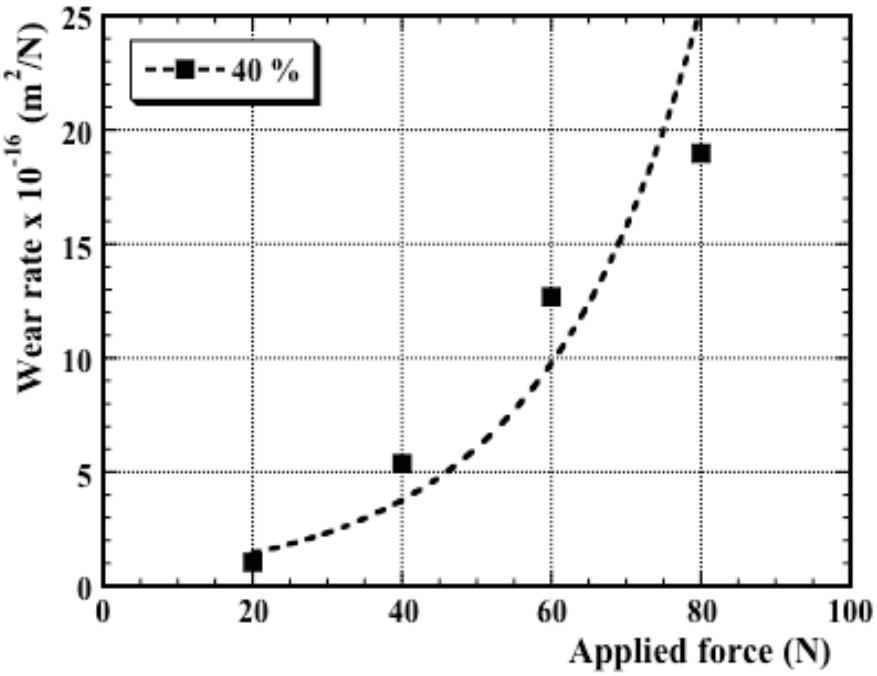
40 %
Wear rate x 10^-16 (m^2/N)
Applied force (N)
0
5
10
15
20
25
0
20
40
60
80
100

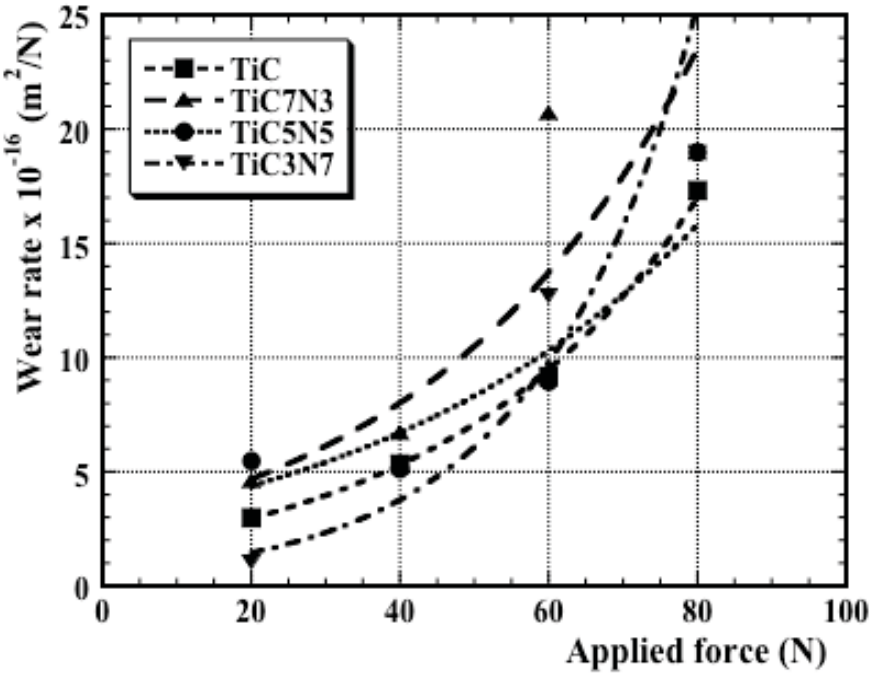
TiC
TiC7N3
TiC5N5
TiC3N7
Wear rate x 10^-16 (m^2/N)
Applied force (N)
0
5
10
15
20
25
0
20
40
60
80
100

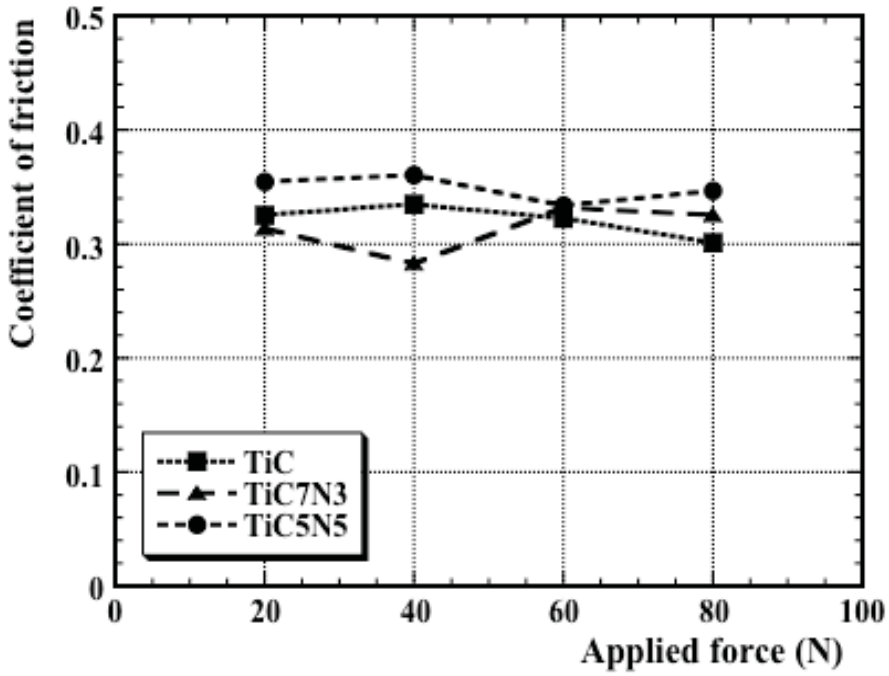

Figure 52. Optical profiles of the cross-sections of the wear track generated at loads of 20 to 80 N (left to right), for TiC, Ti($C_{0.5}$,$N_{0.5}$), and Ti($C_{0.7}$,$N_{0.3}$) with 20 vol. % Ni_3Al, from top to bottom.

The differences in wear resistance between the various materials become clear as the depths of the wear tracks are compared in Figure 47 and, in particular, in Figure 52. Although only a select group of images are displayed in Figures 47 and 52, for the sake of clarity, these comparisons have been completed for all the samples examined in the present work. It may be seen that the depths of the wear tracks compare directly to the results presented in Figures 49 and 50. The wear tracks may also be investigated in greater detail by examining each track individually using the optical profilometer, as demonstrated in Figure 53. This allows for the examination of specific macrostructural (and microstructural) features throughout the wear tracks. The evidence of material being ploughed and accumulated at the ends of the wear tracks, with both ploughing and cutting clearly visible, especially along the centre and of the wear track, are of particular interest as they are indicators of 2 and 3-body wear. Slight indentations and small “black spots” observed throughout the wear track are indications of either small sections of material

being removed or residual porosity. In the former case this is indicative of grain removal, grain pull out, and spalling, all common wear mechanisms for cermets.

(a)

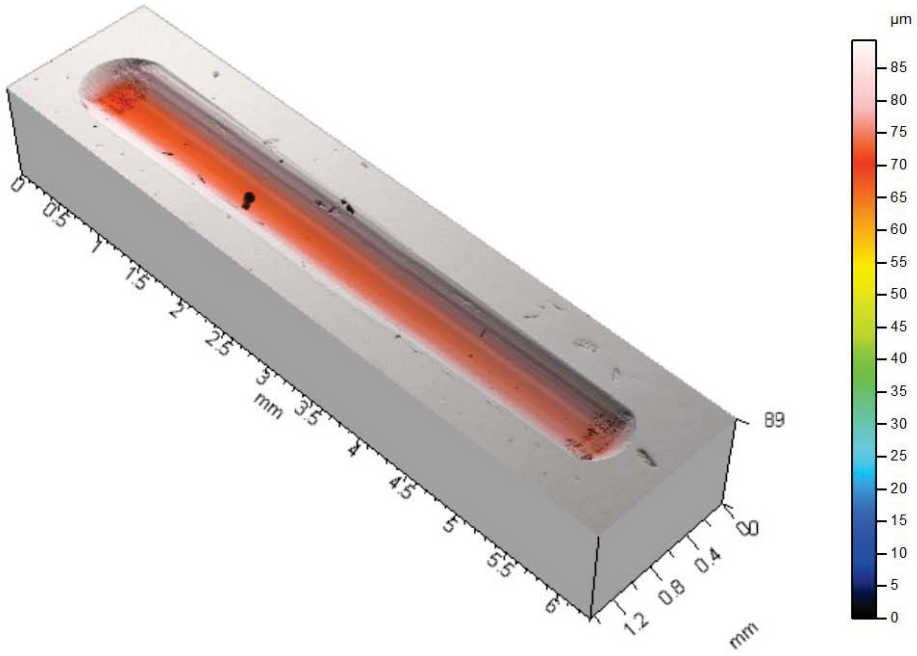

(b)

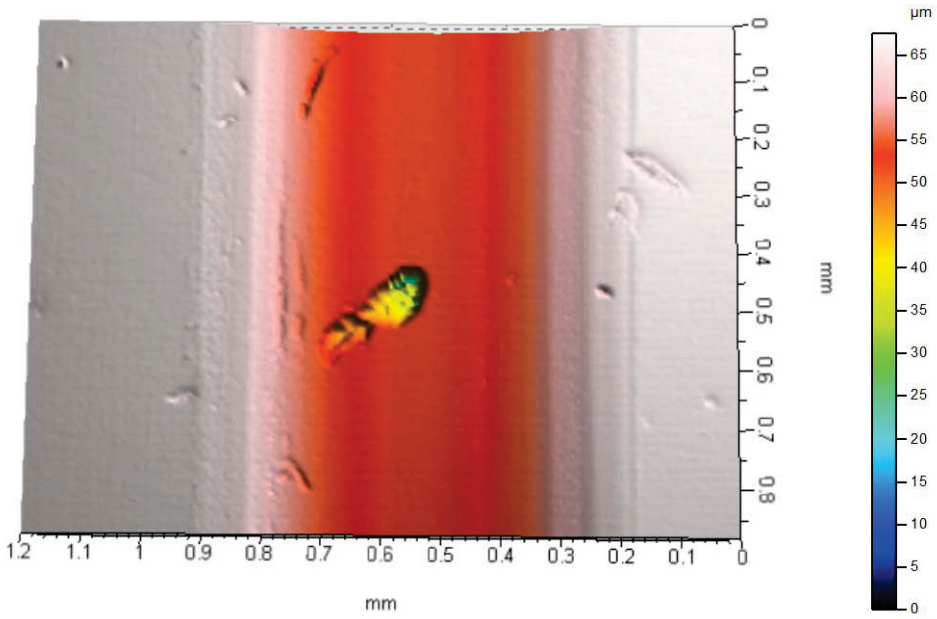

Figure 53. (a) Pseudo three dimensional analysis of a single wear track ($Ti(C_{0.5},N_{0.5})$-Ni_3Al at 20 vol. %). (b) Higher magnification image of a selected wear track feature.

In addition to the use of optical profilometry all of the wear tracks were examined using the SEM, while also performing compositional analysis using EDS. Figures 54 to display 56 micrographs of $Ti(C_{0.7},N_{0.3})$ and $Ti(C_{0.3},N_{0.7})$, each at a binder content of 40 vol. % Ni_3Al, for applied loads between 20 and 80 N. The images displays the changes arising at the ends of the wear tracks caused by the increase in the applied load, along with the effects of the increase in nitrogen content (Figure 54). The presence of the ploughed and deposited material at the ends of the wear tracks is indicative of 2-body and 3-body abrasive wear. 2-body wear is associated with the ploughing and cutting of the material, resulting in gouges within the wear track and uplift/deposition of material around the edges of the wear track, taking the form of pronounced ridges. The presence of the material deposited at the end of the wear tracks along with the gouges throughout the wear track indicate 2-body wear, yet the minimal presence of uplifted edges surrounding the wear track indicates 3-body wear. The combination of 2 and 3-body wear indicate abrasive wear as a dominant wear characteristic, yet the formation of the tribolayer

indicates adhesive wear. Examination of the sides of the wear tracks reveal minimal material uplift (Figure 55), and a relatively sharp transition from the wear track itself to the surrounding unloaded material, which indicates minimal plastic deformation away from the immediate vicinity of the wear track

(a)

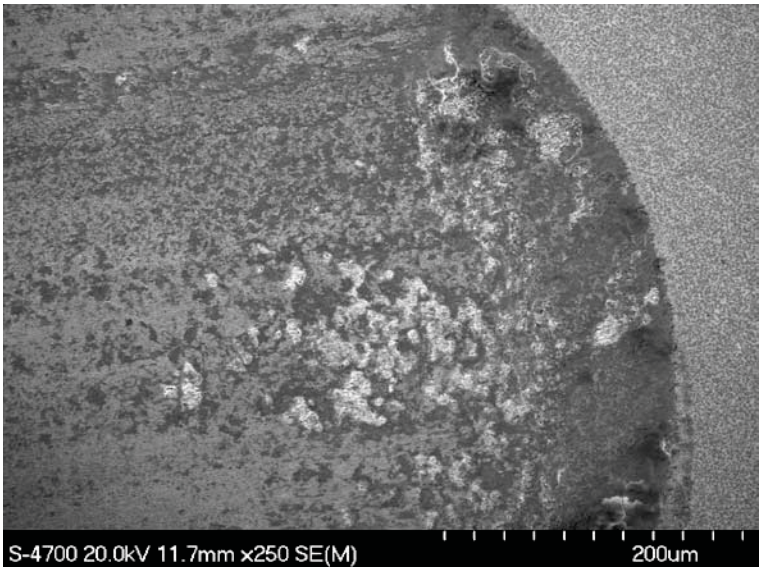

(b)

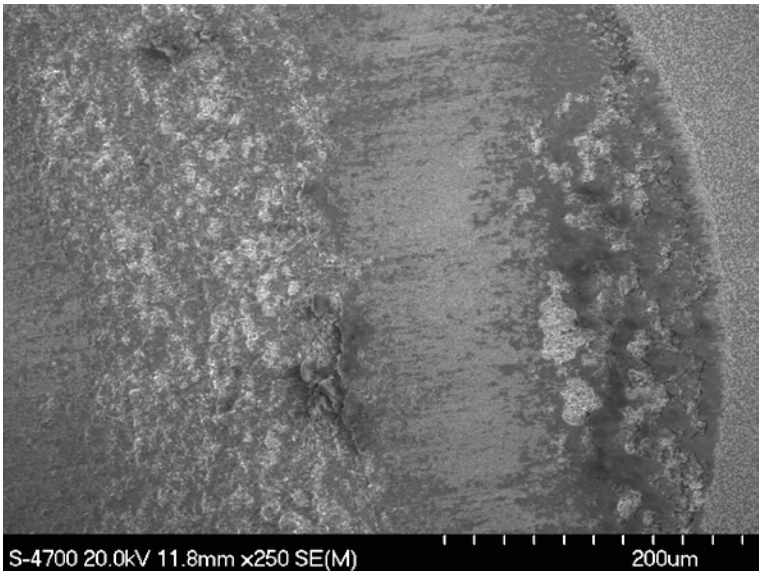

(c)

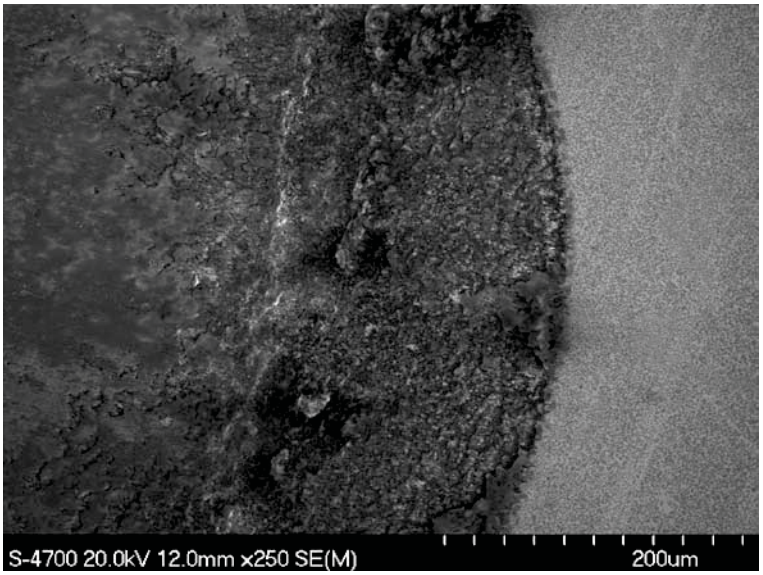

Figure 54. SEM images of the ends of the wear tracks formed for $Ti(C_{0.7},N_{0.3})$ with 40 vol. % Ni_3Al binder at loads of (a) 40 and (b) 80 N, and (c) for $Ti(C_{0.3},N_{0.7})$ with 40 vol. % Ni_3Al at a load of 60 N (nominal reciprocating direction left to right).

Figure 55. SEM image of the wear track edge for a $Ti(C_{0.7},N_{0.3})$ sample, prepared with 40 vol. % Ni_3Al, demonstrating minimal deformation outside of the wear track (nominal reciprocating direction left to right).

(a)

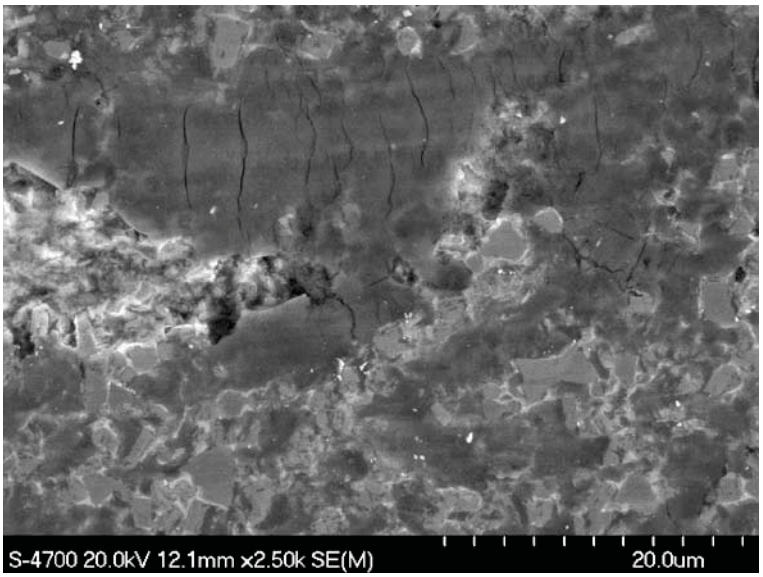

(b)

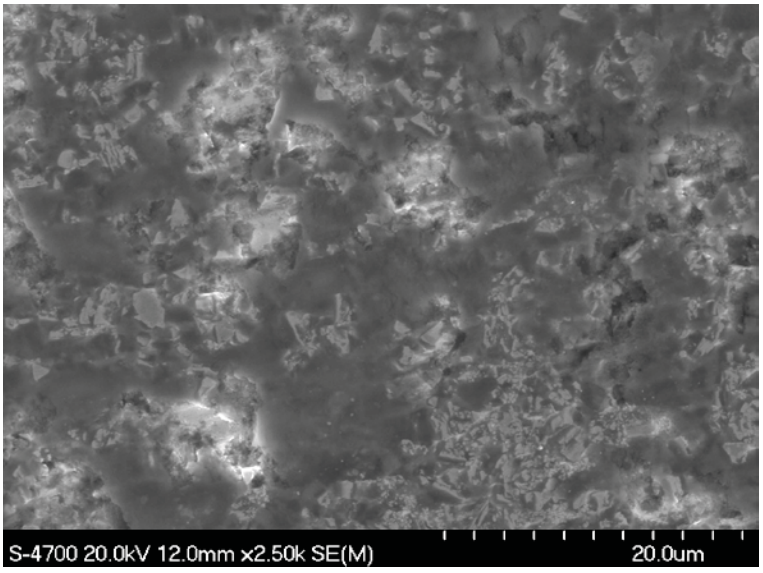

Figure 56. SEM images of the tribolayer formed for $Ti(C_{0.7},N_{0.3})$ with 40 vol. % Ni_3Al binder at loads of (a) 20 and (b) 60 N (nominal reciprocating direction left to right). Note the clear formation of Hertzian cracks perpendicular to the reciprocating direction in (a).

It is also apparent that the extent of tribolayer formation increases with applied load (Figure 56), nitrogen content, and binder content. EDS analysis indicates that the tribolayer consists of large quantities of oxides produced from the binder (i.e. Ni and Al) phase. In addition, the tribolayer also contains large quantities of Ti, from the original

Ti(C,N) and TiC grains, in conjunction with smaller amounts of W (up to 4 at. %). This arises from the breakdown of the ceramic particles (i.e. TiC or Ti(C,N)), as well as incorporation of debris from the WC-Co sphere, and entrainment of the debris within the initially ductile tribolayer; increasing oxidation of these components will, understandably, lead to a more brittle mechanical response.

It should be noted that cermets prepared with Ni_3Al binders show excellent high temperature strength retention,[17] in comparison to WC-Co.[7] The Ni_3Al binders have both excellent resistance to oxidation and an increasing yield strength with temperature.[16] Ni_3Al is known to form a protective, Al_2O_3-based passivating layer during elevated temperature oxidation.[18] In terms of the present work, all of the cermet constituents (with the obvious exception of C) may be expected to form passivating oxide surface layers, even at room temperature. The extensive oxide formation that is apparent within the tribolayer is expected to arise either through significant heat build-up during testing or through the continuous creation of new exposed surfaces during reciprocating wear. However, EDS mapping shows that the oxide formation is entirely restricted to the wear track, indicating that the later mechanism is more probable as some limited oxidation might be expected peripheral to the wear track if solely due to heat build-up.

To investigate the wear processes further, the SEM was also used to observe the wear surface more closely, as shown in Figure 57. Several wear characteristics are demonstrated that are expected to be prominent for reciprocating wear of the cermets; these include the preferential removal of regions of binder (A), which may be associated with Ti(C,N) grain movement, the deposition of wear debris (B), the initiation of cracking within the ceramic phase (C), and the continued fracture and removal of debris (D). As the surface is abraded, the compressive forces cause the binder to undergo “extrusion” and it may then be preferentially removed. As this occurs, the force required to then remove the ceramic grains decreases until they are pushed from the binder, as shown by the dark area within the vicinity of region (B). The abrasive forces also act directly upon the ceramic grains, impinging upon irregularities via Hertzian loading and initiating cracks (C).[44,45] As the abrasion continues, the ceramic particles will continue to break

down and be removed (D). It may be observed that the cracks tend to be perpendicular to the direction of wear. This is due to repeated Hertzian loading, and is typical for fatigue fracture behaviour in brittle materials.

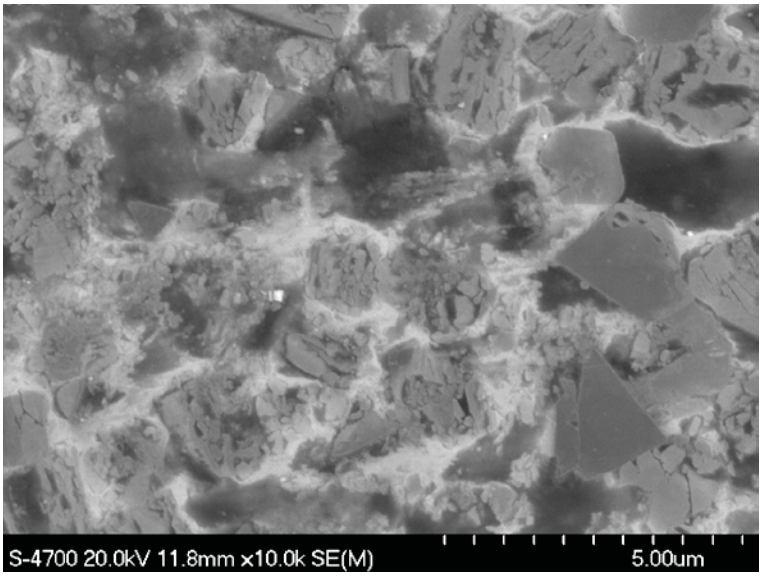

Figure 57. SEM micrograph displaying wear features for $Ti(C_{0.7},N_{0.3})$, with 40 vol. % Ni_3Al, using an applied load of 40 N for the reciprocating test (nominal reciprocating direction left to right). Specific highlighted features are referred to in the text.

The initial accumulation of tribolayer is also apparent in Figure 57, as the Ni_3Al binder can be seen to be partially smeared across the fragmenting Ti(C,N) grains. As the binder and wear debris of both the ceramic particles and the WC-Co spherical indenter undergo wear and are removed, they may become trapped, passing over and/or between the wear surfaces as either an adhered layer or in 3-body wear scenario. In this manner the TiC/Ti(C,N) and WC-Co particles impact and become embedded within the ductile binder, contributing to the tribolayer; an example of a WC-based fragment is shown at point (B). Due to the high repetition of impact, a nearly homogenous layer is formed from the deformed binder and the hard carbide-based particles, which ultimately exhibits a high O content due to the continual formation of new exposed surfaces.

6.5 Conclusions

TiC and Ti(C,N) based cermets with Ni_3Al binder contents between 20 and 40 vol. % were fabricated using a simple melt-infiltration process, and were subsequently evaluated for their fretting wear response using a ball-on-flat configuration, with WC-Co counter-face spheres.. Due to relatively poor infiltration with the lower Ni_3Al binder contents (i.e. 20 and 30 vol. %), the highest N containing samples (i.e. with $Ti(C_{0.3}, N_{0.7})$), could not be evaluated. Hardness and indentation fracture resistance testing were conducted on all of the successfully densified cermets, and it was determined that the hardness decreases while indentation fracture resistance increases, as the Ni_3Al binder content increases for all samples. TiC-Ni_3Al cermets demonstrated the highest combined hardness and indentation fracture resistance at low binder contents, which may be attributed to the slight structural inhomogeneity observed for the Ti(C,N) samples (which increases with N content, combined with an expected larger binder intercept distance due to microstructural coarsening. However, at the highest Ni_3Al binder content (40 vol. %) all the Ti(C,N) cermets exhibit a better combination of hardness and indentation fracture resistance than the equivalent TiC-based material, with $Ti(C_{0.7},N_{0.3})$ performing the best. This may be attributed to an increased hardness with increasing N content, improved homogeneity in the densified cermet due to the high binder content, and a finer ultimate grain size. The addition of N alters the rate at which the hardness decreases with the addition of the binder, allowing the Ti(C,N) samples to retain their hardness while becoming tougher for identical binder contents when compared with TiC.

It was determined for each of the examined compositions that as the load was increased the wear volume, and consequently the rate and extent of wear, increased. This was confirmed through the use of an optical profilometer, allowing for accurate measurements of both the wear track volume and cross-sectional profile. Though each of the compositions displayed this general trend with increasing load, the volumetric wear, for both TiC and $Ti(C_{0.7}, N_{0.3})$, was lowest at 30 vol. % Ni_3Al binder, with the rate being highest for TiC with 20 vol. % binder. Conversely, TiC samples with 40 vol.% binder showed a smooth transition from low wear at low loads (comparable to 30 vol. % Ni_3Al) to high wear at the highest loads (comparable to 20 vol. % Ni_3Al). $Ti(C_{0.5}, N_{0.5})$ and

$Ti(C_{0.3}, N_{0.7})$ both showed a general decrease in the wear rate as binder content increases, with $Ti(C_{0.5}, N_{0.5})$ at 30 vol. % transitioning from low to high wear. This may be explained by the slightly lower level of microstructural homogeneity caused by the increased nitrogen content, with small regions of poorly-infiltrated ceramic matrix.

Observations garnered from optical profilometry and SEM/EDS determined that the cermets (at every nitrogen content, at each load, and each binder content) suffered abrasive wear as the primary form of wear. This took the form of preferential binder removal due to direct loading and abrasion, grain fracture, and grain pull-out (both fracture and pull-out arising from a form of fatigue induced by Hertzian loading). The combination of 2 and 3-body wear caused debris to form and accumulate at the ends of the wear tracks and to form a tribolayer of the mixture of all wear debris throughout the wear track, but without causing significant uplift around the edges of the wear track. As the load increased there was a noticeable increase in formation of the tribolayer. EDS analysis indicated that the tribolayer is comprised of WC and TiC/Ti(C,N) particles, as well as being formed mainly of the Ni_3Al binder and its oxide (having a high oxygen content).

6.6 Acknowledgements

This study was supported by Petroleum Research Atlantic Canada (PRAC) and the Natural Sciences and Engineering Research Council of Canada (NSERC). The support of the Canada Foundation for Innovation, the Atlantic Innovation Fund, and other partners who helped fund the Facilities for Materials Characterisation, managed by the Dalhousie University Institute for Materials Research, are also gratefully acknowledged. The authors would also like to thank Brad Collier for his assistance during the initial stages of this study and Dean Grijm for technical assistance.

6.7 References

1. S. Zhang: 'Titanium carbonitride-based cermets: Processes and properties', *Mater. Sci. Eng. A*, 1993, **163**, (1), 141-148.
2. S. Zhang: 'Material development of titanium carbonitride-based cermets for machining application', *Key Eng. Mater.*, 1998, **138**, (1), 521-543.
3. G. Levi, W.D. Kaplan and M. Bamberger: 'Structure refinement of titanium carbonitride (TiCN)', *Mater. Lett.*, 1998, **35**, (5-6), 344-350.
4. H.Y. Liu, J.H. Huang, C.F Yin, J.G. Zhang and G.B. Lin: 'Microstructure and properties of TiC–Fe cermet coatings by reactive flame spraying using asphalt as carbonaceous precursor', *Ceram. Int.*, 2007, **33**, (5), 827-835.
5. J. Pirso, M. Viljus and S. Letunovitš: 'Friction and dry sliding wear behaviour of cermets', *Wear*, 2006, **260**, (7-8), 815-824.
6. P. Ettmayer, H. Kolaska and K. Dreyer: 'Effect of the sintering atmosphere on the properties of cermets', *Powder Metall. Int.*, 1991, **23**, (4), 224-230.
7. W. Acchar, U.U. Gomes, W.A. Kaysser and J. Goring: 'Strength degradation of a tungsten carbide-cobalt composite at elevated temperatures', *Mater. Charact.*, 1999, **43**, (1), 27–32.
8. Z.N. Farhat: 'Microstructural characterization of WC-TiC-Co cutting tools during high-speed machining of P20 mold steel', *Wear*, 2003, **51**, (2-3), 117-130.
9. D. Mari, S. Bolognini, G. Feusier, T. Cutard, C. Verdon, T. Viatte and W. Benoit: 'TiMoCN based cermets. Part I: Morphology and phase composition', *Int. J. Refract. Met. Hard Mater.*, 2003, **21**, (1-2), 37-46.
10. T.N. Tiegs, P.A. Menchhofer, K.P. Plucknett, P.F. Becher, C.B Thomas and P.K. Liaw: 'Comparison of sintering behavior and properties of aluminide-bonded ceramics', *Ceram. Eng. Sci. Proc.*, 1998, **19**, (3), 447-455.
11. L. Yin, Y. Jin, H. Yu and J. Ye: 'Ultrafine (Ti, M)(C, N)-based cermets with optimal mechanical properties', *Int. J. Refract. Met. Hard Mater.*, 2011, **29**, (1), 104-107.
12. S. Zhang and G.Q. Lu: 'Sintering kinetics of Mo-free cermets', *J. Mater. Process Technol.*, 1997, **67**, (1-3), 162-166.

13. W.T. Kwon, J.S. Park and S. Kang: 'Effect of group IV elements on the cutting characteristics of Ti(C,N) cermet tools and reliability analysis', *J. Mater. Process. Technol.*, 2005, **166**, (1), 9-14.
14. H. Zhang, J. Yan, X. Zhang and S. Tang: 'Properties of titanium carbonitride matrix cermets', *Int. J. Refract. Met. Hard Mater.*, 2006, **24**, (3), 236-239.
15. J. Wang, J. Liu, Y. Feng, J. Ye and M. Tu: 'Effect of NbC on the microstructure and sinterability of $Ti(C_{0.7},N_{0.3})$-based cermets', *Int. J. Refract. Met. Hard Mater.*, 2009, **27**, (3), 549-551.
16. D.M. Dimiduk: 'Dislocation structures and anomalous flow in $L1_2$ compounds', *J. Phys. III*, 1991, **1**, (6), 1025-1053.
17. K.P. Plucknett, P.F. Becher and S.B. Waters: 'Flexure strength of melt-infiltration-processed titanium carbide/nickel aluminide composites', *J. Amer. Ceram. Soc.*, 1998, **81**, (7), 1839-1844
18. S.C. Choi, H.J. Cho, Y.J. Kim and D.B. Lee: 'High-temperature oxidation behavior of pure Ni_3Al', *Oxid. Met.*, 1996 **46**, (1-2), 51-72.
19. G.W. Stachowiak and A.W. Batchelor: 'Engineering tribology', 3rd edn; 2005, Amsterdam, Elsevier Butterworth-Heinemann.
20. E.H. Smith: 'Mechanical engineer's reference book', 12th edn, 9/3-124; 1998, Boston, Butterworth-Heinemann.
21. J.P. Delplanque, S. Johnson, Y. Zhou: 'Spray Deposition and Coating Processes', in 'Materials processing handbook', (ed. M.T. Powers, E.J. Lavernia, J.R. Groza and J.F. Shackelford JF), 11/1-24; 2007, Boca Railton, CRC Press.
22. P. Bowen, C. Bonjour, C. Carry, D. Gonseth, H. Hofmann, D. Mari, R. Mulone and P. Streit: 'Novel alumina titanium-carbonitride nickel composites', *JOM*, 1995, **47**, (11), 56-58.
23. B.V. Manoj Kumar and B. Basu: 'Fretting wear properties of TiCN-Ni cermets: Influence of load and secondary carbide addition', *Metall. Mater. Trans. A*, 2008, **39**, (3), 539-550.
24. K.P. Plucknett and P.F. Becher: 'Processing and microstructure development of titanium carbide-nickel aluminide composites prepared by melt infiltration/sintering (MIS)', *J. Am. Ceram. Soc.*, 2001, **84**, (1), 55-61.

25. R.B. Collier and K.P. Plucknett: 'Spherical indentation damage in TiC-Ni_3Al composites', *Int. J. Refract. Met. Hard Mater.*, 2012, **30**, (1), 188-195.
26. M.I. Mendelson: 'Average grain size in polycrystalline ceramics', *J. Am. Ceram. Soc.*, 1969, **52**, (8), 443-446
27. G.R. Anstis, P. Chantikul, B.R. Lawn and D.B. Marshall: 'A critical evaluation of indentation techniques for measuring fracture toughness. I. Direct crack measurements', *J Am Ceram Soc.*, 1981, **64**, (9), 533-538.
28. ASTM standard C1327: 'Standard test method for Vickers indentation hardness of advanced ceramics', ASTM international, West Conshohocken, US, 2008.
29. S. Buchholz, Z.N. Farhat, G.J. Kipouros and K.P. Plucknett: 'The Reciprocating Wear Behaviour of TiC-Ni_3Al Cermets', submitted to *Int. J. Refract. Met. Hard Mater.*, (Dec. 2011).
30. E.D. Churbanov, V.F. Moisee, V.P. Nechaev, B.L Taubkin, L.G Maskhuliya and N.V. Petrov: 'Wettability of refractory compounds by intermetallic compounds', *Khimicheskoe i Neftekhimicheskoe Mashinostroenie*, 1991, Iss. (10), 34-35.
31. J. Larsen-Basse: 'Abrasive wear of some titanium-carbonitride-based cermets', *Mater. Sci. Eng. A.*, 1988, **105**, (2), 395-400.
32. J. Karthikeyan: 'Ceramic coating technology', *Sādhanā*, 1988, **13**, (1), 139-156.
33. O. Knotek, F. Loffler, G. Kramer: 'Applications to Cutting Tools', in 'Handbook of hard coatings', (ed. R.F. Bunshah), Vol. 1, 370-406; 2001, Park Ridge, NJ, William Andrew Publishing/Noyes.
34. C. Zweben: 'Metal Matrix Composites, Ceramic Matrix Composites, Carbon Matrix Composites, Carbon Matrix Composites, and Thermally Conductive Polymer Matrix Composites' in 'Handbook of plastics, elastomers, and composites', (ed. C.A. Harper), 4th ed., 321-344; 2002, Tow Penn Plaza, McGraw-Hill.
35. B. Bhushan: 'Introduction to Tribology', 207-280, 2002, New York, John Wiley & Sons.
36. H. Czichos: 'Tribology: A systems approach to the science and technology of friction, lubrication, and wear', 1st edn, 45-246, 1978, Amsterdam, Elsevier North Holland.

37. H. Chen and I.M. Hutchings: 'Abrasive wear resistance of plasma-sprayed tungsten carbide-cobalt coatings', *Surf. Coat. Technol.*, 1998, **107**, (2), 106-114.
38. Y. Yeong, J.F. Lin and C.F. Ai: 'Correlation between three-body wear and tribological characteristics of titanium nitride, titanium carbonitride and titanium carbide coatings', *Wear*, 1997, **208**, (1), 147-154.
39. J. Pirso, M. Viljus, K. Juhani and S. Letunovitš: 'Two-body dry abrasive wear of cermets', *Wear*, 2009, **266**, (1-2), 21-29.
40. Y.Y. Guu and J.F. Lin: 'Analysis of wear behaviour of titanium carbonitride coatings', *Wear*, 1997, **210**, (1-2), 245-254.
41. Y.Y. Guu, J.F. Lin and C.F. Ai: 'The tribological characteristics of titanium carbonitride coatings prepared by cathodic-arc ion plating technique', *Thin Solid Films*, 1996, **287**, (1-2), 16-24.
42. C. Wei, J.F. Lin, T.H. Jiang and C.F. Ai: 'Tribological characteristics of titanium nitride and titanium carbonitride multilayer films. Part I: The effect of coating sequence on material and mechanical properties', *Thin Solid Films*, 2001, **381**, (1), 94-103.
43. C. Wei, J.F. Lin, T.H. Jiang and C.F. Ai: 'Tribological characteristics of titanium nitride and titanium carbonitride multilayer films. Part II: The effect of coating sequence on tribological properties', *Thin Solid Films*, 2001, **381**, (1), 104-118.
44. A.C. Fischer Cripps and R.E. Collins: 'The probability of Hertzian fracture', *J. Mater. Sci.*, 1994, **29**, (8), 2216-2230.
45. J. Lu, G.A. Sargent and H. Conrad: 'Study of the mechanisms of erosion in silicon single crystals using Hertzian fracture tests', *Wear*, 1995, **186**, (1), 105-116.

Chapter 7: Conclusions

The initial phase of this project was to develop and optimise a fabrication method for the Ti(C,N)-Ni_3Al cermets. This process was initially hypothesised to follow the same approach used in previous research for TiC-Ni_3Al cermets. However, this proved to not be possible due to the differences in compaction properties. The method used for TiC was successfully adapted to include a ball milling process used to add 1 wt. % PVB to the Ti(C,N) powders prior to compaction. This addition allowed for the successful compaction of Ti(C,N) preforms and their subsequent melt-infiltration.

Difficulty arose with the infiltration of certain samples, due to the decreased wetting and sintering that occurred with increased nitrogen content. Although this was expected, the degree to which the samples were affected was not. Despite the fact that all samples were successfully fabricated using the described sintering methods, the degree of infiltration was decreased to the point where many areas remained uninfiltrated throughout the 20 vol. % Ni_3Al samples for both $Ti(C_{0.7},N_{0.3})$ and $Ti(C_{0.5},N_{0.5})$. Additionally, the $Ti(C_{0.3},N_{0.7})$ samples for 20 and 30 vol. % were not suitable for testing. This difficulty was mitigated by increasing the quantity of binder, allowing $Ti(C_{0.3},N_{0.7})$ to form testable samples.

It was observed that some of the samples suffered from “cupping” during infiltration which worsened as the nitrogen content was increased. This demanded that a grinding and polishing scheme be developed. Due to the extreme hardness of the cermets, traditional grinders were not capable of producing the required finish to allow polishing, therefore a diamond wheel surface grinder was used for the initial preparation stages. Through grinding and polishing, samples for TiC, $Ti(C_{0.7},N_{0.3})$, and $Ti(C_{0.5},N_{0.5})$ were successfully created with Ni_3Al binder contents of 20, 30, and 40 vol. %. For $Ti(C_{0.3},N_{0.7})$, but only samples with 40 vol. % binder were able to be tested.

The reciprocating wear testing was completed using high loads (20 to 80 N), a high frequency, and a long duration. These parameters were chosen because they allow for the production of wear at an observable rate, both visually and using a balance with a resolution in the fifth decimal place. However, the mass loss during wear testing was low

enough that the data could not be reliably used because of inherent error in the scale and environmental factors. Consequently, the extent ofwear was determined through the use of an optical profilometer. Using the method described in Chapter 3, optical profilometry was successfully completed at both high and low resolutions, and was able to determine the volumetric wear rate. It was also used to examine the wear tracks in a pseudo three dimensional image.

When examined together, the Vicker's hardness, indentation fracture resistance, wear rates, SEM imagery, and EDS indicate that each of the samples suffer from a combination of abrasive wear (with a combination of 2 and 3-body wear being evident), adhesive wear (notably present in the form of a new tribolayer), and fretting wear (present in both the breakdown of the ceramic phase and the large quantity of oxide formation). By the presence of scaring, gouging, and the build up of deposited material at the ends of the wear track 2-body wear would be expected, yet the indicative ploughing and pushed up material around the edge of the track is not present. The missing material from the edges of the samples, along with the large volume of embedded wear debris, points to 3-body wear. It is also apparent that the binder is removed preferentially. This ductile material becomes trapped between the two surfaces as either wear debris or as an adhered layer. The other debris, TiC/Ti(C,N) and WC, will contact the ductile material and become embedded within it, forming a tribolayer. Additionally, due to the continual contact and mixing of the tribolayer, it forms a relatively homogenous composition for each of the samples. This includes the large quantity of oxide that is formed. As the tribolayer, especially the Ni_3Al, is impacted and mixed, new exposed surfaces are repeatedly formed. Ni_3Al is known to form a passivating Al_2O_3-based oxide layer in the presence of high temperatures (generated through the vigorous contact between surfaces), and/or form repetitive impact.

The examination of the wear tracks also indicates that each of the samples were affected by the same wear mechanisms. This is apparent from the imagery of the samples and from the COF data. The COF for all of the samples, excluding those with large defects (spalling or porosity) remained relatively constant at 0.325 ± 0.028. While this in itself may not indicate a specific wear type, it does infer that the samples are effected by the same wear mechanisms.

However, through the conducted wear testing several trends are made apparent. It is observed that the TiC-Ni_3Al cermets decrease in wear volume as the binder content increases from 20 to 30 vol. % (the 30 vol. % sample showing the lowest wear). The wear rate then increases as the binder content is increased to 40 vol. %. A smooth transition is observed at this binder content, from low wear rates similar to the 30 vol. % sample at low applied loads to high wear rates behaving like the 20 vol. % sample at high applied loads. This trend is also witnessed in the $Ti(C_{0.7},N_{0.3})$-Ni_3Al samples. This behaviour may be attributed to the increase of binder content, allowing the samples to transition from acting in a brittle fashion to a more ductile one. This will allow for an increased formation of the tribolayer while still retaining the strength of the ceramic phase. However, a further increase in binder content allows for samples to act in a more ductile manner. This reduces the hardness of the cermet to a degree that ploughing and gouging are able to remove material at a faster rate, even though the tribolayer is further increased.

The wear resistance of $Ti(C_{0.5},N_{0.5})$-Ni_3Al and $Ti(C_{0.3},N_{0.7})$-Ni_3Al shows a constant increase from 20 to 40 vol. % binder. Due to poor infiltration, the samples for both of these materials have uninfiltrated areas which greatly reduce the indentation fracture resistance. The volume fraction of these areas increases with increasing nitrogen content, and decreasing binder content. As such, though the materials may in truth follow the same trends as TiC and $Ti(C_{0.7},N_{0.3})$-Ni_3Al, the samples are not fully strengthened until infiltration is complete.

Comparing the samples, it becomes clear that though TiC initially has the best hardness and toughness, as binder content increases, the hardness of TiC decreases at a faster rate than the Ti(C,N) samples. This allows for fully infiltrated samples of Ti(C,N) to show improved properties when compared to TiC for all compositions tested. It is also observed that as nitrogen content increases for the Ti(C,N) samples, the hardness decreases and the toughness increases.

As with any study, time has a limiting effect on the research that may be completed. As such, several avenues of study that have become apparent could not be pursued. One such avenue is research into the sintering properties of the Ti(C,N)-Ni_3Al cermets. The presence of uninfiltrated areas has had a limiting effect, the removal of which will greatly increase the properties of the material. It is recommended that the

effect of sintering time and temperature be investigated. Additionally, it is recommended that the effect of preblending the ceramic and metallic binder phases be examined as a method to increase infiltration.

It is recommended that testing of these cermets be conducted at elevated temperatures. This project has been focussed on the development of a viable production, testing, and evaluation method of these cermets, along with the comparison of the various cermets at room temperature. However, both Ti(C,N) and Ni_3Al are known for their abilities to retain their mechanical properties at elevated temperatures. As such, testing at elevated temperatures may display greatly improved properties to current standard materials.

Sectioning of the wear tracks using a focussed ion beam (FIB) is also recommended. The benefit of this sectioning would be two fold. By sectioning the sample, the tribolayer and the ploughed material at the end of the wear tracks may be investigated further to confirm their thickness and composition throughout the range of examined layer. This will determine if the tribolayer is truly homogenous or if the there is a compositional change throughout the material. Additionally, sectioning will be able to confirm the presence of any subsurface defects which arise from testing. Of particular interest is the presence of Hertzian cone cracking, as this is indicative of fatigue failure.

And finally, it is recommended to conduct the reciprocating testing while adjusting both time and frequency. The testing parameters for this project were created to use mass loss as a parameter. With the profilometry, the degree of wear need not be to such a great extent to produce data. As such, the effect of time and frequency may be investigated to determine the wear mechanisms early in the testing. The mechanisms of wear tends to change over time, and may be different when comparing short periods to long periods of time.

References

References for Chapters 1-4

1. Ellis JL, Goetzel CG. Cermets. ASM Handbook, Properties and Selection, Nonferrous Alloys and Special-Purpose Materials. 1990;2.
2. Zhang S. Material development of titanium carbonitride-based cermets for machining application. Key Eng. Mater. 1998;138:521.
3. Zhang S. Titanium carbonitride-based cermets: Processes and properties. Mater. Sci. Eng., A. 1993;163(1):141.
4. Richerson DW. Modern Ceramic Engineering: Properties, Processing, and Use in Design. 3rd ed. Boca Raton, FL: CRC Taylor & Francis; 2006.
5. Binder S, Lengauer W, Ettmayer P, Bauer J, Debuigner J, Bohn M. Phase equilibria in the systems Ti-C-N, Zr-C-N and Hf-C-N. J. Alloys Compd. 1995;217(1):128.
6. Levi G, Kaplan WD, Bamberger M. Structure refinement of titanium carbonitride (TiCN). Mater. Lett. 1998;35(5):344.
7. Mari D, Bolognini S, Feusier G, Cutard T, Viatte T, Benoit W. TiMoCN based cermets Part II. Microstructure and room temperature mechanical properties. Int. J. Refract. Met. Hard Mater. 2003;21(1):47.
8. Churbanov ED, Moiseev VF, Nechaev VP, Taubkin BL, Maskhuliya LG, Petrov NV. Wettability of refractory compounds by intermetallides. Khimicheskoe i Neftekhimicheskoe Mashinostroenie. 1991(10):34.
9. Rahaman MN. Ceramic Processing. Boca Raton: CRC; 2006.
10. Callister WDJ. Materials Science and Engineering an Introduction. 6th ed. Hoboken, N.J.: John Wiley & Sons, Inc.; 2003.
11. Stachowiak GW, and Batchelor AW. Engineering Tribology. 3rd ed. Amsterdam: Elsevier Butterworth-Heinemann; 2005.
12. Bhushan B. Introduction to Tribology. New York: John Wiley & Sons; 2002.
13. Czichos H. Tribology : A Systems Approach to the Science and Technology of Friction, Lubrication, and Wear. Amsterdam ; New York : Elsevier Scientific Pub. Co. ;

New York: distributors for the U.S. and Canada, Elsevier North Holland; 1978.
14. Smith EH,. Mechanical Engineer's Reference Book. 12th ed. Oxford, England ; Boston: Butterworth Heinemann; 1998.
15. Guu Y, Lin JF. Analysis of wear behaviour of titanium carbonitride coatings. Wear. 1997;210(1-2):245.
16. Pirso J, Viljus M, Juhani K, Letunovitš S. Two-body dry abrasive wear of cermets. Wear. 2009 1/5;266(1-2):21-9.
17. Yeong Y, Lin JF, Ai CF. Correlation between three-body wear and tribological characteristics of titanium nitride, titanium carbonitride and titanium carbide coatings. Wear. 1997;208(1):147.
18. Manoj Kumar BV, Basu B. Fretting wear properties of TiCN-ni cermets: Influence of load and secondary carbide addition. Metall. Mater. Trans. A. 2008;39(3):539.
19. Wei C, Lin JF, Jiang TH, Ai CF. Tribological characteristics of titanium nitride and titanium carbonitride multilayer films. part I. the effect of coating sequence on material and mechanical properties. Thin Solid Films. 2001;381(1):94.
20. Larsen-Basse J. Abrasive wear of some titanium-carbonitride-based cermets. Mater. Sci. Eng., A. 1988;105(2):395.
21. Pirso J, Viljus M, Letunovitš S. Friction and dry sliding wear behaviour of cermets. Wear. 2006 4/7;260(7-8):815-24.
22. Wei C, Lin JF, Jiang TH, Ai CF. Tribological characteristics of titanium nitride and titanium carbonitride multilayer films. Part II. The effect of coating sequence on tribological properties. Thin Solid Films. 2001;381(1):104.
23. Mari D, Bolognini S, Feusier G, Cutard T,Verdon C, Viatte T, Benoit W. TiMoCN based cermets: Part I. Morphology and phase composition. Int. J. Refract. Met. Hard Mater. 2003;21(1):37.
24. Ettmayer P, Kolaska H, Dreyer K. Effect of the sintering atmosphere on the properties of cermets. Powder Metall. Int. 1991;23(4):224.
25. Kwon WT, Park JS, Kang S. Effect of group IV elements on the cutting characteristics of ti(C,N) cermet tools and reliability analysis. J. Mater. Process. Technol. 2005;166(1):9.
26. Wang J, Liu J, Feng Y, Ye J, Tu M. Effect of NbC on the microstructure and

sinterability of Ti($C_{0.7}$, $N_{0.3}$)-based cermets. Int. J. Refract. Met. Hard Mater. 2009;27(3):549.
27. Zhang H, Yan J, Zhang X, Tang S. Properties of titanium carbonitride matrix cermets. Int. J. Refract. Met. Hard Mater. 2006;24(3):236.
28. Ettmayer P, Kolaska H, Dreyer K. Effect of the sintering atmosphere on the properties of cermets. Powder Metall. Int. 1991;23(4):224-30.
29. Cordoba JM. Properties of Ti(C,N) cermets synthesized by mechanically induced self-sustaining reaction. J. Eur. Ceram. Soc. 2009;29(1):1173-82
30. Perez TA, Battez HA, Garcia-Atance G, Viesca JL, Gonzalez R, HadField M. Use of optical profilometry in the ASTM D4172 standard. Wear. 2011 6;271(2963-2967).
31. Gahlin R, Jacobson S. A novel method to map and quantify wear on a micro-scale. Wear. 1998; 5;222(93-102).
32. Qu J, Truhan JJ. An efficient method for accurately determining wear volumes of sliders with non-flat wear scars and compound curvature. Wear. 2006; 8; 261(848-855).
33. Arhab S, Soriano G, Belkebir K, Sentenac A, Giovannini H. Full wave optical profilometry. J. Opt. Soc. Am. A. 2011;28(4):576-80.
34. Urchegui MA, Tato W, Gomez X. A METHOD FOR EVALUATING FRETTING WEAR SCARS IN THIN STEEL ROPING WIRES BASED ON CONFOCAL IMAGING PROFILOMETRY. J. Test. Eval. 2011;35(4):1-7.
35. Collier RB, Plucknett KP. Spherical indentation damage in TiC-Ni_3Al composites. Int. J. Refract. Met. Hard Mater. 2012;30(1):188-95.

References for Chapter 5

1. Zhang SY. Titanium carbonitride-based cermets: Processes and properties. Materials Science and Engineering A. 1993;163(1):141.
2. Zhang S. Material development of titanium carbonitride-based cermets for machining application. Key Engineering Materials. 1998;138:521.
3. Liu HY, Huang JH, Yin CF, Zhang JG, Lin GB. Microstructure and properties of TiC–Fe cermet coatings by reactive flame spraying using asphalt as carbonaceous precursor. Ceramics International. 2007 7;33(5):827-35.
4. Ettmayer P, Kolaska H, Dreyer K. Effect of the sintering atmosphere on the properties of cermets. Powder Metallurgy International. 1991;23(4):224.
5. Kwon WT, Park JS, Kang S. Effect of group IV elements on the cutting characteristics of Ti(C,N) cermet tools and reliability analysis Journal of Materials Processing Technology. 2005;166(1):9.
6. Wang J, Liu J, Feng Y, Ye J, Tu M. Effect of NbC on the microstructure and sinterability of $Ti(C_{0.7},N_{0.3})$-based cermets. International Journal of Refractory Metals and Hard Materials. 2009;27(3):549.
7. Zhang H, Yan J, Zhang X, Tang S. Properties of titanium carbonitride matrix cermets. International Journal of Refractory Metals and Hard Materials. 2006;24(3):236.
8. Plucknett KP, Becher PF. Processing and microstructure development of titanium carbide-nickel aluminide composites prepared by melt infiltration/sintering (MIS). Journal of the American Ceramic Society. 2001;84(1):55.
9. Asthana R, Kumar A, Dahotre NB. Materials Processing and Manufacturing Science. Butterworth-Heinemann; 2006.
10. Bowen P, Bonjour C, Carry C, Gonseth D, Hofmann H, Mari D, Mulone R, Streit P. Novel alumina titanium-carbonitride nickel composites. JOM. 1995;47(11):56.
11. Acchar W, Gomes UU, Kaysser WA, Goring J. Strength degradation of a tungsten carbide-cobalt composite at elevated temperatures. Materials Characterization. 1999;43:27–32.

12. Ying L, Jin Y, Yu H, Ye J. Ultrafine (Ti, M)(C, N)-based cermets with optimal mechanical properties. International Journal of Refractory Metals and Hard Materials. 2011;29(1):104-7.
13. Manoj Kumar BV, Basu B. Fretting wear properties of TiCN-Ni cermets: Influence of load and secondary carbide addition. Metallurgical and Materials Transactions A. 2008;39(3):539.
14. Bunshah RF, editor. Handbook of Hard Coatings. William Andrew Publishing/Noyes.; 2001.
15. Harper CA, editor. Handbok of Plastics, Elastomers, and Composites. Fourth Edition ed. McGraw-Hill Companies, Inc., McGRAW-HILL; 2002.
16. Stachowiak GW, and Batchelor AW. Engineering Tribology. 3rd ed. Amsterdam: Elsevier Butterworth-Heinemann; 2005.
17. Czichos H. Tribology: A Systems Approach to the Science and Technology of Friction, Lubrication, and Wear. Amsterdam ; New York : Elsevier Scientific Pub. Co. ; New York: distributors for the U.S. and Canada, Elsevier North Holland; 1978.
18. Smith EH. Mechanical Engineer's Reference Book. 12th ed. Oxford, England; Boston: Butterworth Heinemann; 1998.
19. Powers MT, Lavernia EJ, Groza JR, Shackelford JF, editors. Materials Processing Handbook. CRC Press; 2007.
20. Collier RB, Plucknett KP. Spherical indentation damage in TiC-Ni_3Al composites. International Journal of Refractory Metals and Hard Materials. 2012;30(1):188-95.
21. Collier RB, Plucknett KP. A comparison of anionic and cationic polyelectrolytes for the aqueous colloidal processing of titanium carbide ceramics. International Journal of Refractory Metals and Hard Materials. 2011;29(2):298-305.
22. Anstis GR, Chantikul P, Lawn BR, Marshall DB. A critical evaluation of indentation techniques for measuring fracture toughness. I. direct crack measurements. Journal of the American Ceramic Society. 1981;64(9):533-8.
23. Yount HJ. Hardness and fracture toughness of heat-treated advanced ceramic materials for use as fuel coating and inert matrix material in advanced reactors. MSc dissertation, University of Wisconsin-Madison; 2006.

24. ASTM standard C1327; 2008; Standard test method for Vicker's indentation hardness of advanced ceramics; ASTM International; West Conshohocken, PA, 2008; DOI: 10.1520/C0033-03; www.astm.org.
25. Bhushan B. Introduction to tribology. New York: John Wiley & Sons; 2002.
26. Chen H, Hutchings IM. Abrasive wear resistance of plasma-sprayed tungsten carbide-cobalt coatings. Surface and Coatings Technology. 1998;107(2):106-14.
27. Yeong Y, Lin JF, Ai CF. Correlation between three-body wear and tribological characteristics of titanium nitride, titanium carbonitride and titanium carbide coatings. Wear. 1997;208(1):147.
28. Pirso J, Viljus M, Juhani K, Letunovitš S. Two-body dry abrasive wear of cermets. Wear. 2009 1/5;266(1-2):21-9.
29. Guu YY, Lin JF, Ai C. The tribological characteristics of titanium carbonitride coatings prepared by cathodic-arc ion plating technique. Thin Solid Films. 1996 10/30;287(1-2):16-24.
30. Guu Y, Lin JF. Analysis of wear behaviour of titanium carbonitride coatings. Wear. 1997;210(1-2):245.
31. Wei C, Lin JF, Jiang TH, Ai CF. Tribological characteristics of titanium nitride and titanium carbonitride multilayer films. Part II. the effect of coating sequence on tribological properties. Thin Solid Films. 2001;381(1):104.
32. Wei C, Lin JF, Jiang TH, Ai CF. Tribological characteristics of titanium nitride and titanium carbonitride multilayer films. Part I. the effect of coating sequence on material and mechanical properties. Thin Solid Films. 2001;381(1):94.
33. Plucknett KP, Becher PF, Waters SB. Flexure strength of melt-infiltration-processed titanium carbide/nickel aluminide composites. Journal of the American Ceramic Society.1998;81:1839–44.
34. Dimiduk DM. Dislocation structures and anomalous flow in $L1_2$ compounds. Journal de Physique III. 1991;1:1025-53.
35. Choi SC, Cho HJ, Kim YJ, LeeDB. High-temperature oxidation behavior of pure Ni_3Al. Oxidation of Metals. 1996;46:51-72.
36. Fischer Cripps AC, Collins RE. The probability of Hertzian fracture. Journal of Materials Science. 1994;29(8):2216-30.

References for Chapter 6

1. S. Zhang: 'Titanium carbonitride-based cermets: Processes and properties', *Mater. Sci. Eng. A*, 1993, **163**, (1), 141-148.
2. S. Zhang: 'Material development of titanium carbonitride-based cermets for machining application', *Key Eng. Mater.*, 1998, **138**, (1), 521-543.
3. G. Levi, W.D. Kaplan and M. Bamberger: 'Structure refinement of titanium carbonitride (TiCN)', *Mater. Lett.*, 1998, **35**, (5-6), 344-350.
4. H.Y. Liu, J.H. Huang, C.F Yin, J.G. Zhang and G.B. Lin: 'Microstructure and properties of TiC–Fe cermet coatings by reactive flame spraying using asphalt as carbonaceous precursor', *Ceram. Int.*, 2007, **33**, (5), 827-835.
5. J. Pirso, M. Viljus and S. Letunovitš: 'Friction and dry sliding wear behaviour of cermets', *Wear*, 2006, **260**, (7-8), 815-824.
6. P. Ettmayer, H. Kolaska and K. Dreyer: 'Effect of the sintering atmosphere on the properties of cermets', *Powder Metall. Int.*, 1991, **23**, (4), 224-230.
7. W. Acchar, U.U. Gomes, W.A. Kaysser and J. Goring: 'Strength degradation of a tungsten carbide-cobalt composite at elevated temperatures', *Mater. Charact.*, 1999, **43**, (1), 27–32.
8. Z.N. Farhat: 'Microstructural characterization of WC-TiC-Co cutting tools during high-speed machining of P20 mold steel', *Wear*, 2003, **51**, (2-3), 117-130.
9. D. Mari, S. Bolognini, G. Feusier, T. Cutard, C. Verdon, T. Viatte and W. Benoit: 'TiMoCN based cermets. Part I: Morphology and phase composition', *Int. J. Refract. Met. Hard Mater.*, 2003, **21**, (1-2), 37-46.
10. T.N. Tiegs, P.A. Menchhofer, K.P. Plucknett, P.F. Becher, C.B Thomas and P.K. Liaw: 'Comparison of sintering behavior and properties of aluminide-bonded ceramics', *Ceram. Eng. Sci. Proc.*, 1998, **19**, (3), 447-455.
11. L. Yin, Y. Jin, H. Yu and J. Ye: 'Ultrafine (Ti, M)(C, N)-based cermets with optimal mechanical properties', *Int. J. Refract. Met. Hard Mater.*, 2011, **29**, (1), 104-107.
12. S. Zhang and G.Q. Lu: 'Sintering kinetics of Mo-free cermets', *J. Mater. Process Technol.*, 1997, **67**, (1-3), 162-166.

13. W.T. Kwon, J.S. Park and S. Kang: 'Effect of group IV elements on the cutting characteristics of Ti(C,N) cermet tools and reliability analysis', *J. Mater. Process. Technol.*, 2005, **166**, (1), 9-14.
14. H. Zhang, J. Yan, X. Zhang and S. Tang: 'Properties of titanium carbonitride matrix cermets', *Int. J. Refract. Met. Hard Mater.*, 2006, **24**, (3), 236-239.
15. J. Wang, J. Liu, Y. Feng, J. Ye and M. Tu: 'Effect of NbC on the microstructure and sinterability of $Ti(C_{0.7},N_{0.3})$-based cermets', *Int. J. Refract. Met. Hard Mater.*, 2009, **27**, (3), 549-551.
16. D.M. Dimiduk: 'Dislocation structures and anomalous flow in $L1_2$ compounds', *J. Phys. III*, 1991, **1**, (6), 1025-1053.
17. K.P. Plucknett, P.F. Becher and S.B. Waters: 'Flexure strength of melt-infiltration-processed titanium carbide/nickel aluminide composites', *J. Amer. Ceram. Soc.*, 1998, **81**, (7), 1839-1844
18. S.C. Choi, H.J. Cho, Y.J. Kim and D.B. Lee: 'High-temperature oxidation behavior of pure Ni_3Al', *Oxid. Met.*, 1996 **46**, (1-2), 51-72.
19. G.W. Stachowiak and A.W. Batchelor: 'Engineering tribology', 3rd edn; 2005, Amsterdam, Elsevier Butterworth-Heinemann.
20. E.H. Smith: 'Mechanical engineer's reference book', 12th edn, 9/3-124; 1998, Boston, Butterworth-Heinemann.
21. J.P. Delplanque, S. Johnson, Y. Zhou: 'Spray Deposition and Coating Processes', in 'Materials processing handbook', (ed. M.T. Powers, E.J. Lavernia, J.R. Groza and J.F. Shackelford JF), 11/1-24; 2007, Boca Railton, CRC Press.
22. P. Bowen, C. Bonjour, C. Carry, D. Gonseth, H. Hofmann, D. Mari, R. Mulone and P. Streit: 'Novel alumina titanium-carbonitride nickel composites', *JOM*, 1995, **47**, (11), 56-58.
23. B.V. Manoj Kumar and B. Basu: 'Fretting wear properties of TiCN-Ni cermets: Influence of load and secondary carbide addition', *Metall. Mater. Trans. A*, 2008, **39**, (3), 539-550.
24. K.P. Plucknett and P.F. Becher: 'Processing and microstructure development of titanium carbide-nickel aluminide composites prepared by melt infiltration/sintering (MIS)', *J. Am. Ceram. Soc.*, 2001, **84**, (1), 55-61.

25. R.B. Collier and K.P. Plucknett: 'Spherical indentation damage in TiC-Ni_3Al composites', *Int. J. Refract. Met. Hard Mater.*, 2012, **30**, (1), 188-195.
26. M.I. Mendelson: 'Average grain size in polycrystalline ceramics', *J. Am. Ceram. Soc.*, 1969, **52**, (8), 443-446
27. G.R. Anstis, P. Chantikul, B.R. Lawn and D.B. Marshall: 'A critical evaluation of indentation techniques for measuring fracture toughness. I. Direct crack measurements', *J Am Ceram Soc.*, 1981, **64**, (9), 533-538.
28. ASTM standard C1327: 'Standard test method for Vickers indentation hardness of advanced ceramics', ASTM international, West Conshohocken, US, 2008.
29. S. Buchholz, Z.N. Farhat, G.J. Kipouros and K.P. Plucknett: 'The Reciprocating Wear Behaviour of TiC-Ni_3Al Cermets', submitted to *Int. J. Refract. Met. Hard Mater.*, (Dec. 2011).
30. E.D. Churbanov, V.F. Moisee, V.P. Nechaev, B.L Taubkin, L.G Maskhuliya and N.V. Petrov: 'Wettability of refractory compounds by intermetallic compounds', *Khimicheskoe i Neftekhimicheskoe Mashinostroenie*, 1991, Iss. (10), 34-35.
31. J. Larsen-Basse: 'Abrasive wear of some titanium-carbonitride-based cermets', *Mater. Sci. Eng. A.*, 1988, **105**, (2), 395-400.
32. J. Karthikeyan: 'Ceramic coating technology', *Sādhanā*, 1988, **13**, (1), 139-156.
33. O. Knotek, F. Loffler, G. Kramer: 'Applications to Cutting Tools', in 'Handbook of hard coatings', (ed. R.F. Bunshah), Vol. 1, 370-406; 2001, Park Ridge, NJ, William Andrew Publishing/Noyes.
34. C. Zweben: 'Metal Matrix Composites, Ceramic Matrix Composites, Carbon Matrix Composites, Carbon Matrix Composites, and Thermally Conductive Polymer Matrix Composites' in 'Handbook of plastics, elastomers, and composites', (ed. C.A. Harper), 4th ed., 321-344; 2002, Tow Penn Plaza, McGraw-Hill.
35. B. Bhushan: 'Introduction to Tribology', 207-280, 2002, New York, John Wiley & Sons.
36. H. Czichos: 'Tribology: A systems approach to the science and technology of friction, lubrication, and wear', 1st edn, 45-246, 1978, Amsterdam, Elsevier North Holland.

37. H. Chen and I.M. Hutchings: 'Abrasive wear resistance of plasma-sprayed tungsten carbide-cobalt coatings', *Surf. Coat. Technol.*, 1998, **107**, (2), 106-114.
38. Y. Yeong, J.F. Lin and C.F. Ai: 'Correlation between three-body wear and tribological characteristics of titanium nitride, titanium carbonitride and titanium carbide coatings', *Wear*, 1997, **208**, (1), 147-154.
39. J. Pirso, M. Viljus, K. Juhani and S. Letunovitš: 'Two-body dry abrasive wear of cermets', *Wear*, 2009, **266**, (1-2), 21-29.
40. Y.Y. Guu and J.F. Lin: 'Analysis of wear behaviour of titanium carbonitride coatings', *Wear*, 1997, **210**, (1-2), 245-254.
41. Y.Y. Guu, J.F. Lin and C.F. Ai: 'The tribological characteristics of titanium carbonitride coatings prepared by cathodic-arc ion plating technique', *Thin Solid Films*, 1996, **287**, (1-2), 16-24.
42. C. Wei, J.F. Lin, T.H. Jiang and C.F. Ai: 'Tribological characteristics of titanium nitride and titanium carbonitride multilayer films. Part I: The effect of coating sequence on material and mechanical properties', *Thin Solid Films*, 2001, **381**, (1), 94-103.
43. C. Wei, J.F. Lin, T.H. Jiang and C.F. Ai: 'Tribological characteristics of titanium nitride and titanium carbonitride multilayer films. Part II: The effect of coating sequence on tribological properties', *Thin Solid Films*, 2001, **381**, (1), 104-118.
44. A.C. Fischer Cripps and R.E. Collins: 'The probability of Hertzian fracture', *J. Mater. Sci.*, 1994, **29**, (8), 2216-2230.
45. J. Lu, G.A. Sargent and H. Conrad: 'Study of the mechanisms of erosion in silicon single crystals using Hertzian fracture tests', *Wear*, 1995, **186**, (1), 105-116.

Appendix A - Optical Profilometry

The following are the pseudo 3-dimensional images generated using optical profilometry that have not been displayed in Chapters 5 or 6. They display all wear tracks generated for each tested cermet for all volume percentages of binder. Some images display more than four wear tracks, and are the product of interrupted wear tests.

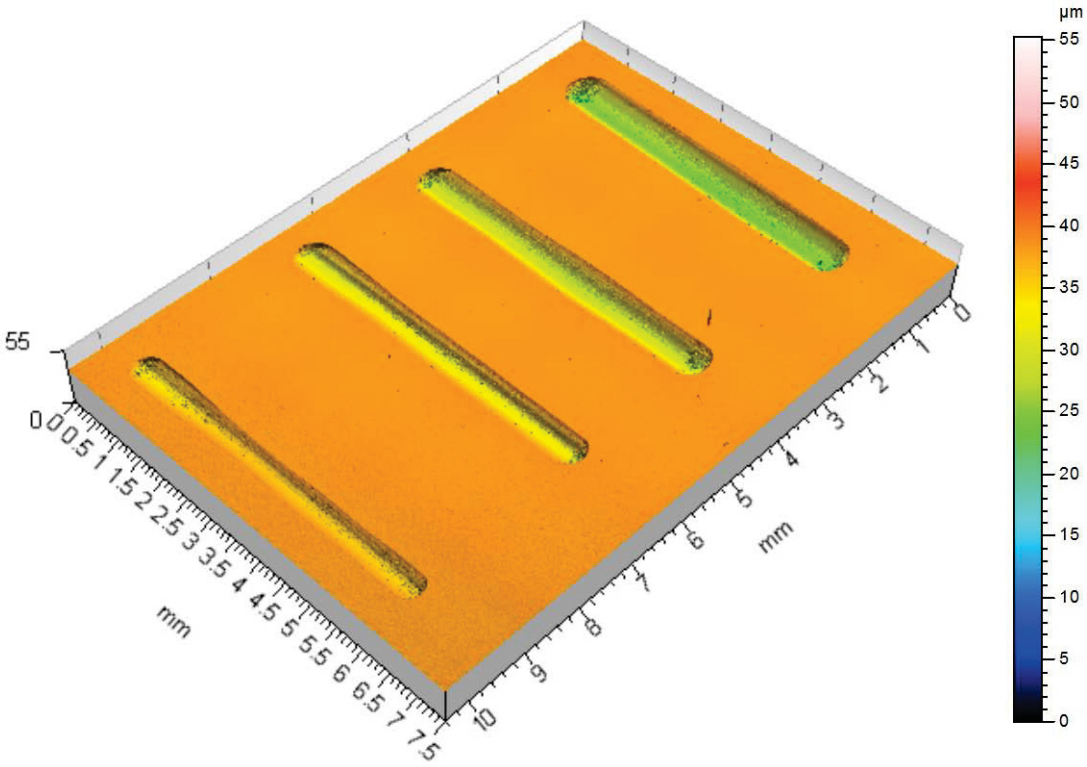

Figure 58. Pseudo 3-D optical profilometry of TiC-Ni_3Al with 30 vol. % binder.

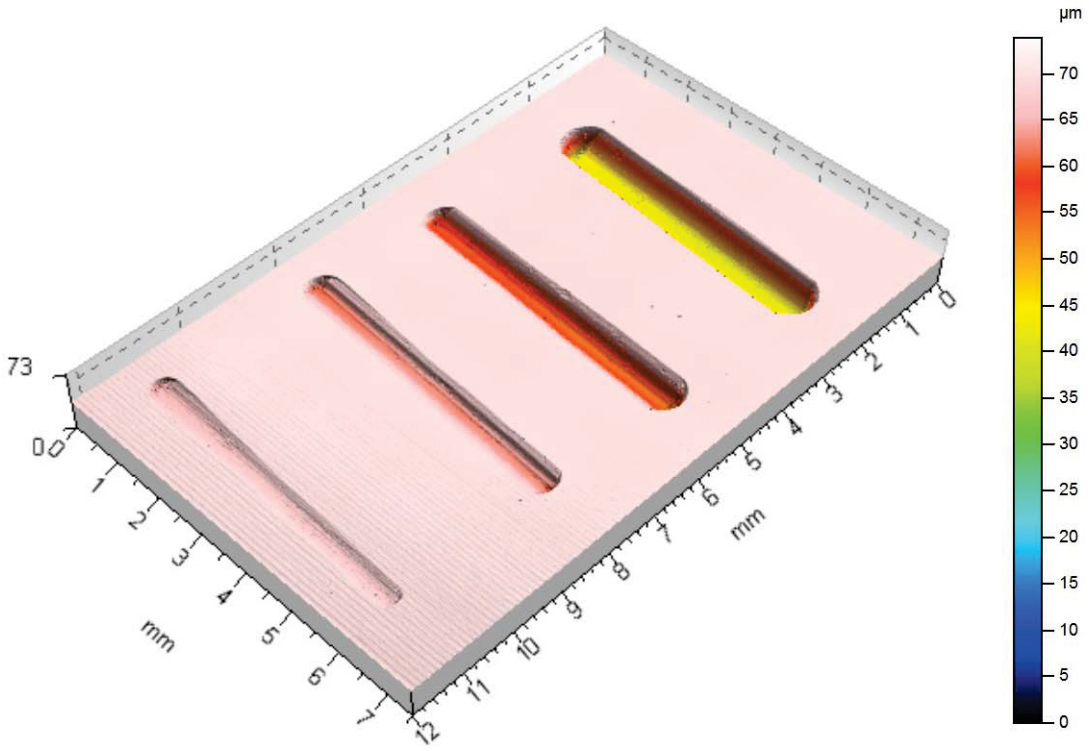

Figure 59. Pseudo 3-D optical profilometry of TiC-Ni_3Al with 40 vol. % binder.

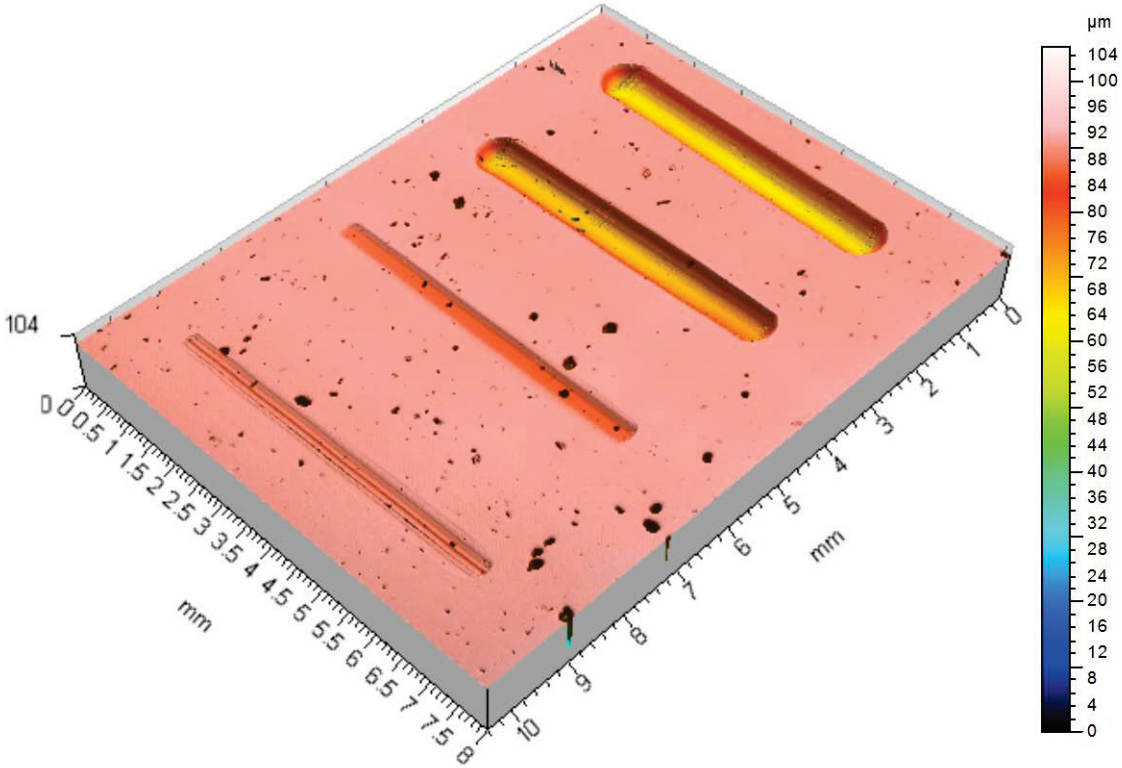

Figure 60. Pseudo 3-D optical profilometry of $Ti(C_{0.7},N_{0.3})$-Ni_3Al with 20 vol. % binder.

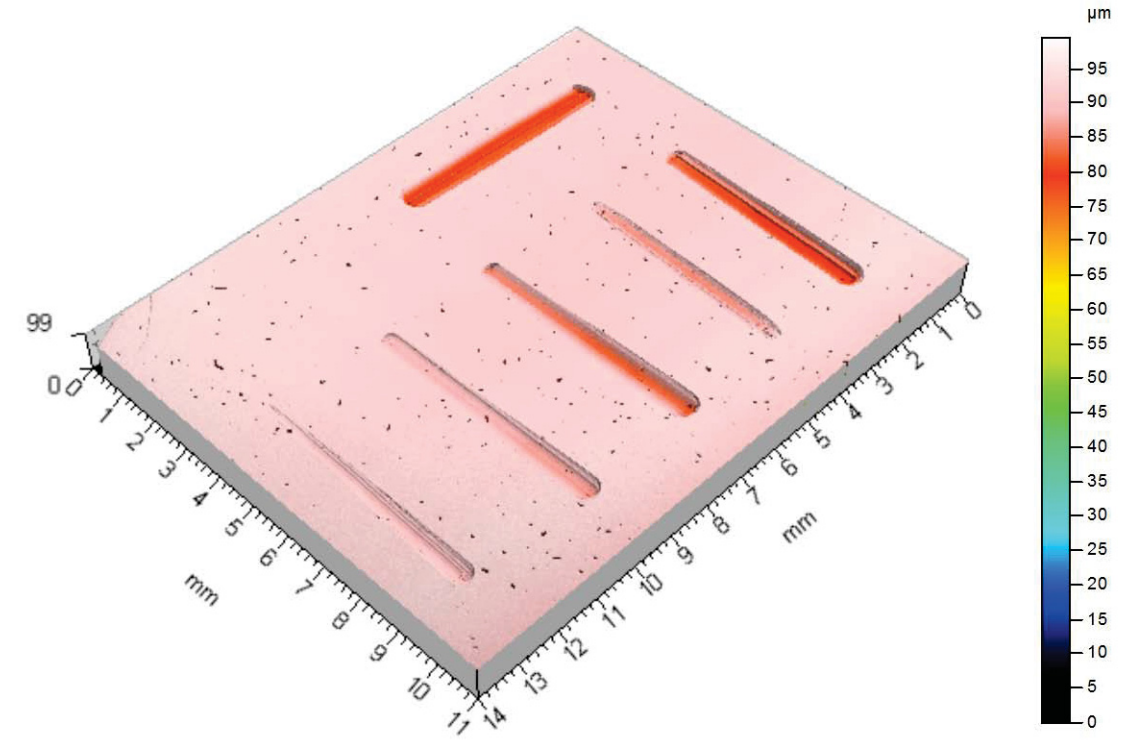

Figure 61. Pseudo 3-D optical profilometry of $Ti(C_{0.7},N_{0.3})$-Ni_3Al with 30 vol. % binder.

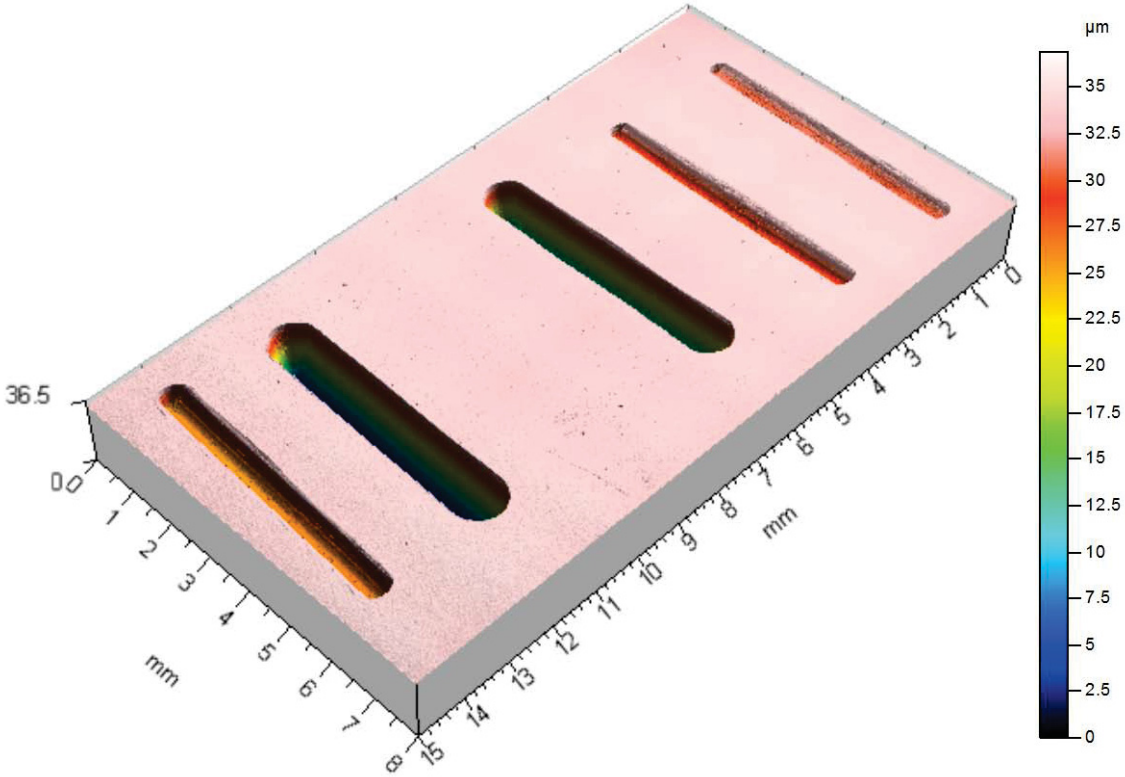

Figure 62. Pseudo 3-D optical profilometry of $Ti(C_{0.7},N_{0.3})$-Ni_3Al with 40 vol. % binder.

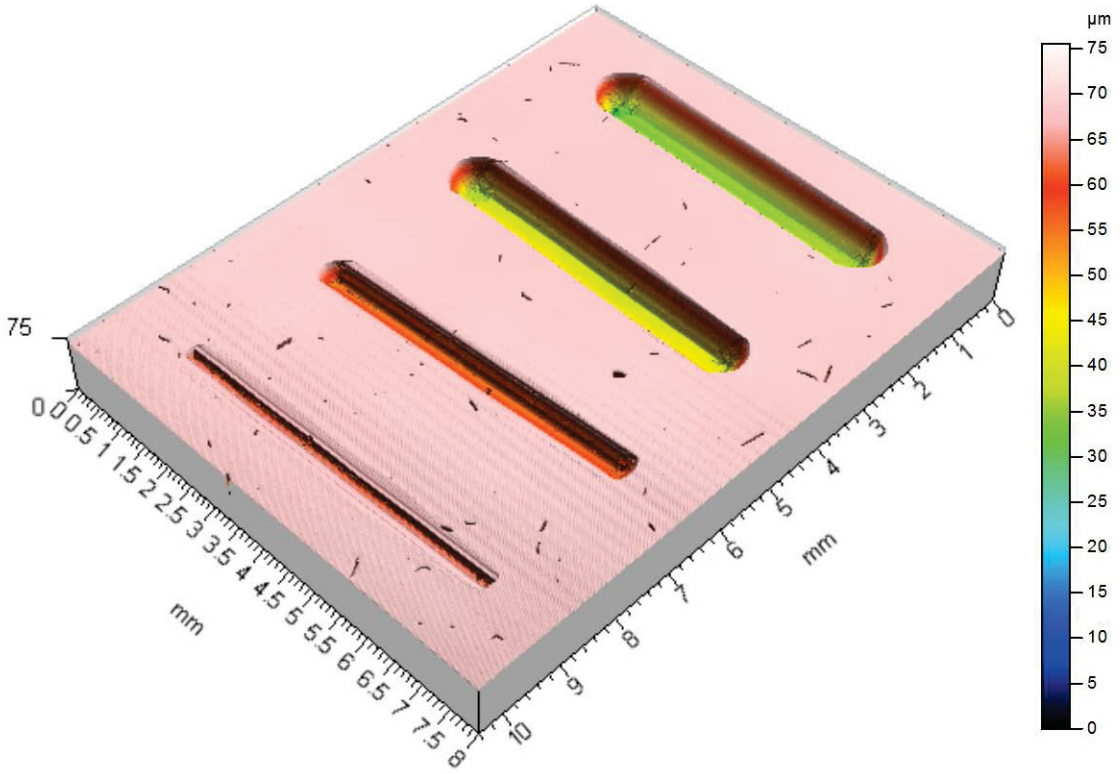

Figure 63. Pseudo 3-D optical profilometry of $Ti(C_{0.5},N_{0.5})$-Ni_3Al with 30 vol. % binder.

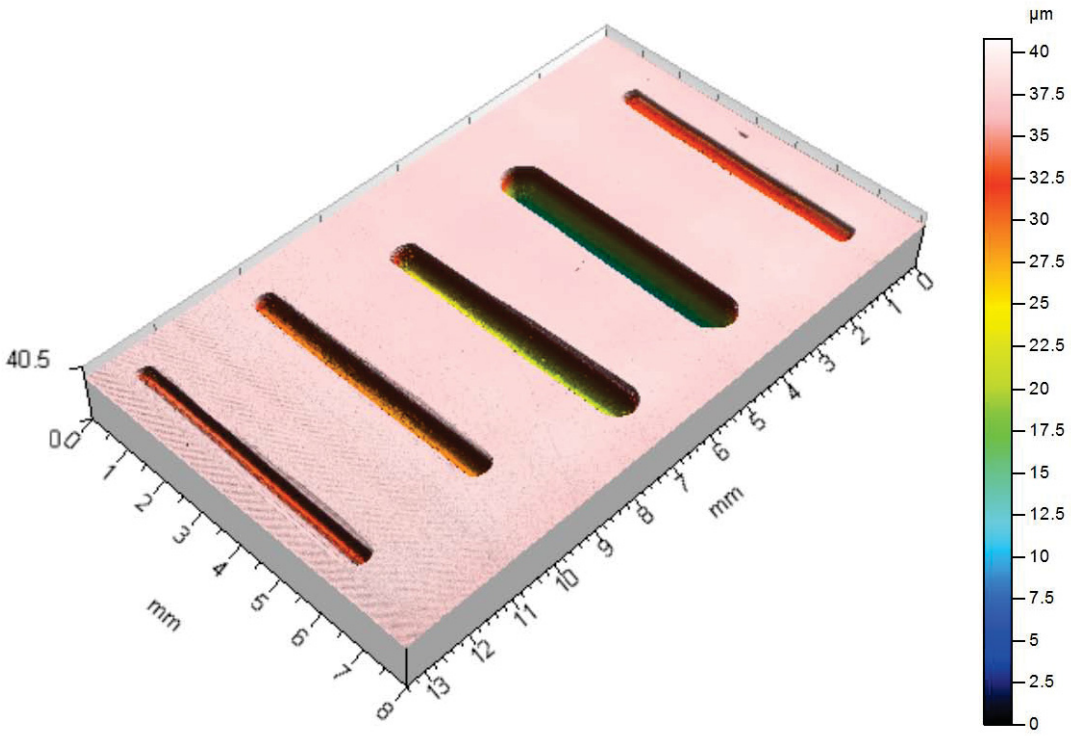

Figure 64. Pseudo 3-D optical profilometry of $Ti(C_{0.5},N_{0.5})$-Ni_3Al with 40 vol. % binder.

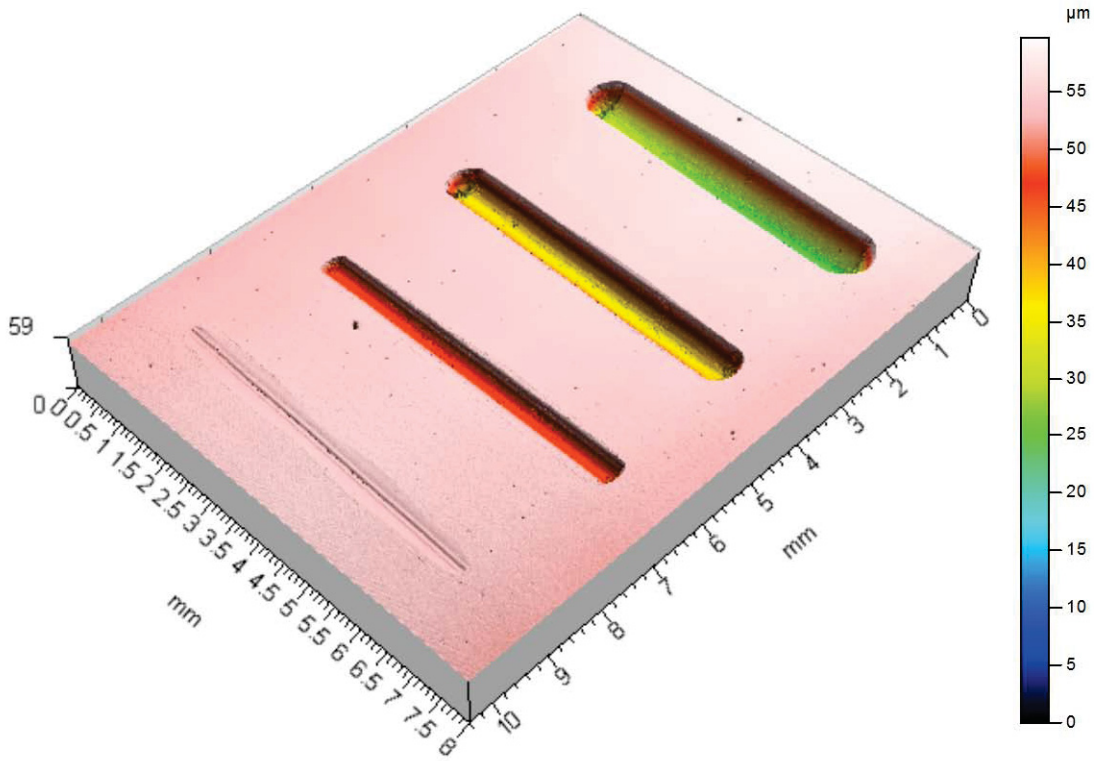

Figure 65. Pseudo 3-D optical profilometry of $Ti(C_{0.3},N_{0.7})$-Ni_3Al with 40 vol. % binder.